Synthesis And Characterization of Nanoparticles Using Keratin Extracted From Sheep Hooves for Industrial Applications

Cheptoo Caroline

2025-10
UoK
https://ir-library.kabianga.ac.ke/handle/123456789/1161

SYNTHESIS AND CHARACTERIZATION OF NANOPARTICLES USING KERATIN EXTRACTED FROM SHEEP HOOVES FOR INDUSTRIAL APPLICATIONS

CHEPTOO CAROLINE

A Thesis Submitted to the Board of Graduate Studies in Partial Fulfilment of the Requirements for the degree of Doctor of Philosophy in Chemistry of the University of Kabianga.

UNIVERSITY OF KABIANGA

OCTOBER, 2025

DECLARATION AND APPROVAL

DECLARATION

I declare that this thesis is my original work and has not been presented for the conferment of a Degree or award of a Diploma in this or any other institution.

Signature…… Date…….

Cheptoo Caroline
PHD/CHE/002/19

APPROVAL

This thesis has been submitted with our approval as the University supervisors.

Signature…… Date ……

Dr. Wycliffe Chisutia Wanyonyi
Department of Mathematics Actuarial and Physical Sciences,
University of Kabianga

Signature…… Date ……

Prof. Kiplimo Jepkorir Joyce
Department of Mathematics Actuarial and Physical Sciences,
University of Kabianga

Signature…… Date ……

Dr. Edwin S. Madivoli
Department of Chemistry
Jomo Kenyatta University of Agriculture and Technology

COPYRIGHT

DEDICATION

To everyone who prayed and wished me well during the research journey.

ACKNOWLEDGEMENT

I thank God for the far HE has taken me. HE makes my feet like the feet of a deer and enables me to go on greater heights. I thank my supervisors Dr. Wanyonyi C. Wycliffe, Prof. Kiplimo Joyce and Dr. Edwin Madivoli for their guidance and mentorship that enabled me to get the right methodology, collect data and come out with the research report. I acknowledge the advice and encouragement from all the Chemistry lecturers from the University of Kabianga that enabled me to improve the quality of this research. I thank the following laboratory technologist for their assistance in the laboratory: Mr. Gilbert Cheruiyot and Ms. Sharon Mercy Onderi from chemistry laboratory, Mr. Allan Soimo and Mr. Paul Onyango from microbiology laboratory, Mr. Robert Korir and Mr. Gilbert Limo from Physics laboratories all from University of Kabianga. I thank Mr. Sammy Indire Wanakai and Ms. Joyline Jemutai from Chemistry and Mr. John Kamau Muchuku from Botany Departments of Jomo Kenyatta University, Mr. Robert Bii and Mr. Samwel Lelgo from Tea Research Institute for their assistance. I thank my husband Mr. Wilbon Langat for his advice, encouragement and financial support, my mother Mrs. Zeddy Barng´oino for her encouragement and my sister Ms. Fancy Chelangat for her support and assistance. I thank my uncles Mr. Jonathan Lang´at and Mr. Joseph Lang´at for their encouragement and motivation throughout my studies. This work was graciously supported by the National Research Fund (NRF) Kenya through Dr. Wycliffe C. Wanyonyi multidisciplinary research grant.

ABSTRACT

Environmental degradation is a concern in developing countries due to industrial development, constantly rising population which practice agriculture, industrial development, urbanisation and poor waste management. The waste disposed to the environment contributes to environmental pollution. Industrial effluents and water runoff from urban regions and farms contribute to water pollution in rivers and other water bodies. In various parts of the world persons lack access to clean water for drinking, due to pollutants from industries and residential waste. Some of the pollutants in water include: Dyes from industries such as the textile and leather industries, steroids and antibiotics from industries and hospital waste water. Wastes from slaughter houses are source pollution and landfills occupy space which could have been used for farming and other purposes. The aim of this research was to extract keratin from sheep hooves using NaOH and use it as a reducing and capping agent in synthesis of nanoparticles for use in adsorption of selected organic dyes in water. Sheep hooves were collected from a slaughter house in Litein, cleaned with detergent and distilled water and 70 % ethanol before drying. The optimum conditions for Keratin hydrolysis were: A time of 9 hours, temperature of 70 °C, NaOH concentration of 1 % (w/v) and a pH of 12. The pH of Keratin solution was adjusted to 3.2 to obtain keratin precipitate which was used as a reducing and stabilizing agent in synthesis of Cu, Ag, ZnO and Fe_3O_4 nanoparticles. The optimum conditions for synthesis of copper and silver nanoparticles were: A time of 90 minutes, temperature of 80 °C and a concentration of 0.01 mol/dm^3 of the salt containing the metal ions. Characterisation of the synthesized nanoparticles was done using UV-VIS to determine optical properties, FT-IR to determine functional groups on nanoparticles, SEM to determine shape and particle size distribution and XRD to determine crystallinity of the nanoparticles. UV-VIS analysis confirmed the formation of nanoparticles. FT-IR results indicated the involvement of keratin in formation of nanoparticles. Efficiency of adsorption of methylene blue using copper nanoparticles and adsorption of crystal violet dyes using AgNps and Fe_3O_4 was investigated. Residual dye concentrations were determined by UV-VIS. Adsorption of CV using silver nanoparticles attained equilibrium after 60 minutes at room temperature with 97.9 % efficiency of the dye removal. Copper nanoparticles were used in removal of methylene blue with equilibrium attained after 330 minutes at room temperature with 95% efficiency. Adsorption of crystal violet using Fe_3O_4 attained equilibrium after 8 minutes with 99.2 % efficiency. Influences of preliminary concentration, pH and temperature on dye removal were investigated. Optimum conditions for removal of crystal violet by silver were pH of 5-6, 60 minutes of contact time and a temperature of 45 °C. The optimum conditions for the removal methylene blue dye by copper nanoparticles were a pH range of 2-5 and a dosage of 8 mg/10 ml of the colorant. The optimum conditions for adsorption of CV using Fe_3O_4 nanoparticles were a time of 8 minutes and a dosage of 6 mg/10 ml. Adsorption kinetics were investigated using Pseudo first order and second order kinetics. Adsorption isotherms were investigated by plotting Langmuir and Freundlich isotherms. The results followed Langmuir and Freundlich isotherms and Pseudo second order kinetics. The findings of this research will add knowledge on the probable use of CuNps, AgNps and Fe_3O_4 in removal of organic dyes in waste water. These results demonstrate that keratin capped nanoparticles are effective, eco-friendly and low-cost adsorbent material for removal of dyes from aqueous solutions and industrial effluents.

TABLE OF CONTENTS

LIST OF TABLES

LIST OF FIGURES

ABBREVIATIONS AND ACRONYMS

AgNps	Silver nanoparticles
$(C_6H_4NH_2)_2$	Benzidine
CuNps	Copper nanoparticles
CV	Crystal violet
ECM	Extracellular matrix
EDS	Energy dispersive spectroscopy
F-C	Folin Ciocalteu
FCC	Face centred cubic
Fe_3O_4-NPs	Magnetic iron (III) oxide nanoparticles
$FeSO_4$	Iron (II) Sulphate
$FeCl_3.6\ H_2O$	Iron (III) chloride hexahydrate
FTIR	Fourier transform infra-red spectroscopy
K	Distribution coefficient
KEBS	Kenya Bureau of Standards.
ln	Natural logarithm
LSPR	Localised Surface Plasmon Resonance
MB	Methylene blue
MIP	Metal Induced Photo catalysis.
NaOH	Sodium hydroxide
NH_2	Amine
NPs	Nanoparticles.
PL	Photoluminescence
R	Gas constant (8.314 J/K/mol)

RO	Reverse osmosis
SDGs	Sustainable Development Goals
SEM	Scanning Electron Microscopy.
SH	Thiols
SODIS	Solar disinfection
T	Absolute temperature
TBT	Tri-biphenyl triazine
TEM	Transmission Electron Microscopy
TGA	Thermo gravimetric analysis
UV-VIS	Ultra violet- Visible Light
WHO	World Health Organization.
XRD	X-ray diffraction

DEFINITION OF TERMS

Azo dyes: These are dyes characterized by vibrant color and by the existence of one or more azo groups (–N=N–) aromatic rings in their structure.

Characterization: To give distinctive features of something. It involves determining chemical and physical properties of substances using various analytical techniques.

Effluents: An effluent is water-treated or untreated that flows out of a treatment plant, sewer or industrial outfall.

Keratin: A fibrous cysteine-rich structural insoluble protein which is the key structural material making up feathers, hair, horns, claws, hooves, and the outer layer of human skin.

Nano materials: Materials which are made up of particles with size that ranges from 1-100 nm.

Nanotechnology: It is designing of devices, materials, and systems through control of matter on the nanometer length scale.

Synthesis: Combination of elements or parts to obtain a more complete system.

.

CHAPTER ONE

INTRODUCTION

1.1 Overview

This chapter entails the background information of the study that involves local industries such as food and textile industries, impact of the industrial effluents on environmental filth, waste management, technologies used to remove the contaminants and the need to improve and develop new techniques to reduce the cost of operation, improve efficacy and prevent generation of noxious sludge during water purification. Objectives of the study, statement of the problem, justification and limitation of the study area are also presented here.

1.2 Background of the Study

Water contamination is a global problem since it has damaging effects on humans and ecosystem (Ray et al., 2020). Manufacturing actions have augmented with increase in population in India, China, Kenya, Nigeria and other developing countries (Ehiomogue et al., 2021). The extensive human activities which include industrial development, domestic, municipal and agricultural practices is currently a major source of environmental degradation (Ray et al., 2020). Due to rapid growth and development of local industries, there has been a subsequent increase in environmental degradation due to discharge of effluents into the environment. Moreover, increase in population has further escalated this problem as this increase subsequently leads to demand for fertilizers, petroleum-based products and antibiotics which are emerging pollutants (Wasike et al., 2019). A large population in Africa practice agriculture using chemicals for controlling pests and diseases on crops and animals. These chemicals used contain impurities which contribute to environmental pollution. The population also consumes industrial products and disposes

waste materials into the environment. Some of the disposed materials are non-biodegradable for example plastics and polythene hence they accumulate in the environment causing pollution (Rada-Mendoza et al., 2018). Some waste degrade slowly releasing bacteria and fungi affecting ecological conditions such as the soil pH and also the pathogens released affect human health as fungal infections from dermatophillic fungi (Bitew et al., 2018).

Although access to clean water and sanitation is an SDG goal number six (6), this has become a challenge because of human activities that lead to pollutants from agricultural chemicals and effluents released into the environment. Poor waste management, irrigation with contaminated water containing high concentrations of impurities from industries, use of contaminated manure, pesticides, herbicides and phosphate fertilizers have led to their presence being detected in various foods (Rai et al., 2019). Some contaminants such as colorants persist in the environment and build up in living organisms with time since they are non-biodegradable (Rada-Mendoza et al., 2018). These environmental pollutants are harmful to humans when they exceed WHO and KEBS limits (Wasike et al., 2019). There is an extensive use of organic dyes in textile industries. The quantity of colorant applied that stick to the substrate during coloring process significantly varies hence large quantities of the dye applied may be lost (Meili et al., 2019). The untreated industrial water find its way into environment and water bodies where they persist for a long time lowering esthetic quality of water, affecting photosynthesis of aquatic plants and causing harm to microorganism (Al-Tohamy et al., 2022). Waste water from industries containing organic dyes which are harmful to human beings and microorganisms since the dyes are resistant to degradations, toxic and carcinogenic (Shanker et al., 2017). Use of contaminated water

for irrigation impacts negatively the soil hence slowing germination rates (Al-Tohamy et al., 2022).

Food industry is one of the industries which contribute to environmental pollution due to improper disposal of bio wastes. Slaughterhouses on the other hand produces large quantity of discharge due to slaughtering of animals such as sheep, goats and cows, meat processing and cleaning of equipment used in the facility (Bustillo-Lecompte and Mehrvar, 2015). Discharge of untreated slaughterhouse waste causes threat to human well-being and deteriorate environs due to waste accumulation caused by existence of lipids and protein which cannot easily be degraded in the waste (Musa and Idrus, 2021). Keratin rich bio waste such as feathers, sheep wool, horns and scales are some of the solid wastes released to environment (Sharma and Gupta, 2016). The wastes accumulate as landfill and over burden water bodies owing to high frequency of release (Musa and Idrus, 2021). Various methods have been employed in cleaning environment such as incineration of accumulated solid waste, burning of wastes in the open releases poisonous or greenhouse gases to the environment. However designing of special chambers for burning of waste to prevent the release of gases to environment can be expensive and involves consumption of high amount of energy (Sharma and Gupta, 2016); (Sinkiewicz et al., 2017). Methods developed for removing pollutants in water these include: Use of chemical adsorbents, extraction using solvents, sedimentation, electrochemical techniques, oxidation or reduction, use of ion exchanger, reverse osmosis and biological methods. These methods can be slow consuming a lot of time to remove impurities or uneconomical, making it difficult to sustain the purification processes. Using chemicals can result in products which need further treatment (Czikkely et al., 2018). Nanotechnology plays a significant role in enhancing water

treatment due to their unique features such as surface area multi-functionality, reusability, surface chemistry, high efficiency and flexibility (Hu et al., 2016). Nanoparticles are synthesized using top-down methods which involves size lessening using various chemical treatments and physical techniques to obtain Nano sized particles from an appropriate preliminary bulk material (Mittal et al., 2013). Bottom-up methods involves nanoparticles synthesis starting with molecules or atoms which assemble to form nanoparticles (Jamkhande et al., 2019). Keratin can be extracted from keratin rich bio waste and used as a reducing and capping agent during synthesis of nanoparticles due to the presence of amine and carboxyl which can reduce metal ions and act as the capping agents for the nanoparticles (Mittal et al., 2013).

This study therefore aimed at synthesizing nanoparticles using keratin extracted from sheep hooves for use in removal of selected organic dyes in water. Characterization of the synthesized nanoparticles was done using UV-VIS, SEM, XRD and FT-IR techniques. Efficiency of the synthesized nanoparticles in water purification (removal of selected organic dyes) was determined by adding synthesized nanoparticles to aqueous solution containing the dye and monitoring the changes in concentration with time using UV-VIS spectroscopy under different conditions of pH, amount of adsorbent and temperature.

1.3 Statement of the Problem

There is a high demand for mutton and leather products manufactured using sheep skin in Kenya and other part of the world. For example, Segero slaughter house in Litein town, Kericho County is mainly for cows, sheep and goats. Its highest number of animals slaughtered per day is as follows; 24 sheep, 10 cows and 4 goats. The high numbers of

sheep is because they are more in this area and are sold at a price of about Ksh 4,000-5,000 while goats are sold for Ksh 7,000-9,000. Sheep hooves from these slaughterhouses and local hotels that make soup are carelessly disposed to the environment as bio waste. The waste disposed into the environment accumulates leading to increase in environmental pollution. The bio waste takes the space which should be used for other purposes such as farming or construction of houses. In addition the huge quantities of bio waste accumulating in landfill may cause leaching of the soil when it rots, hence altering the soil pH. Scattered hooves in rural areas and small towns may cause accidents if their sharp edges are accidentally stepped on. In addition the keratinous waste cause a foul smell when it degrades resulting in discomfort at the surrounding (Bhat et al., 2021). Pathogens resulting from rotten waste affect human health and cause diseases especially during rainy season since they contain fungi and bacteria which act as degrading agents on the bio waste. The rotting biomasses are in turn washed into rivers or other water bodies increasing water pollution. This makes improper disposal of the biomass to be a health hazard. Some slaughterhouses are known to burn the wastes, while this may be a short term solution, burning of the bio wastes releases toxic sulphur (IV) oxide fumes due to presence of sulphur in the hooves. This also leads to the loss of a potential source of revenue, since the bio waste which could be collected and sold for use in industries which require keratin are destroyed by burning. Using keratin bio waste in industrial processes will reduce environmental pollution due to accumulation of bio waste in environment. This protein can be extracted and used in the fusion of nanoparticles for various industrial applications (Bhat et al., 2021).

On the other hand, a large amount of dyes are used for coloring in industries, mainly the textile industries. These industries in turn release their effluents containing dyes to rivers and other parts of the ecosystem, this is another concern due to their high toxicity, high persistence and the possibility of these dyes can bio-accumulate in an organism (Shanker et al., 2017). When the effluents containing dyes get to water bodies, it becomes a health hazard to the people using the water. Purification of water has been done using several chemical and physical techniques however these techniques are limited by factors such as high operational cost, noxious muck production which require surplus treatment and low confiscation efficacy at low concentration (Adeola and Forbes, 2021). Therefore there is need for efficient, fast and cheap methods of removing the dyes in order to maintain a healthy population that can access clean water and are exposed to a clean environment. This project is aimed at synthesis of nanoparticles using keratin extracted from sheep hooves for industrial use in removal of organic dyes in water.

1.4 Objectives of the Study

1.4.1 General Objective

To synthesize and characterize nanoparticles using keratin extracted from sheep's hooves, characterize and evaluate their ability to remove organic dyes (methylene blue and crystal violet dyes).

1.4.2 Specific Objectives

i. To optimize factors affecting chemical hydrolysis and extraction of keratin from sheep hooves.

ii. To synthesize silver, copper, zinc oxide and magnetic iron (III) oxide nanoparticles using keratin extracted from sheep hooves.

iii. To characterize the synthesized nanoparticles using UV-VIS, FT-IR, SEM and XRD.

iv. To determine efficiency of keratin stabilized nanoparticles in removal of organic dyes (methylene blue and crystal violet dyes) in water.

1.5 Hypothesis

i. There are no optimum conditions for chemical hydrolysis and extraction of keratin from sheep hooves.

ii. Keratin extracted from sheep hooves cannot be used as reducing and capping agents in fusion of nanoparticles.

iii. The UV-VIS, FT-IR, SEM and XRD techniques might not be sufficient to characterize the synthesized nanoparticles.

iv. Keratin capped nanoparticles are not efficient in removal of organic colorants such as methylene blue and crystal violet from water.

1.6 Justification

The success of this project will guarantee a clean environment as the sheep hooves bio waste, which contributes to a higher quantity of disposed hooves will be used, preventing accumulation of waste in the environment. Keratin is a fibrous protein substance which builds up the structure of hooves and other parts of animals. It is eco-friendly, non-abrasive, decomposable, unsolvable in organic thinners and has good mechanical properties. The use of green technology to clean water will eliminate health hazards and pollutants in drinking

water. This has economic benefits since the cost of purification of water is reduced and access of clean water by the population will improve their health reducing the cost spent on treatment of diseases caused by the pollutants, while ensuring that the healthy population get to work to improve the economy. The space initially used for dumping waste can be used for other purposes such as farming, construction of houses and other economic activities this helps in the national development. Water purification using a cheaper technology has economic benefits and can be sustained, this ensures that a higher number of people can access clean water and live a healthy life.

1.7 Significance of the Study

Contaminated water contains pollutants such as heavy metals, agricultural residues from farms and synthetic dyes released from industries among other pollutants. Hooves are released from slaughter house as bio waste which accumulates in the environment filling land which can be used for development purposes in terms of agriculture and housing. Accumulated hooves discharge pathogens which can lead to diseases due to the presence of fungi and bacteria which acts as degrading agents on the biomass. Accumulated hooves provides a breeding ground for mosquitoes and hiding place for rodents, snakes and other poisonous animals which are harmful to human. Elimination of hooves will save space and reduce diseases. Using the hooves for industrial processes generate revenue which can improve the livelihood and wellbeing of the people. Synthetic colorants discharged into waste water by industries are mutagenic and cause cancer (Paşka et al., 2014). Fusion of nanoparticles using keratin as a reducing and capping agent will make the synthesis to be cheap since keratin can be obtained from bio wastes released from slaughter houses. Synthesized keratin capped nanoparticles used to eliminate synthetic dyes in industrial

waste water helps in reducing contaminants getting to water bodies. This will ensure sustainability of aquatic life and preventing diseases in humans caused by the dyes in water such as cancer, gene mutation, dermatitis and asthma among others (Lellis et al., 2019). Healthy population can go to work and improve the economy of the country. Adsorbed dyes can be recycled, cutting down the cost of buying dyes in industries and reduce the effluent from industries discharged to water. Cleaned waste water can be used for economic activities like irrigation, domestic and industrial application.

The outcomes will guide policy makers on whether there is need to design keratin bio waste collection points to prevent accumulation of the wastes in the environment and design keratin extraction points for use in industries for green synthesis of nanoparticles. The findings on efficiency of the nanoparticles in adsorption of dyes will guide the industries using dyes on suitability of keratin capped nanoparticles on treatment of effluents containing dyes before releasing into the water bodies.

1.8 Scope and Limitation of the Study

Optimization of chemical hydrolysis and extraction of keratin using NaOH was investigated on sheep hooves only. Keratin capped copper, silver, magnetic iron (III) oxide and zinc oxide nanoparticles were synthesized. Suitability of keratin in synthesis and capping of other nanoparticles was not investigated due to limited time and resources. UV-VIS and FT-IR techniques were used to characterize the synthesized nanoparticles. XRD and SEM techniques were used in analysis of synthesized copper nanoparticles only due to limited access of the equipment.

1.9 Assumptions

It was assumed that the nanoparticles remained stable during analysis and adsorption of organic dyes. It was also assumed that the room temperature remained constant and the room light intensity did not influence the adsorption of dyes using nanoparticles.

CHAPTER TWO

LITERATURE REVIEW

2.1 Introduction

This chapter gives a review of an exhaustive literature exploration related to the research in question. In other words it supports the study and the objectives, creating a research gap that needs to be filled through a scientific adoption of related theories or modifications of the existing ones. It comprises a literature pursuit on nanotechnology, water treatment technologies, water scarcity and water pollutants.

2.2 Nanotechnology

Nanotechnology refers to manipulation and controlling of matter on the nano-scale dimensions by use of scientific knowledge of various bio medical and industrial applications (Jeevanandam etal., 2018). It involves generation of useful material systems and devices by control of matter in the range between 1–100 nm and their ability to working at a molecular level, to generate larger structures with a primarily new arrangement of molecules. Nanoparticles are very minute materials with proportions that ranges from 1-100 nm. they have particles with at least one facet less than 100 nm (Khan et al., 2019). Nanoparticles have gained more attention in technological development compared to their macro sized counterparts. The unique properties of nanomaterial results from their nano-scale size and shape. Bottom-up approaches have been adopted for the synthesis of nanoparticles because in addition to the ability to regulate the magnitude and shapes of the nanomaterial, their chemical and biological properties could be controlled and turned to yield unique materials (Lukman et al., 2011). The need for clean, non-toxic methods for synthesizing nanomaterials especially those utilized for biological applications has

increased the focus on biological/biogenic fusion of nanoparticles by means of microorganisms, whole plants, plant extracts, animal products and marine algae. These methods of synthesis of nanomaterials are environmentally friendly and cost effective.

2.2.1 Nanotechnology in Medicine

Nanoparticles find its usages in biomedicine and drug conveyance systems(Aygün et al., 2020). Nano medicine investigates the possibility of application of nanotechnology in identification, curing and preclusion of various ailments (Almatroudi, 2020). In addition their nano scale size, nanoparticles offer low resistance to diffusion and can easily move into cells, small capillaries and reach targeted organs (Nanthavanan et al., 2019). It is a promising substance for drug delivery (Foglietta et al., 2018). Nanotechnology is currently applied in pain relieve and to design medical tools and to generate new processes (Malik et al., 2023). The nanotechnology helps in production of items with improved functionality using greener method at lower cost, improving drug delivery (Sim and Wong, 2021). It is effective in regulating and repairing biological systems through planned nanostructures and nano devices operating at molecular level (Haleem et al., 2023). It has helped in minimizing side effects of medicine and to raise efficiency of drug delivery through specific drug delivery (Malik et al., 2023). Nanotechnology is effective in controlling and repairing biological systems through designed nanostructures and nano devices operating at molecular levels (Haleem et al., 2023). It is applied for imaging by using magnetic iron (III) oxide in magnetic resonance imaging (Wegmann and Scharr, 2018).

2.2.2 Nanotechnology in Cleaning Environment

Nanotechnology offers a promising lasting solution to removal of persistent and emerging water contaminants (Bhati and Rai, 2017). Nanoparticles have large surface area and more active sites, which plays a vital role in partitioning water and solids (Nanthavanan et al., 2019). The nano-scale particle size enhances high adsorbent capacity and efficiency, photo catalysis and rapid removal dynamics (Ajith and Rajamani, 2021). Nanotechnology enables sensing, detection, treatment and remediation of impurities in water at low levels (Bhati and Rai, 2017). When nanotechnology is applied in treatment of water, the approaches involved include binding the nanoparticles to polymers or membranes, a granule or powder or can be used individually (Sharma and Bhattacharya, 2017). Nano filtration membranes which are cheaper than other filtration methods such as ultrafiltration and microfiltration membranes are highly effective in removal of biological impurities such as virus, bacteria and protozoa (Tlili and Alkanhal, 2019). Nano filters with membrane diameter range of 0.2 – 0.5 nm is currently applied in treatment of wastewater containing colorants. It removes the colorant molecules using molecular size and electrostatic repulsion mechanism (Al-Tohamy et al., 2022).

2.2.3 Nanotechnology in Manufacturing and Construction Industries

Nanotechnology has also been applied in industries for designing renewable energy sources, hence reducing carbon emission (Santos et al., 2014). Nano materials have been applied in nuclear technology. It has been in designing of sensors and batteries, LED, super capacitors and micro batteries. It is applied in designing of reedy films and fitting of electronic assembly for solar energy (Yildiz et al., 2019).

In cosmetic, nanoparticles such as zinc oxide and titanium oxide are used to reduce unwanted skin whitening by scattering light to give lovely skin aesthetics. UV filters have been designed using tri-biphenyl triazine (TBT), with unit extent in the range of 290-340 nm. TiO_2 aerosols with nano scale size is used as a key ingredient in white paints (Stark et al., 2015). Epoxy coating using nanoparticles is used in designing maritime components and ships. The coating prevents corrosion and bio fouling on the components due to exposure to various environmental conditions (Santos et al., 2014).

In electronics nanoparticles have been applied in printing electronic devices where they are used as conducting tracks. They are used as catalysts in some reactions, as fillers to enhance materials properties and as mediums to detect signals in micro and macroscopically vital event.

Nanoparticles such as ZrO_2, TIO_2, Fe_3O_4, and Al_2O_3 are added to concrete to increase its strength and produce lasting structures. TiO_2 coating on walls ensure cooling effects from sun radiations and ensure self-cleaning on the walls (Hu et al., 2016).

2.3 Water Treatment Technologies

Numerous chemical, microbial and physical means have been advanced for use in water purification for exclusion of water contaminants such as heavy metals, suspended solids, protozoan parasites, bacteria and organic pollutants among others (Priya et al., 2020). Chemical processes include precipitation, solvent extraction, flocculation, electrolysis and chlorination. Physical methods include filtration, distillation, sedimentation, adsorption, reverse osmosis (RO) and solar disinfection (SODIS) among others (Popescu et al., 2017). SODIS is an inexpensive, simple and effective physical method of water treatment. It

involves exposure of water to bursting sunlight for a period of at least six hours. Pathogens in water become inactive during the progression owing to the effects of UV emissions and heat (Nuño Martínez et al., 2020). UV radiations kill the microorganism by damaging their genetic components (Sharma and Bhattacharya, 2017). Limitations of SODIS include long duration of purification that is usually affected by sunlight intensity (Cowie et al., 2020). It involves low batch volume of water and at longer wavelength, bacteria will not absorb the radiation (García-Gil et al., 2021).

Reverse osmosis on the other hand is a process driven by pressure and concentration (Sharma and Bhattacharya, 2017). This process is governed by pore size and membrane characteristics. Membrane prepared using polyamide and cellulose derivatives are used (Priya et al., 2020). Pressure exerted in excess of the osmotic pressure is applied to drive solvent molecules across the membrane. This makes the solvent molecules to migrate from the solution side to the solvent side (Sharma and Bhattacharya, 2017). In reverse osmosis, membrane get clogged with time due to fouling of the membrane and the purified water is devoid of important minerals since they are eliminated during the process (Ray et al., 2020).

Adsorption involves mass transfer which can be used to accumulate gaseous molecule, liquid molecules, atoms, ions or dissolved solid at a boundary between two phases which comprises gas-solid or liquid-solid interfaces. The method is easy to operate and cheap (Priya et al., 2020). Bio sorption involves the use of biological materials such as plant material, animal material, microorganism and enzymatic reactions in degradation and detoxification of contaminants in water (Adeola and Forbes, 2021). They have a high

selectivity, efficiency and affinity for metal ions (Martella et al., 2018). They also have a high efficiency in degrading organic compounds such as polycyclic aromatic hydrocarbons (PAHs). The mechanisms involved in bio sorption can be electrostatic force, precipitation or ion exchange (Matouq et al., 2015). Bio sorption is a low cost method due to employing of cheap adsorbents, flexible and provides high pollutant removal efficiency (Cheruiyot et al., 2019).

Electro dialysis is water purification method which involves application of electric potential on membrane material. Fixed charged groups attached to the membrane attract impurities with opposite charge from aqueous solutions. The method is used to remove or separate electrolytes due to the charge on ions (Sharma and Bhattacharya, 2017). Electro dialysis is limited by fouling that influence selectivity of the membrane raising energy consumption due to precipitation of organic anions on the membrane raising resistance to electric current (Oztekin and Altin, 2016). Electro catalytic oxidation involves oxidation of impurities on anodic surface. This process is affected by pH, temperature and rate of diffusion of oxidants (Sharma and Bhattacharya, 2017). Electro catalytic oxidation of organic water pollutants is costly due to high electrical energy consumption and costly anodes which have over potential towards oxygen (Singh and Goldsmith, 2020).

2.4 Water Scarcity

Water demand has turned into a noticeable challenge to livelihood in many parts of the world. Climate change projections indicate that the problem will deteriorate in future resulting in tough competition between water used for irrigation and other sectors of the economy (Mancosu et al., 2015). A number of indicators have been in use to investigate the water scarcity status. The key elements of the indicators of water scarcity include water

availability, population and the water use (Liu et al., 2017). Water crisis has been worsened by urbanization, rapid increase in population and industrial development. A country is considered to be water stressed if per capita water obtainability is lower than 1700 m^3 per capita per year. Kenya has a few renewable sources of fresh water (lower than 1000 m^3 per capita per year), hence it is one of the water stressed countries. The United Nations Sustainable Development Goal (SDG) number six (6) has put in place several objectives to ensure water sustainability by 2030. The SDG 6 aims at increasing access to clean water, sanitation, efficient use and sustainable withdrawals of water, lowering water pollution, implementation of incorporated water resource supervision and shielding water related ecosystem (Lele, 2017); (Ho et al., 2020).

Diverse methods are used in alleviating and controlling water sources. The initiatives include policies that ensure reduction of water pollution, protection of water sources, reduction of surface water runoff through catchment re-establishment, water conveyance and storing technologies, conservation, recycling and reuse of water. These will increase access to sanitation and clean water it will also ensure that the Kenyan population which has been constantly increasing can attain good health, food security and education which is not taken seriously in places where people travel for long distances in search of water or food (Mulwa et al., 2021).

2.5 Water Pollutants

Water pollutants are released to the water bodies as an end result of human undertakings such as industrialization, urbanisation and agricultural practices. The pollutants are produced from point sources of which these are pollutants whose sources can be identified effluents from an industry while non-point sources which pollutants arriving from different

sources are run off from urban waste. Water pollutants are classified into inorganic and organic. Inorganic pollutants are found in agricultural runoff, heavy metals in industrial effluents, silt found in surface and fertilizers. Some organic pollutants include organohalides, herbicides, colorants and insecticides. Urbanisation has increased industrial discharges and run off from industrial area polluting urban streams (Singh and Gupta, 2016).

Industrial waste causes water pollution since most of industrial plants are located near rivers such as paper and steel industries due to the large amount of water during the industrial process. Waste from industries which contain dyes, acids and alkalis among other chemicals are disposed into water bodies as effluents. Acids and alkalis alters the water pH affecting aquatic life (Singh and Gupta, 2016).

Presence of azo dyes in water affects transparency due to colouration. The dyes are mutagenic and cause cancer. These dyes causes water pollution affecting aquatic life and human health (Paşka et al., 2014).

Steel plant on the other side release cyanide while fertilizer industries produce a large amount of ammonia. Agricultural chemical waste such as pesticides, herbicides and fertilizer discharged from crop fields may find its way to rivers through surface run off and spraying. These chemical wastes are reported to contribute to soil and water pollution since most of them are persistent in environment or are non-biodegradable. Antibiotics used for feed efficiency improvement in agriculture, treating and preventing human and animal diseases and promoting growth. Antibiotic wastes are released into domestic sewage, the industrial waste water by the manufacturers and hospital waste, which are released into

sewage treatment plant. Due to incomplete removal by engineered treatment methods, antibiotics released may find its way to water bodies. Presence of antibiotics such as trimethoprim, clarithromycin, ofloxacin, roxithromycin and erythromycin in rivers has been reported. Uptake of the antibiotic pollutants may cause antibiotic resistance. In rivers, the antibiotics alters microbial communities, cause evolution and extent antibiotic resistance genes, threatening human life (Kuang et al., 2020).

Other pollutants include oil spillage discharged from petrol tankers and oil exploration offshore. Thermal pollution caused by industrial boilers, electric power plant, steel smelting and petrol refineries reduces oxygen dissolved and affect aquatic reproduction. Pollution from acid rains alters pH levels harming aquatic plants. Radioactive pollution results from presence of radioactive waste in water. In large amounts, the radioactive waste causes gene mutation or damage organisms (Singh and Gupta, 2016).

Heavy metals are pollutants which get to the environment through industrial wastes and agricultural inputs such as pesticides and fertilizers. The heavy metals present in these pollutant sources are carried to underground and surface water as a result of diffusion and leakage (Yardimci, 2021). Water overflow from heavily trafficked and paved areas like roads and parking lots found in urban areas and industries is considered as a main non-point source of organic and heavy metal contaminants to environment (Yardimci, 2021).

2.6 Chemistry and Functions of Keratin in nanoparticles synthesis

Keratin are fibrous, mechanically strong biomolecules found in vertebrates such as birds, reptiles and mammals (Sharma and Gupta, 2016). They are produced in the cytoplasm

making up to 90 % - 95 % of the epidermal cells. The cells undertake keratinization to maturity and drift from basal layer towards the skin exterior (Guarino et al., 2018). Keratin is insoluble, biocompatible and decomposable biological material. It has filament forming protein molecules founding the greater part of epidermal appendages such as claws, hair, turtle scutes, beaks, feathers, nails, skin, horns, scales, birds, reptiles, connecting tissues and quills (Pan et al., 2016); (DeFrates et al., 2018); (Wang et al., 2016). Keratins are rich in cysteine and are interconnected by intermediate filaments (Sharma and Gupta, 2016). Due to high cysteine content, keratin molecules have a high sulphur content (Ramirez et al., 2022). The cysteine residues form disulphide bonds which makes the biomolecules to be insoluble in water, have enhanced mechanical and thermal properties (Guarino et al., 2018).

Keratin exists in three different form: α-, β-, and γ-keratin. The most prevalent types are α- and β- keratins. The α-keratin has a structure which is a left-handed alpha-helix that is coiled with other keratin molecules to form a polymerized complex. The α-keratin has intermediate filaments which are involved in the cytoskeleton and they are mainly located in soft tissues. β- keratin are located in hard tissues, such as scales and nails. They also have intermediate filaments. γ-keratin is a form of keratin which is not involved in the cytoskeleton structural elements (DeFrates et al., 2018).

Keratins are moreover classified based on levels of sulphur as hard or soft. Soft keratins have low cysteine content, weak cross linking and small resistance to other chemicals in the outer epidermis layer. The presence of peptide, disulfide, carboxylic and amino groups makes it reactive under certain conditions (Sharma and Gupta, 2016). It undergoes reduction reactions to form disulphide links which are fragmented into thiols (-SH) group

(Donato and Mija, 2019). The amino (-NH_2) groups are protonated to form positive charge on the biomolecules (Sharma and Gupta, 2016). Keratin has a distinctive order of amino acid such as “Arg-Gly-Asp” and“Leu- Gly-Val” that can bind to receptors over expressed by numerous cancer cells (Ferroni and Varchi, 2021).

2.7 Dyes

Colorants are chromogenic organic aromatic compounds which absorb visible light and impart color of the visible expanse (Khan et al., 2022). Colorings are ordered into various sorts according to their molecular structure, origin and application (Al-Tohamy et al., 2022). Natural colors are extracted from plants while synthetic dyes are designed by humans. Use of synthetic dyes is common practice since they are inexpensive, can be easily prepared and the raw materials are easily available. Auxochrome radicles which come from OH, COOH, SO_3H or NH give colorant salts and are either basic or acidic. Coloring power of a compound is due to auxochromes and chromophoric groups which have structures joined by azo (- N= N-) groups that may appear repeatedly (Osagie et al., 2021). Amongst all the known dyes being sold are azo dyes are commonly used. Other groups of dyes include anthraquinone, phthalocyanine, aryl-carboniums and polymethine (Shanker et al., 2017).

The levels of oxygen dissolved in water reduce due to dye molecules which prevent sunlight into the water system. The contamination also increases biological oxygen demand. Azo dyes synthesized from aromatic amines are carcinogens and explosive. They also have a common carcinogen, the benzidine $(C_6H_4NH_2)_2$ (**1**) which should be treated efficiently before aryl-carboniums are released to the environment.

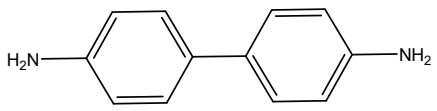

1

Dyes are removed by employing biological methods which involves biodegradation, physical methods such as coagulation-flocculation, adsorption, oxidation, catalytic degradation, membrane filtration, or chemical methods such as chemical precipitation and ion exchange method. Adsorption is considered to be an inexpensive and effective method of dye removal and is the most efficient. Adsorbents such as chitosan, activated carbon and natural waste are frequently engaged (Shanker et al., 2017). Some of the organic dyes include congo red, methylene blue and crystal violet among others.

2.7.1 Congo Red

This is an anionic dye with a chemical formula of $C_{32}H_{22}N_6Na_2O_6S_2$ (**2**) and a molecular weight of 696.66 g/mol (Paşka et al., 2014). It is a non-biodegradable commonly used in leather, plastic, printing, textile and paper industries.

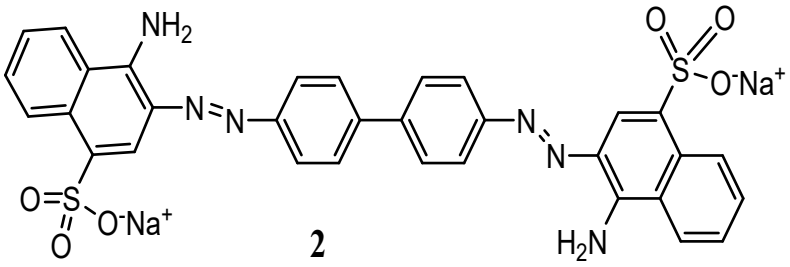

2

It can also be used as a pH indicator, detection of free HCl in gastric substances, in histological stain and in the diagnosis of amyloidosis (Shanker et al., 2017).

2.7.2 Methylene Blue

Methylene blue is a primary thiazine cationic dye, which is dark green powder which dissolves in water to form a blue solution. Its molecular weight is 319.85 g/ mol and molecular formula is $C_{16}H_{18}N_3ClS$ (**3**) (Khan et al., 2022).

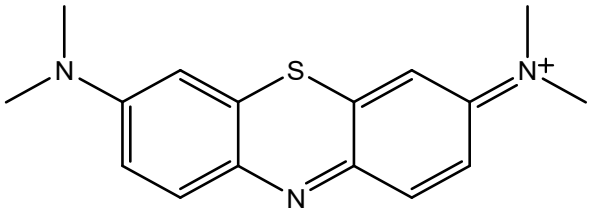

3

2.7.3 Crystal Violet

Crystal violet is a cationic synthetic dye with a molecular formula of $C_{25}H_{30}ClN_3$ (**4**) and a molecular weight 408.0 g/ mol (Rashad et al., 2019). It has been used extensively for histological staining, detergents, paper printing, as antiseptic for example in athletes foot, as anti-freezers, leather and fertilizers the dye is also used in textile industries (Abdi etal., 2020). Industrial effluents released to environment create a major concern when it gets to water bodies due to its noxious effect on aquatic plants and animals (Abdi et al., 2020). The dye is toxic to humans as it is attracted to negatively charged cell membrane where its molecules get into the cell where it concentrate in the cytoplasm. This may cause cancer. The dye is mitotic poison and it is mutagenic (Rashad et al.,2019).

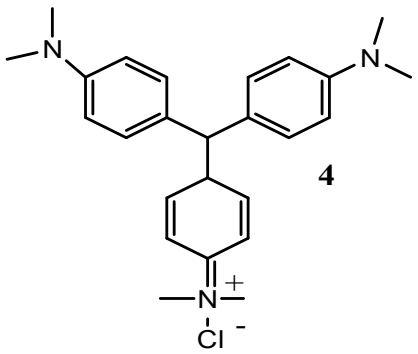

4

2.8 Environmental Dye Pollution

A large quantities of dyes of different types are unconfined into the environs from industries such as the textile, cosmetic, plastic, paper, rubber, leather and food industries, where they are used as the coloring agents (Oloo et al., 2020). The harmful and carcinogenic colorants contaminate water sources, making it unhealthy for human consumption and unsafe for aquatic plants and animals (Khanet al., 2022). Dye contaminants in water absorb sunlight and prevent photosynthesis of aquatic plants and inhibit growth of microorganism. Harmful prolonged effects of dyes on microorganisms are determined by exposure time and colorant concentration (Mohammad and Atassi, 2020).

Due to the fast growing industrialization, effluents which contain dyes, phenols, pesticides and other tenacious organic contaminants are increasing at a high rate, exposing living organisms to danger because they are toxic and harmful. In some cases, their metabolites are more toxic than the parent compound (Shanker et al., 2017).

2.9 Adsorption of Dyes

Adsorption is a low-cost swift and effective technique used in colorant removal from water (Ray et al., 2020). It is chiefly used due to its simplicity in process scheme, outstanding adsorbent restorability and outstanding parting progression (Zhang et al., 2020). Adsorption is categorized into two types: chemisorption and physisorption. The basis of classification is built on how colorant molecules are attached to the adsorbent exterior (Al-Tohamy et al., 2022). In physisorption feeble van der Waals forces, hydrogen bonding and dipole-dipole connections at the interface are involved. It is a non-selective and reversible process. Chemisorption arises by means of strong links such as covalent or ionic bonding. The progression is discriminating and irrevocable (Li et al., 2022). Enthalpy change in physisorption is lower than 40 kJ/mol, while enthalpy change in chemisorption is much higher (Chakraborty et al., 2020). In adsorption, adsorbent ingredients with a permeable edifice which upsurges surface area for effective and rapid process are used (Al-Tohamy et al., 2022).

Several exploration on colorant adsorption by means of activated carbon derived from biomass have been reported. Biomass is varied, profuse and maintainable, this makes the use of carbon to be cost-effective, but pore dimensions of activated carbon is far-off from ideal henceforth larger quantity of adsorbent is employed (Li et al., 2022).

2.10 Adsorption Isotherms

Adsorption isotherm refers to a curve used to describe a phenomenon which governs the retention (or the release) or motion of a substance from aqueous environment into a solid phase under a constant pH and temperature conditions (Wanyonyi et al., 2014). Some of

the isotherms commonly used include: Langmuir isotherm, Freundlich and Temkin isotherms. The curves are beneficial in membrane optimization (Mohammad and Atassi, 2020).

Langmuir isotherm assumes that the adsorbed molecules form a monolayer. The model presented in equation (2.1).

$$q_e = \frac{q_{ax} b_o c_e}{1 + b_o c_e} \quad \text{..... (2.1)}$$

q_{ax} represent the maximum adsorption capacity in mg of dye/g of keratin capped nanoparticles.

C_e is the equilibrium concentration of the dye being investigated in mg/L.

b_o is the Langmuir isotherm constant in L/mg, which is related to affinity of binding sites.

q_e represents the amount of dye adsorbed by the adsorbent at equilibrium in mg/ g.

In linear form, the Langmuir isotherm is described as follows

$$\frac{c_e}{q_e} = \frac{1}{b_o q_{ax}} + \frac{1}{q_{ax}} c_e \quad \text{..... (2.2)}$$

q_{ax} and b_o are obtained from the slope and intercept of a graph of $\frac{c_e}{q_e}$ (y- axis) against C_e (x axis) (Matouq et al., 2015).

Freundlich isotherm model is used to determine the relationship between reversible and non-ideal adsorption. The model suggests that the energy of sorption process decreases exponentially upon completion of sorption centers on the adsorbent. Freundlich isotherm adopts a multilayer non ideal sorption which takes place on a heterogeneous surface (Wanyonyi et al., 2014). The Freundlich isotherm is presented in equation 2.3 below.

$$q_e = K_f C_e^{\frac{1}{n}} \quad \text{(2.3)}$$

K_f is the Freundlich constant which is related to the energy of bonding in $(mg/g)(L/g)^{1/n}$.

n is the heterogeneity factor.

Freundlich equilibrium constant can be obtained from a graph of ln qe against ln C_e by using the following equation:

$$\log q_e = \log K_f + \frac{1}{n} \log Ce \quad \text{(2.4)}$$

The slope which represents $\frac{1}{n}$ is a value between 0 and 1 and it is used to measure the heterogeneity or intensity of adsorption (Matouq et al., 2015). K_f and n are calculated from the y intercept and the slope of the graph respectively. When n is greater than 1, it means that the adsorption conditions are favorable (Wanyonyi et al., 2014).

Tempkin model considers the adsorbate and the impurity to interact resulting in a chemical adsorption procedure (Zhang et al., 2020). Tempkin isotherm is presented in equation 2.5 and 2.6.

$$q_e = \frac{RT}{b} \ln A + \frac{RT}{b} \ln C_e \quad \text{(2.5)}$$

$$B = \frac{RT}{b} \quad \text{(2.6)}$$

A (L/g) represents the binding constant for the model at equilibrium.

b (mg/L) is the isotherm constant for Tempkin model

B relates to enthalpy of adsorption in J/ mol.

Gas constant R= 8.314 J/mol K.

2.11 Adsorption Kinetics

Kinetics of adsorption are used in the study of the rates of reaction between adsorbates and adsorbent and conditions which affect the reaction rates (Zhang et al., 2020). Kinetic modelling is applied to investigate mechanism of adsorption and the probable rate shaping steps. Pseudo first (Lagergren model) and second order kinetics were applied to analyse the sorption kinetics of the organic dyes by keratin capped nanoparticles. The pseudo first order kinetic model considers adsorption rate to be proportional to concentration of the dye molecules in the aqueous medium and assume that the process is governed by steps in particles diffusion process (Zhang et al., 2020). The integral Pseudo first order kinetic model equation is expressed in equation (2.7)

$$\log (q_e - q_t) = \log q_e - \frac{tk_1}{2.303} \quad \text{.....(2.7)}$$

From the equation;

k_1 represents the rate constant for adsorption in the pseudo first order model equation.

q_e represents the quantity of the dye adsorbed by the metal nanoparticles at equilibrium

q_t is the quantity of the dye adsorbed by the metal nanoparticles at time t.

By plotting a graph of graph of log $(q_e - q_t)$ against t, k_1 and q_e calculated can be obtained from the slope and log $(q_e - q_t)$ intercept respectively. Pseudo second order model undertakes that the rate of adsorption of impurities is proportionate to the number

of vacant sites on the surface of the adsorbent and the reaction rate is reliant on the quantity of adsorbate on the surface of the adsorbent (Kajjumba et al., 2019). When experimental results fit Pseudo second order kinetics, it indicates that the reaction is controlled by chemical processes which involve charge transfer or sharing between the adsorbent and adsorbate (Cheruiyot et al., 2019). Pseudo second order kinetic model equation is expressed in equation (2.8).

$$\frac{dq_e}{d_t} = k_2(q_e - q_t)^2 \quad \text{(2.8)}$$

The conditions of q_e and t = 0 at the beginning of the adsorption process. The integration of the equation 2.8 leads to the following equation

$$\frac{t}{q_t} = \frac{1}{K_2 q_e^2} + \frac{t}{q_e} \quad \text{(2.9)}$$

K_2 represents a rate constant for pseudo second order adsorption ($mg^{-1}min^{-1}$).

q_t represents the amount of dye adsorbed by nanoparticles in mg/g at time t

q_e is the amount of dye adsorbed by nanoparticles in mg/g at equilibrium.

By plotting a graph of $\frac{t}{q_t}$ against time t, q_e and K_2 can be obtained from the slope and y-intercept of the graph (Wanyonyi et al., 2014).

2.12 Thermodynamics Studies

Study of thermodynamic behavior is used to describe the type and nature of adsorption. The variables which include Gibbs free energy change ΔG° (kJ/mol) (equation 2.10),

enthalpy change (ΔH°) (kJ/mol) (equation 2.12) and enthropy change ΔS° (J/kg/mol) (equation 2.14) are presented in the following equations (Cheruiyot et al., 2019).

$$\Delta G° = -RT\ln K \quad (2.10)$$

$$K = \frac{C_{Solid}}{C_{Solution}} \quad (2.11)$$

$$-RT\ln K = \Delta H° - T\,\Delta G° \quad (2.12)$$

$$\ln K = -\frac{\Delta H°}{RT} + \frac{\Delta S°}{R} \quad (2.13)$$

$$\Delta G° = \Delta H° - T\Delta S° \quad (2.14)$$

K is the distribution coefficient for adsorption. It is the ratio of colorant concentration on solid phase to the concentration of the dye in aqueous solution at equilibrium.

T is the absolute temperature used to carry out the investigation. R represents the gas constant (8.314 J/K/mol) (Zhang et al., 2020).

ΔG° (negative) indicates a spontaneous and favorable process. The ΔH° is positive when adsorption process is endothermic and negative when adsorption process is exothermic (Piri et al., 2019). ΔH° is lower than 20 kJ for physisorption and higher for chemisorption process (Cheruiyot et al., 2019). ΔS° specifies the randomness of the solution/solid interface (Zhang et al., 2020).

2.13 Synthesis of Nanoparticles

Diverse approaches have been used to synthesize nanoparticles; these approaches have been classified into two main groups. These groups are: Top-down and bottom-up methods (Figure 2.1). Top-down method involves starting with larger materials which are broken down into nanomaterial by using physical, chemical or biological reactions. The top-down methods are physical vaporization, lithography, laser ablation, photo irradiation, spray pyrolysis and ultra-sonication (Keat, 2015). The second approach is known as bottom-up method (also known as building up approach), in which synthesis of nanoparticles is performed from simpler substances such as the constituents of molecular or atomic sizes using various physical, chemical or biological reaction. The bottom up methods are green or bio synthesis using fungus, plants, bacteria, virus or algae, sol gel, bio chemical synthesis, reverse micelles, co-precipitation, photochemical reduction, electrochemistry and spinning (Khan et al., 2019). In bottom-up method sizes of the nanoparticles can be controlled. In physical methods, nanoparticles are formed through evaporation condensation using a tube furnace. The methods are fast and the processes involved don't require harmful chemicals; however, there is high energy consumption and small amount of nanoparticles is formed. Chemical processes employ water or organic solvents. This method requires a metal precursor, reducing agents and stabilizers for synthesis of metal nanoparticles. Advantages of this method include: ease of production, cost involved is low and the nanoparticles are formed in large quantities (Ying et al., 2022). In this study bottom up approach was employed in synthesis of nanoparticles using keratin extracted from sheep hooves as a reducing and capping agent for the nanoparticles.

Figure 2.1: Steps followed during synthesis of nanoparticles (a) Bottom up method (b) Top down method

2.14 Synthesis of Metal Nanoparticles

Mode of metal nanoparticles fusion is essential due to the impact of various experimental techniques on physicochemical, morphology and stability of the nanoparticles. The experimental technique used influences interaction kinetics of the ions with electron donor and the adsorption procedure of the stabilizing agent (Jamkhande et al., 2019). Synthesis and stabilization of metal nanoparticles involves the use of various chemical, physical and biological methods (Thakkar et al., 2010). Chemical approaches engaged include electrochemical, photochemical and chemical reduction among others (Jamkhande et al., 2019). Some of the physical methods employed are mechanical methods using ball mill, pyrolysis, vapor deposition and aerosol processes (Mittal et al., 2013). In biological procedures bacteria, fungi, actinomycetes, viruses, yeast and plant extracts are employed in synthesis and capping of nanoparticles (Mittal et al., 2013). Bacteria have exterior membrane protein which provide amino acid moieties which act as nucleation sites for the metal nanoparticles. Use of microorganisms is inexpensive, environmentally safe and maintainable but culturing is time consuming, production rate is slow and nanoparticles obtained are amassed (Narayanan and Sakthivel, 2010). Plant extract contain bio molecules such as flavonoids, proteins amino acids and polysaccharides which are in charge of metal ion reduction (Mittal et al., 2013).

2.15 Keratin Derived Nanoparticles

Capping agents based on biopolymers have received more attention due to their stability bio mimicry and biocompatibility (Annesi et al., 2021). Proteins have been applied in synthesis of due to strong affinity of metals to –SH, -COOH and $–NH_2$ groups which are found in keratin (Lü and Cui, 2010). Biomolecules which contain NH_2, COO, C-N and C=O have been used in synthesis of nanoparticles such as selenium, copper, silver, gold, zinc oxide and others. Presence of amine and carbonyl groups in keratin makes it suitable for use in synthesis of nanoparticles. These act as reducing agents by supplying electrons to reduce the metal ions (Husen and Siddiqi, 2014). Electron transfer occurs from carboxylic group to metal ions under certain conditions (Jiang et al., 2019). Amine group has a lone pair of electrons which can easily be donated to metal ions (Mbewana-Ntshanka et al., 2020). High surface energy causes agglomeration of the nanoparticles. The groups such as NH_2, COO^-, C-N and C=O acts as stabilizers and capping agents which hold keratin biomolecules to AgNps, lowering surface energy by coating the nanoparticles producing steric, electrostatic and electro steric interaction stabilizing nanoparticles (Restrepo and Villa, 2021); (Husen and Siddiqi, 2014).

Keratin proteins have gained attention due to the renewability of the sources and its biocompatibility. The sequence of the monomers in keratin is similar to the sequence found in extracellular matrix (ECM), hence appropriate for generating materials that can be accepted in human bodies, improve cellular propagation, migration and attachment. It has been used in fusing nanoparticles employed in technological and biomedical sectors (Annesi et al., 2021). Keratin is a most common protein which is rich in cysteine HOOCCH (NH_2) CH_2SH,which is biocompatible and is harmless to cells (Foglietta et al.,

2018). The high concentration of cysteine (**5**) protein makes it to be unique as compared to other forms of protein since it is tough and durable. This toughness and durability makes keratin have diverse protective functions for vertebrates which makes them to adapt to the external environment as it provides mechanical support (Wang et al., 2016).

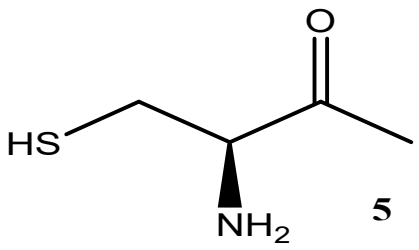

5

Synthesis of nanoparticles using keratin as a capping agent has been reported in some studies. Annesi et al synthesized gold nanoparticles in two steps involving reduction of the metal ions using sodium citrate followed by adding keratin solution extracted from wool to bind the AuNps (Annesi et al., 2021). Lü and Cui synthesized AgNps by using $NaBH_4$ reducing agent and wool keratin solution as stabilizing agent for AgNps (Lü and Cui, 2010).

In this study keratin extracted from sheep hooves was used as a reducing and stabilizing agent in synthesis of metal nanoparticles and as a capping agent in synthesis of metal oxide nanoparticles.

2.16 Extraction of Keratin

Keratin can be extracted using thermal hydrolysis by using superheated water and steam flash explosion use of ionic liquids, steam explosion, chemical or biological methods

(Chilakamarry et al., 2021); (Tasaki, 2020). Biological methods involve the use of plants and microorganisms in synthesis of nanoparticles. This method is a green synthesis technology. It is considered to be environmentally friendly, cost effective and biologically safe (Ying et al., 2022). Chemical methods involve reductive, sulfitolysis, oxidative, use of ionic liquids, enzyme hydrolysis and chemical hydrolysis using strong alkalis and acids hydrolysis (Chilakamarry et al., 2021). Use of chemicals such as sulfides, sulfanylbutane-2, 3-diol, peroxides and thiols (SH) with breaking of disulfide bonds to produce keratin. These chemical methods have some disadvantages, for instance some of the chemicals such as 2-sulfanylethanol and 2-sulfanyl acetic acid are harmful hence cannot be handled easily. Moreover, the molecular weight of keratin extracted by using sulfites or peroxides is low. The use of ionic liquids and enzyme hydrolysis to extract keratin has received greater attention. However, use of enzymes for industrial application is slowed down by the long production cycle of enzymes. L-Cysteine with the chemical formula HOOCCH (NH_2) CH_2SH, is α- amino acid. Thiols of L- cysteine, (SH) group take part in redox reactions, in which it gets oxidized to protein disulfides. L-Cysteine can be used in place of 2-Sulfanylethanol since it can give a good yield of undamaged keratin. L-Cysteine can be oxidized or may form disulfide bridge R-S-S-$CH_2CH(NH_2)COO^-$. The disulfide link is broken in keratin as shown below:

$$\text{R-S-S-R} + \text{2-SCH}_2\text{CH(NH}_2\text{)COO}^- \longleftrightarrow 2\text{RS}^- + {}^-\text{OOC(NH}_2\text{)CHCH}_2\text{S-SCH}_2\text{CH(NH}_2\text{)COO}^-$$

Keratin (2.15)

2.17 Metal Nanoparticles as Photo Catalyst.

Photo catalysis involves speeding up a photoreaction by using a catalyst (Santos et al., 2014). Catalysts such as TiO_2 are used to hasten photoreactions. TiO_2 semiconductor photo catalyst is used in treating waste water since it is cheap and has a low toxicity. Photo catalysis is brought about by absorption of ultra violet radiations by nanoparticles (Santos et al., 2014). Absorption of light radiations by nanoparticles give them a characteristic property which gives the nanoparticles a specific colour. This property is applied in surface enhanced Raman spectroscopy. This property is applied in water splitting, photochemical application and in medical therapy. Metal induced photo catalysis (MIP) has been used in synthesis of light responsive composite materials (Liu et al., 2017).

When light is incident on nanoparticles, some proportion is scattered, while some proportion is absorbed. The ratio of light scattered to light absorbed varies with change in particle size. A larger proportion is scattered by larger particles, while smaller particles absorb a larger proportion. Absorption of light has received more attention in photo catalysis (Liu et al., 2017). Photo catalysis has been used to break down poly aromatic hydrocarbons such as pyrene and phenanthrene by using ultra violet irradiation on titanium oxide catalyst (Adeola and Forbes, 2021).

It has been reported that heterogeneous photocatalysis has a high efficiency in breaking down coloured substances. It can break down organic contaminants into products such as water and carbon (IV) oxide which is harmless. Irradiation of the nanoparticles results in formation of electron-hole pairs on the catalyst. The charge carriers produced react with hydroxyl, water and oxygen molecules to produce hydroxyl radicals and superoxide radical anions radicals (Santos et al., 2014). The two models of excitation related to MIP are

interband transition and Localised Surface Plasmon Resonance (LSPR). In LSPR, light interacting with particles which are smaller than the wavelength of the incident radiation, produces a plasmon oscillating around a nanoparticle. Inter band transition occurs due to transitions between *d*-band of the nanoparticles and the conduction band (Liu et al., 2017). The population decay in LSPR occurs through non-radioactive decay into electron-hole excitation and through change of plasmon into photons. Absorption of light by transitional metals induces water splitting, degradation of dyes, removal of organic dyes, CO_2 photo reduction and synthesis of fine chemicals among others. Roles played by these metals are photosensitization of semiconductors and activity enhancement. In solar harvesting, semiconductors integrated with plasmonic metal nanoparticles have been used to form a composite with improved ability to harvest solar light (Liu et al., 2017).

2.18 Characterization of Nanoparticles and Sample Analysis

Characterization of nanoparticles is carried out to determine formation of nanoparticles and to characterize the nanoparticles to find out properties such as the shape, size and surface morphology. Some of the characterization techniques used to characterize nanoparticles include: Fourier transform infrared spectroscopy used to determine functional groups present in the nanoparticles, this helps in determining the involvement of molecules in formation and capping of the nanoparticles (Ezealisiji et al., 2019), X-ray diffraction (XRD) analysis is used to give the structural characteristics of nanoparticles (Puneetha et al., 2021). Scanning electron microscopy (SEM) is used to determine surface morphology of the nanoparticles, while transmission electron microscopy (TEM) analysis is done to investigate the internal fine structure of the nanoparticles (Patra and Baek, 2014). Thermo gravimetric analysis (TGA) is used to determine the thermal properties of the nanoparticles

(Guo et al., 2021) and UV-VIS method of analysis is used to determine the optical properties of nanoparticles (Muhammad et al., 2019).

2.18.1 Fourier Transform Infrared Spectroscopy (FTIR)

Fourier transform infrared spectroscopy (FTIR) is used to analyze organic and inorganic compounds. This method is based on the measurement of the absorption of electromagnetic radiation with wavelengths that fall within the mid-infrared region (4000-400 cm^{-1}) (Mourdikoudis et al., 2018).When electromagnetic radiations are directed into a substance placed in the path of IR radiations, the radiations can be transmitted, absorbed, scattered or have photoluminescence (PL). This gives important information on the energy level transition of the substance and also the molecular structure. The sample absorbs and transmit light, which passes to a detector which measures intensity of radiations entering the sample and the intensity of the radiations transmitted (Mourdikoudis et al., 2018).

In FTIR, interferometer is used to generate an infrared spectrum. The intensity of transmitted signal is used to generate an IR fingerprint (Raja and Barron, 2020). The output of the spectrometer as a function of time is changed into a plot of absorption against wave number by a computer using a Fourier transform method. When a molecule absorbs infra-red radiation, the dipole moment is somehow adjusted and the molecule becomes Infrared active (Mourdikoudis et al., 2018). IR radiations do not have sufficient energy to cause electron transitions but makes the bonds in molecules to undergo stretching or bending vibration (Khan et al., 2018) A recorded spectrum gives the position of bands associated to the nature and strength of bonds, and also exact functional groups, providing the information concerning molecular structures and interactions (Mourdikoudis et al., 2018).

2.18.2 Ultraviolet-Visible Light Spectroscopy

Ultraviolet-Visible light spectroscopy (UV-VIS) is a moderately simplistic and low-cost method of characterization that is often used in analysis of nanoscale materials (Mourdikoudisetal., 2018). UV region occurs in the wavelength range between 200 nm-400 nm, visible light is has a lower energy and occurs in the wavelength range between 400 nm- 800 nm (Abdolkarimi-Mahabadi et al., 2021).

When an organic molecule containing a double bond or hetero atoms is irradiated with UV-VIS light, they absorb the radiations resulting in electronic transition from ground state to excited states. The ground state orbitals are π- (bonding) molecular orbital, σ- bonding molecular orbital and n- (non-bonding) atomic orbital. The anti-bonding orbitals include π^* and σ* orbitals. The electron transitions which occurs when a sample absorbs UV-VIS rays are π-π^*, n-π^*, n-σ* and σ-σ*(Abdolkarimi-Mahabadi et al., 2021). When returning to ground state, radiative processes (fluorescence or phosphorescence) occurs. The electronic transitions which occurs when a sample absorbs UV-VIS radiations are UV-VIS analysis is used to determine the presence of the analyte in the sample by identifying the wavelength at which maximum absorption of the radiation occurs and to determine the concentration of the analyte by measuring the absorbance of the sample and using a standard curve to determine the concentration corresponding to the measured absorbance (Antosiewicz and Shugar, 2016).

Nanoparticles (NPs) have optical properties which are sensitive to shape, agglomeration state, size, concentration and refractive index near the nanoparticle surface, which makes UV-Vis spectroscopy a significant tool used to identify, characterize and to study

nanomaterial and in evaluating the stability of nanoparticles colloidal solutions (Mourdikoudiset al., 2018).

2.18.3 X-Ray Diffraction (XRD)

X-ray diffraction (XRD) is based on constructive interference of monochromatic X-rays and the crystalline sample. X-ray diffraction (XRD) is a nondestructive powerful method of analysis for describing crystalline materials. It delivers information on structures, phases, preferred crystal orientations and other structural parameters like grain size, average crystallinity, crystal defects and strain. XRD peaks are formed as a result of constructive interference of a monochromatic beam of X-rays which is scattered at precise angles from each set of lattice planes in a sample. These X-rays are generated by a cathode ray tube, when fast moving electrons hit a target, and some of its kinetic energy is converted to X-rays, filtered to obtain a monochromatic radiation, collimated to focus, and directed to the sample (Bunaciu et al., 2015).

The interaction of the monochromatic incident X-rays with the sample results in constructive interference (and a diffracted ray) when the conditions satisfy Bragg's law, presented in equation (2.16).

$$(n\lambda = 2d \sin \Theta) \ldots \ldots (2.16)$$

Where n is an integer, λ is the wavelength of the incident X-rays, d is the spacing between the planes of the material investigated generating the diffraction and Θ is the angle of diffraction of the rays. The diffracted monochromatic X-rays are then detected, processed, and counted. When a sample is scanned through a range of 2Θ angles, all the possible

diffraction directions of the sample lattice can be attained because of the random orientation of the particles in a powdered material. Arrangement of particles in a material can vary from random to extremely ordered (Raja and Barron, 2020).

Changing of the diffraction peaks into *d*-spacings is used to identify the compound since each compound has a set of *d*-spacings which are unique. This is achieved by comparison of *d*-spacings of the sample material with a standard reference patterns. An X-ray diffractometer is made up of three basic elements: an X-ray tube, where X-rays are generated, a sample holder, and an X-ray detector. X-rays are produced in a cathode ray tube through thermionic emission, in which a heating current passing through a filament heats the cathode to eject electrons, accelerated toward a target by applying an accelerating voltage to the electron beam, and bombarding the target material with electrons. When electrons have sufficient energy to remove inner shell electrons of the atoms in the target material, characteristic X-ray spectra are produced (Bunaciu et al., 2015).

The spectra obtained is made up of numerous components, with the most common being the Kα and Kβ. Kα contains in portion, $K\alpha_1$ and $K\alpha_2$. $K\alpha_1$ has a slightly shorter wavelength and is twice the intensity of $K\alpha_2$. The specific wavelengths are determined by the element used in the target material (Cu, Fe, Mo, and Cr). Filtering, by using monochromators or foils, is essential to yield monochromatic X-rays required for diffraction (Bunaciu et al., 2015).

2.18.4 Electron Microscopy

Electron microscopy has been an innovative imaging technology used by engineers and scientists over the past 80 years. This method of analysis has opened up the world of nanomaterials and made it possible to characterize their exclusive properties. The ability

of electron microscopes to image very small-sized objects, even to the level of single atomic positions, has resulted in development of entirely new nanotechnologies, and aided in notable developments to take place by nanoscale engineering of macro sized components (Inkson, 2016).

There are two major classes of electron microscopy. These include transmission electron microscopy (TEM) and scanning electron microscopy (SEM). In electron microscope a beam of electrons is used in image formation. The electron beam used replaces light beam used in light microscopy. Even though the light microscopes are robust, cheap and normally noninvasive ensuring the object is not changed by imaging process, there is a limit of the light microscope's ability to differentiate objects and features smaller than 0.1 mm (100 nm) (Akhtar et al. 2018).

Ability of a microscope to separate two features at a given distance apart as distinct objects in the image is the resolution. In light microscopes, resolution limit depends on the wavelength of light used. Wavelength of visible light ranges from 400 nm in the blue region to 700 nm for the red light. Light with a smaller wavelength interact more strongly with the sample resulting in higher resolution images (Inkson, 2016).

In electron microscopy, a beam of highly accelerated electrons are brought to focus on the surface of materials, in order to create an image. Accelerated electron beam in electron microscopy has shorter wavelength hence makes diffraction to occur at a much smaller physical dimension. This helps in resolving features of a material starting from nanometre to micrometre particle size range. Electron microscopy gives images with a better resolution and higher magnification than optical microscopy, since accelerated and focused

beam of electrons is used to see through a material on a fine and very small scale (Akhtar et al. 2018).

2.19 Identification of the Knowledge Gap

There are a number of methods used for treatment of contaminated waste water containing organic dyes. Some of these methods include precipitation, solvent extraction, flocculation, electrolysis, distillation, sedimentation, reverse osmosis (RO) and solar disinfection (SODIS) among others (Popescu et al., 2017). These methods have numerous drawbacks which include low efficiency in removal of dyes, generation of secondary pollutant, high cost, difficulty to regenerate dyes, unavailability in large quantities, disposal challenges and not environmentally friendly. In addition, advancement of technology has made it possible for the production of synthetic dyes which are difficult to treat using the traditional methods. There is an urgent need to develop a super-efficient adsorbent that is cheap, versatile, eco-friendly and easy to regenerate for treatment and purification of waste water contaminated with organic dyes. In extraction of keratin, there is need to determine optimum conditions for extraction of keratin in keratinous bio waste for industrial application in synthesis of nanoparticles. This would inform on suitability of keratin-rich bio waste in synthesis of nanoparticles.

CHAPTER THREE

MATERIALS AND METHODS

3.1 Introduction

This chapter addresses methods that were used in achieving the specific objectives of the study: the research design, sample collection and preparation, procedure for extraction and optimisation of hydrolysis of keratin, synthesis and analysis of nanoparticles, application of synthesised nanoparticles on adsorption of selected organic dyes, adsorption kinetics and isotherms is presented.

3.2 Research Design

Experimental design was conducted on optimization of chemical hydrolysis and extraction of keratin from sheep hooves collected randomly from Litein town in Kericho county Kenya, Synthesis and characterization of nanoparticles using UV-VIS, SEM, X-ray diffraction and FT-IR analysis techniques and determining efficiency of nanoparticles in adsorption of methylene blue and crystal violet dyes.

3.3 Location of the Study

Litein town in Bureti sub-county was purposely selected for the study. Bureti sub- County is one of the five sub-counties Kericho County in Kenya. Bureti is located in 0.5 ^{o}S and 35.25 ^{o}E. It covers a total area of 955 km^2 and it is sub divided into 4 administrative divisions (Sigei et al., 2015). The main ethnic group in Bureti is the Kipsigis. The inhabitants earn a living through small scale subsistence farming, dairy farming, rearing of sheep and goats, trade, vegetable, tea pineapple and coffee farming (Omari and Masimba 2018).

3.4 Sample Collection

A sample of 5 kg of sheep hooves was collected using purposive random sampling method from a slaughter house in Litein town, Bureti sub-County in Kericho County. The collected samples were washed thoroughly with warm water and alcohol based detergent to remove blood stains, dust and any other dirt on the hooves. The samples were sun dried for two days and stored in a zipper bag before taking to the laboratory.

3.5 Sample Preparation

Samples of sheep hooves were washed with distilled water and soap detergent, rinsed with distilled water followed by 70 % ethanol and dried at 50 °C in an oven for 24 hours before extracting keratin.

3.6 Chemicals and Reagents

All reagents and chemicals used were supplied by Ranbaxy Fine Chemicals Nairobi, Kenya Ltd and they were of analytical grade. They included: Sodium hydroxide 98%, Hexane 85 %, Dichloromethane 99 %, absolute Ethanol 99.5 %, Zinc sulphate 99 %, Copper sulphate 98 %, Silver nitrate 49.9 %, Iron (II) sulphate 99 %, Iron (III) chloride 97 %, Hydrochloric acid 37 %, Nitric acid 69 %, Folin ciocalteu (F-C) 99.5 %, Trichloroacetic acid 99 % and Sodium carbonate 98 %, Ammonia 25 % and Acetic acid 99.7 %.

3.7 Optimization of Factors Affecting Chemical Hydrolysis and Extraction of Keratin

3.7.1 Effect of Time on Hydrolysis of Keratin.

Effect of time on hydrolysis of keratin was investigated by accurately measuring 0.5 g of clean hooves and transferring to a conical flask containing 2.5 % w/v of NaOH. The mixture was covered with aluminium foil and incubated for 12 hours in a water bath at

60 ºC. The amount of tyrosine released was measured after every 1 hour using Folin-Ciocalteu method as follows: Using a micropipette, 1 ml of the aliquot was measured and transferred into a clean boiling tube, followed by addition of 520 µl of trichoroacetic acid. The mixture was incubated at 37 ºC for 20 min and centrifuged for 10 min using a centrifuge (90-2 model), to remove any coagulated protein. A 2.5 ml of 0.5 M Na_2CO_3 was added to the mixture, followed by 520 µl of F-C solution diluted 1:3 with distilled water. The mixture was further incubated at 37 ºC for 30 min and analysed using UV-VIS spectrometer at 660 nm. The experiment was carried out in duplicate and the average results were used for analysis (Kamarudin et al., 2017);(Martins et al., 2021).

3.7.2 Effect of % Weight/Volume of NaOH on Hydrolysis of Keratin

Eight sets of clean hooves with a mass of 0.5 g was accurately measured and transferred into conical flasks containing 200 ml of NaOH in varying concentrations of 0.5 %, 1.0 %, 1.5 %, 2.0 %, 2.5 %, 3.0 %, 3.5 % and 4.0 % w/v at a temperature of 50 ºC. Concentration of tyrosine released was determined hourly for 12 hours using Folin-Ciocalteu method (Sinkiewicz et al., 2017).

3.7.3 Effect of pH on Hydrolysis of Keratin

Effect of pH on hydrolysis of hooves keratin was investigated by selecting a pH range of 2-13. The pH of the solution was varied using 0.1 M HCl and 0.1 M NaOH solutions. Clean hooves with a mass of 0.5 g was accurately measured and transferred into conical flasks containing 200 ml of solutions at different pH. The mixture was covered using aluminium foil and incubated at 60 ºC in a water bath for 12 hours. The concentration of hydrolysates was determined using F-C method of analysis hourly for 12 hours.

3.7.4 Effect of Temperature on Hydrolysis of Keratin

Hydrolysis of keratin was carried out at temperatures of 30 ºC, 40 ºC, 50 ºC, 60 ºC, 70 ºC and 80 ºC. Clean hooves with a mass of 0.5 g was accurately measured and transferred into a conical flask containing 200 ml of 1.0 % w/v of NaOH solution at varied temperatures. The mixture was covered and incubated in a water bath at varied temperatures. Amount of tyrosine released was measured after every hours using Folin-Ciocalteu method of analysis as described above.

3.7.5 Effect of Mass of Hooves on Hydrolysis of Keratin

Hydrolysis of keratin from hooves was carried out using 200 ml of 1.0 % w/v sodium hydroxide in a water bath set at 70 ºC. The masses of hooves selected was 1.0, 3.0, 5.0, 7.0, 9.0, 11.0 and 14.0 g. Amount of hydrolysates released was measured hourly for 12 hours using Folin-Ciocalteu method.

3.7.6 Changes in pH of Solution during Hydrolysis of Keratin

Changes in pH of solution were investigated using 200 cm^3 of 1.0 % sodium hydroxide in a water path set at 70 ºC. Masses of hooves used were 11.0 and 14.0 g. The pH of the solution was measured hourly using HI 98129 pH/EC/TDS/temperature meter, for 12 hours.

3.8 Extraction of Keratin from Sheep Hooves Samples

Clean dry hooves with a mass of 200 g were defatted using 500 $cm^3$of hexane and dichloromethane (1:1 v/v) mixture for 24 hours. The defatted hooves were dried at 30 °C in hot air oven and ground using a grinder CM-5000 model to obtain a powder which was used for keratin extraction. Keratin was extracted by adding 50 g of the hooves powder to

500 ml of NaOH solution with a pH of 12 in a 500 ml pyrex Erlenmeyer flask. The mixture was covered with aluminium foil and heated in a water bath on magnetic stirrer Eyela RC-12 model set at 70 °C for 9 hours. The mixture was centrifuged using a centrifuge MRC 6000 series model set at 6000 rev per minute to remove any undissolved hooves. The pH of the hydrolysates was adjusted to 3.8 using 0.2 M HCl to obtain keratin precipitate, which was washed with distilled water and dried at 40 °C in a hot air oven for 3 hours (Sinkiewicz et al., 2017) (Shankar and Rhim, 2019). The percentage yield of keratin was determined as follows:

$$\%\, Yield \;= \frac{Mass of keratin precipitate}{Mass of hoovesu} \times 100$$

3.9 Synthesis of Metal Nanoparticles.

The metal nanoparticles were synthesized using keratin extracted from sheep hooves in the methods listed below.

3.9.1 Synthesis of Silver Nanoparticles

To synthesize silver nanoparticles, 1 g of Keratin was added to 50 cm^3 of aqueous $AgNO_3$ solution with a concentration of 0.01 mol/L in a 250 ml Erlenmeyer flask coated and covered at the top with aluminium foil to prevent photo catalysis of the silver ions. The mixture was placed on an orbital shaker (GS-20 AKMLab) model set at 140 revolutions per minute at 25 ºC for 10 minutes followed by addition of 15 cm^3 of 2 M NaOH with continuous stirring for another 30 minutes. The mixture was heated at 80 ºC for 90 minutes. Formation of silver nanoparticles was marked by formation of a brown solution (Ying et

al., 2022). The presence of silver nanoparticles was confirmed by wavelength scan from 800 nm to 200 nm using a UV-1800 Shimadzu UV model spectrophotometer (Shimadzu, Japan). The resultant mixture was allowed to settle for 24 hours, decanted to obtain silver nanoparticles as the residue and filtered using Whatman filter paper No.1 to obtain silver nanoparticles, which were washed using double distilled water followed by absolute ethanol three times to remove impurities on the surface of nanoparticles and dried at room temperature (Agarwal et al., 2014). Synthesis of silver nanoparticles was optimised by synthesizing silver nanoparticles at different conditions of time, temperature, amounts of keratin and concentrations of silver nitrate. The levels of silver nanoparticles formed in solution were determined by determining absorbance at the λ_{max} peak which was obtained for silver nanoparticles at around 410 nm.

3.9.2 Synthesis of Copper nanoparticles

Copper nanoparticles were synthesized by adding 1 g of keratin to 50 ml of 0.01 M $CuSO_4$ in 250 ml Erlenmeyer flask and sealed using aluminium foil to prevent spillage. The mixture was shaken using an orbital shaker (GS-20 AKMLab) set at 25 ^oC and 140 rpm for 10 minutes. To the mixture, 15 ml of 2 M NaOH was added with continuous shaking at 140 rpm for 30 minutes, and transferred to a water path at 80 ^oC where the mixture was heated for 90 minutes to obtain copper nanoparticles, which was allowed to rest for 24 hours, decanted, washed with distilled water, rinsed with ethanol and filtered using whatman filter no1 to obtain nanoparticles. The nanoparticles collected were left to air dry and preserved in a clean vial for use in adsorption (Khan, 2016). Synthesis of the nanoparticles was optimized by carrying out the reaction at different conditions of time, temperature, concentrations of $CuSO_4$ and amounts of keratin.

3.10 Synthesis of Zinc Oxide Nanoparticles

Zinc sulphate with a mass of 1g was dissolved in 100 ml of water in a 250 cm^3 Erlenmeyer flask and placed on a magnetic stirrer set at 120 rpm, 60 °C. To the solution, 5 ml of keratin solution was added with continuous stirring. The mixture was heated for 2 hours to obtain zinc nanoparticles. The precipitate obtained was dried at 60 ºC and kept in amber-coloured vial before analysis (Ezealisiji et al., 2019).

3.11 Magnetic Iron (III) Oxide Nanoparticles (Fe_3O_4-NPs)

Magnetic Iron (III) oxide nanoparticles were prepared by adding 2 g of keratin to 100 cm^3 of solution containing 0.1 moles $FeCl_3.6H_2O$ and 0.05 moles of Fe_2SO_4 solution. The mixture was placed on a Stuart magnetic stirrer set at 120 rpm, 60 ºC. To the mixture, 20 ml of NaOH with a concentration of 2 M was added with continuous stirring for 90 min and then allowed to stand at room temperature for another 30 min. The procedure was repeated using Fe^{3+}:Fe^{2+} with mole ratio of 0.02:0.01. Formation of magnetic iron (III) nanoparticles was marked by appearance of a black precipitate when the ratio of Fe^{3+}:Fe^{2+} was 0.02:0.01. The color was brown when the moles of the Fe^{3+}:Fe^{2+} was raised to 0.1:0.05. The obtained suspensions was centrifuged using a centrifuge (centurion 6000 series UK) set at 10000 rpm and washed several times with distilled water followed by absolute ethanol and dried at 40 ºC in an oven for 2 hours to obtain dry Fe_3O_4-NPs. The procedure was repeated using 100 ml of solution 0.02 moles $FeCl_3.6H_2O$ and 0.01 moles of Fe_2SO_4 solution, mixed with 2 g of keratin, and using 100 ml of solution 0.02 moles $FeCl_3.6H_2O$ and 0.01 moles of Fe_2SO_4 solution without keratin in order to determine the effect of adding keratin to the synthesis of magnetic Fe_3O_4-NPs (Rashid et al.,2020). The levels of nanoparticles formed was determined using (UV-1800 Shimadzu, Japan).

3.12 Characterization of Synthesized Nanoparticles using UV-VIS, FT-IR, SEM and XRD

3.12.2 X-ray Diffraction (XRD) Study

XRD analysis was done using XRD diffractometer Bruker D8 advance diffractometer (Bruker, Ettlingen, Germany). For the XRD analysis, 1 g of nanoparticles was accurately measured using a weighing balance. The sample was ground using a clean pestle and motor to obtain a fine powder, which was transferred into a sample holder and pressed using a clean block to avoid contamination of the sample. Excess powder was removed using a glass slide to obtain a flat surface on the top of the sample. The sample holder was placed at the base of sample chamber, lifted to the right position and locked using a sample stage fixture. Using the instrument software, Scan range, number of steps per scan and time for the scan can be selected. Scan commander application was used to start the scan. The sample and the detector were rotated at various angles to obtain the structure and lattice of the nanoparticles. The data was obtained using a X-ray diffractometer with Bragg-Brentano parafocusing geometry, a diffracted beam monochromator and a conventional copper target X-ray tube set (λ = 1.54 Å) to 40 kV and 44 mA at 26 ºC. Diffraction intensities were recorded with 2θ ranging from 3° to 40° at a scan speed of 0.02°/s (Xu et al., 2014).

3.12.3 Ultraviolet-Visible Analysis

The optical properties of synthesized particles were carried out using double beam ShimadzuUV-1800 UV–Vis spectrophotometer (Shimadzu, Japan) as follows. The UV-VIS equipment was auto zeroed using blank solution. Nanoparticles solution with a

volume of 3 ml was transferred to a clean cuvette. While holding the cuvette with the translucent sides, the cuvette was carefully wiped using micro fiber cloth to remove any spilled solution on the surface. The cuvette with the solution was placed in a sample holder, with the transparent sides facing the beam path, while a blank solution in another cuvette was kept in another sample holder. The cuvettes were slided to the beam bath to ensure that the UV VIS light passed through the sample. On the computer screen, wavelength range of 200-800 nm was selected. By selecting and pressing start, the solution was scanned using UV-VIS light with a wavelength scan from 800 nm to 200 nm. Maximum absorption peaks were obtained at a specific wavelength, which correspond to specific nanoparticles (Nanthavanan et al., 2019).

3.12.4 Scanning Electron Miscroscopy

The morphology was analyzed using a Scanning electron microscope Tescan mira 3 LMFE SEM microscope (Tescan Brno-Kohoutovice, Czech Republic) as follows: Using a micropipette 7 µl of nanoparticles solution was transferred to a flat surface of a carbon coated aluminium stub with a sticker sheet. The solvent was allowed to evaporate. The stub with nanoparticles was placed on the stage in the specimen chamber which was closed and evacuated by turning on the vacuum pump. Accelerating voltage of 4 KV was turned on followed by thermionic cathode. The stage was moved in the microscope by changing set to find the position of the sample. Magnification was increased and the position of the sample was readjusted. By increasing magnification to 47700X, the shape and size of the nanoparticles was determined (Nanthavanan et al., 2019).

3.12.5 Fourier Transform Infrared Spectroscopy

FTIR spectrum was obtained using IRAffinity-1S Fourier transform infrared spectrophotometer (Shimadzu, Japan). Grinding of 0.2 g of nanoparticles was carried out to form a pellet for which FTIR analysis was be performed. The sample was placed on the center of a platform which had been cleaned by wiping with cotton wool soaked in ethanol. The knob of FTIR analysis machine was lowered gently until it came in contact with the sample. Sample scan was carried out by clicking sample scan on the screen of the computer used to control the FTIR machine. IR spectra was obtained with an operating range of 4500-500 cm^{-1} (Nanthavanan et al.,2019).

3.13 Batch Adsorption Studies on removal of organic dyes in water using nanoparticles

3.13.1 Reusability of nanoparticles and Desorption Experiments

Experiments for reusability of silver nanoparticles was investigated by adding 0.115 g of loaded silver nanoparticles to 30 cm^3 of 0.1 M acetic acid and shaking the mixture for 120 minutes and allowed to settle for 1 hour. The mixture was filtered with whatman filter no1 to obtain nanoparticles. The nanoparticles were rinsed with distilled water and air dried. The washed nanoparticles were reused in adsorption of CV. MB desorption from CuNps was performed using different eluents including distilled water, HNO_3, HCl, NaOH, NH_3 and CH_3COOH. Desorption of MB dye was carried out by adding 0.024 g of dye loaded copper nanoparticles to 30 cm^3 of various desorption reagents and shaking the mixture. The mixture was allowed to rest at room temperature. Absorbance of the mixture was recorded after 20 minutes for 100 minutes. The experiment was repeated carried out at 40 °C. The amount of desorbed dye was determined by measuring the amount of dye in the

solution. The batch mode and experimental conditions for adsorption of dyes are presented in table 3.1.

Table 3.1:

Batch Mode Experimental Conditions for Adsorption of Dyes.

Experimental Conditions	Experiment Parameter
Time interval	30 minutes interval for MB adsorbed using CuNps for 360 minutes (initial concentration 5 ppm), 20 minutes interval for CV adsorbed with AgNps for 160 minutes, initial colorant concentration of 10 $mg \cdot L^{-1}$. 1 minute interval for CV adsorbed by Fe_3O_4Nps, Initial colorant concentration 10 ppm at 25 °C and contact time of 10 minutes.
Dosage of nanoparticles	1 mg, 2 mg, 4 mg, 8 mg, 10 mg and 12 mg of CuNp adsorbent for MB was used, 2 mg, 4 mg, 6 mg, 8 mg, 10 mg and 12 mg of AgNp adsorbent for CV used and 1 mg, 2 mg, 4 mg, 6 mg and 8 mg of Fe_3O_4 Nps adsorbent was used on CV (20ppm at 25 °C)
Initial dye concentrations	10, 5, 2.5, 1.25 and 0.625 $mg \cdot L^{-1}$; contacting time 6 h; pH = 5 for MB and CuNps. 20, 10, 5, 2.5, 1.25 and 0.625 $mg \cdot L^{-1}$ for CV at 25 °C. Initial colorant concentrations of 20, 10, 2.5, 1.25 and 0.625 $mg \cdot L^{-1}$ for CV adsorbed using Fe_3O_4 Nps (dosage 6 mg/ 10 ml at 25 °C).
Initial pH values	2, 3, 4, 5, 6, 7, 8, 9,10, 11, 12 and 13 with initial concentration of 5 $mg \cdot L^{-1}$; for MB contact time 6 h. 2, 3, 4, 5, 6, 7, 8, 9 and 10 for CV.
Effect of Temperature	The experiment was carried out at a temperature of 25 ºC, 30 ºC, 40 ºC, 50 ºC and 60 ºC using 8mg/10 ml of CuNPs on 5 ppm MB and 8mg/10 ml of AgNPs on 10 ppm CV.

3.14 Validation of the Technique of Analysis

To ensure that the UV-VIS analysis was unwavering, calibration technique was used, by measuring absorbance of the standard and blank solutions. Calibration of F-C method was done using tyrosine which is one of the amino acids released during hydrolysis of keratin. The procedure for Folin-Ciocalteu (F-C) analysis according to Martins et al., 2021 was used as follows: Tyrosine solution with a volume 1 ml of 0.0012 M was incubated at 37 ºC for 5 min and mixed with 520 µl of trichloroacetic acid. The mixture was kept in a water

path at 37 ˚C for 20 min and centrifuged for 10 min using a centrifuge (90-2 model). A 2.5 ml of 0.5 M Na_2CO_3 was added to the mixture, followed by 520 µl of F-C solution diluted 1:3 with distilled water. The mixture was further incubated at 37 ºC for 30 min and analysed using UV-VIS spectrometer at 660 nm. The procedure was repeated for different concentrations of tyrosine, to obtain values which were used to plot a standard curve (Martins et al., 2021). To calibrate the analysis of adsorption of dyes, respective dyes under investigation were used to obtain a standard curve. Methylene blue and crystal violet dyes with various concentrations were analyzed using UV-VIS spectrophotometer to determine absorbance used to plot regulation curves. The measurement was done three times, to obtain average values used to plot a graph for regulation, basing on R^2 values.

3.15 Determination of Dye Decolourization rate

Amount of the pollutant adsorbed q_t in (mg/g) was calculated as follows:

$$q_t = \frac{C_o - C_t)\, V}{W} \quad \text{..... (3.1)}$$

C_o is the initial concentration of the dye under investigation.

C_t is the concentration of the dye under investigation at any time, t in mg/L.

V is the volume of the colorant solution used.

W is the mass of the nanoparticles used for adsorption in grams.

Removal efficiency, R (%) of dyes was calculated as shown below.

$$R = \frac{C_\circ - C_e}{C_\circ} * 100 \quad \text{..... (3.2)}$$

$C_\circ$ is the initial concentrations of the dye under investigation in mg/ L

C_e is the equilibrium concentrations of the dye under investigation in mg/ L(Paşka et al., 2014). A graph of adsorption efficiency against the parameter under investigation was plotted to find out how it affect adsorption process.

CHAPTER FOUR

RESULTS AND DISCUSSION

4.1 Introduction

This chapter addresses the data obtained from research and a comprehensive discussion supporting the experimental data, the results on optimization of hydrolysis of keratin, synthesis of nanoparticles, characterization of nanoparticles, application of nanoparticles in adsorption of dyes and data analysis is presented herein.

4.2 Optimisation of Hydrolysis of Keratin

4.2.1 Tyrosine Standard Curve

Tyrosine is one of the amino acids present in keratin and the rate of sheep hooves hydrolysis was monitored with the amount of tyrosine liberated (Kamarudin et al., 2017). A calibration curve (Figure 4.1), was plotted using tyrosine solution Folin ciocalteur test and was used as a reference for determining levels of hydrolysates released during optimization of keratin hydrolysis. Absorbance values obtained from experiment were related with the standard curve equation to determine concentration of tyrosine in hydrolysates. From the graph in figure 4.1, it was noted that with increase in concentrations a straight line is obtained with R^2 value = 0.999. Therefore this indicated reliable measurements using F-C method.

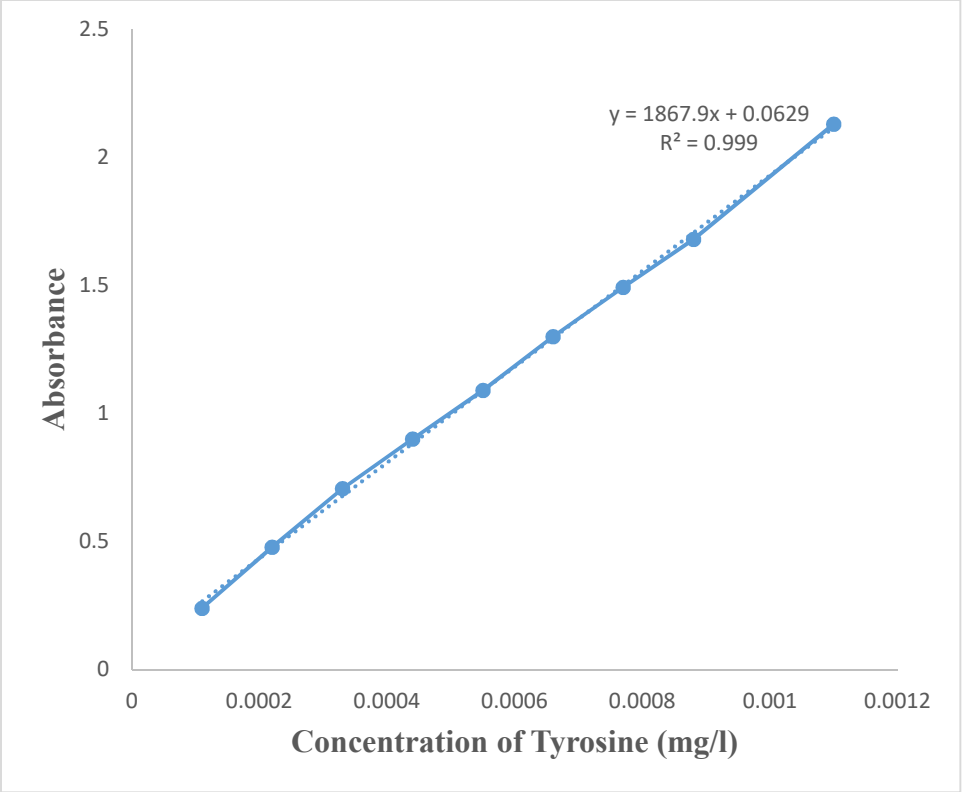

Figure 4. 1: Calibration plots for tyrosine

Determination of the levels of keratin hydrolysates in reacting mixture of hooves and sodium hydroxide was done by comparing measured absorbance with the absorbance on the calibration curve and corresponding concentrations.

4.2.2 Effect of Time on Hydrolysis of Keratin

Time is an important factor when determining equilibrium point for a reaction process. The effect of time on alkaline hydrolysis of keratin using NaOH was investigated and the results obtained are presented in figure 4.2. Generally it was observed that amount of hydrolysates released increased with time. The graph also shows that the rate of hydrolysis was high during the first two hours and the maximum yield was attained after 9 hours. Previous research reported that optimum time for keratin hydrolysis varied depending on the

chemicals used, concentration of chemicals and the reaction temperature for hydrolysis. Kamarudin et al reported an optimum hydrolysis time of 9.5 hours for hydrolysis of keratin from chicken feathers using 0.05 M sodium sulphide at a temperature of 80.9 °C (Kamarudin et al., 2017). Wang et al reported a dissolution time of 5 hours for wool keratin at a temperature of 75 ºC using 0.165 M l-cysteine (Wang et al., 2016). An optimum time of 5.53 hours has also been reported by Admassu on hydrolysis of chicken feathers using 0.43 M sodium sulfide (Admassu, 2020). Dąbrowska et al reported an optimum time of 32 hours using 1M NaOH during hydrolysis of chicken feathers at room temperature (Dąbrowska et al., 2022), while Sinkiewicz et al reported a maximum keratin yield after 3 hours from chicken feathers using 0.08 M sodium bisulphite (Sinkiewicz et al., 2017), Bhat et al reported optimum time of 24 hours using 4 % NaOH on human hair at room temperature (Bhat et al., 2021), while Fagbemi et al reported an optimum time of 2 hours during hydrolysis of chicken feather keratin using 1.75 % NaOH (Fagbemi et al., 2020).

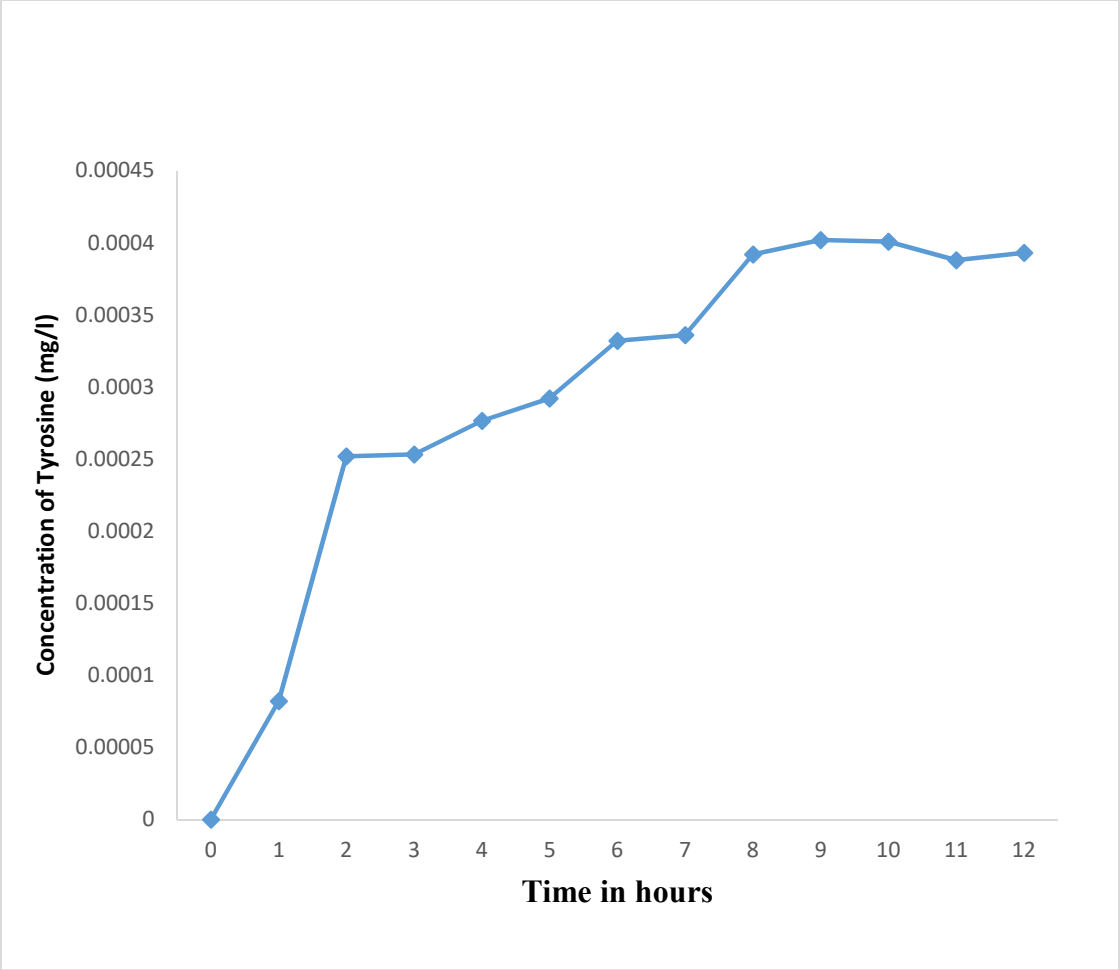

Figure 4. 2: Concentration of keratin hydrolysates against time

4.2.3 Effect of % Weight/Volume of NaOH on Hydrolysis of Keratin

The amount of hydrolysates released increased with increase in % weight/volume of sodium hydroxide from 0.5 % NaOH to 1 %, followed by a decrease from 1.5 % up to 4% NaOH. Highest amount of hydrolysates was obtained by using 1 % NaOH. This corresponds fairly with what was reported in other studies, Bhat reported an increase in the concentration of hydrolysates with increase in concentration of KOH used up to 3% then there was no more further increase in amount of hydrolysates released even when the

concentration of KOH was increased (Bhat et al., 2021). Sinkiewicz reported an increase in the yield of hydrolysates with increase in concentration of NaOH from 1 % to 2.5 %, with the yield being highest when 1.5 % of NaOH was used (Sinkiewicz et al., 2017). Admassu reported an increase in keratin yield from chicken feathers when the concentration of Na_2S was increased from 0.2 M to 0.4 M, followed by a decrease in keratin yield, with a further increase in Na_2S concentration (Admassu, 2020). The concentration of hydrolysates obtained after 9 hours is shown in the figure 4.3 below.

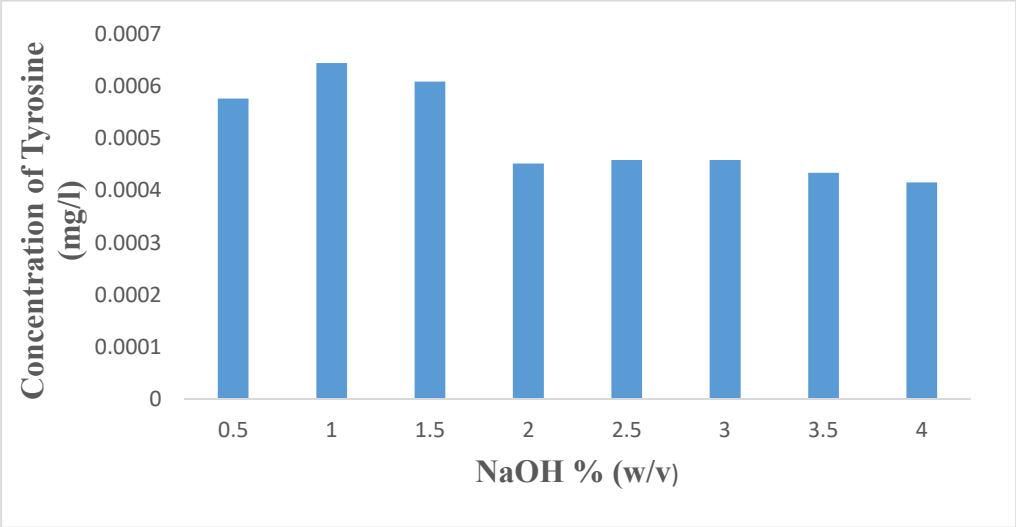

Figure 4.3: Concentration of tyrosine in keratin hydrolysates obtained using different concentrations of NaOH

The results indicates that the yield of hydrolysates increases with increase in concentration of NaOH due to increase in fragmentation of the protein as concentration of alkali increases. This in turn increases the yield of hydrolysates. The yield of hydrolysates obtained using NaOH contains all the amino acid found in the native protein, unlike in the acid hydrolysis in which some amino acid such as methionine, histidine and tryphtophan

are lost (Mustățea et al., 2019). Therefore the concentration of hydrolysates is expected to increase when an alkali is used during hydrolysis unlike in acid hydrolysis.

4.2.4 Effect of pH of solution on Hydrolysis of Keratin

It was noted that the amount of hydrolysates released from sheep hooves increased with increase in pH as shown in figure 4.4. Higher amount of hydrolysates was obtained in alkaline pH. The amount of tyrosine released was highest when solutions of pH 12- 13 were used. At pH close to the isoelectronic point of keratin (pH 4.9-5.4), solubility of keratin was found to below, hence more peptides are precipitated (Dąbrowska et al., 2022). At high pH, it was observed that keratin undergoes decomposition, releasing more hydrolysates (Sharma and Gupta, 2016).

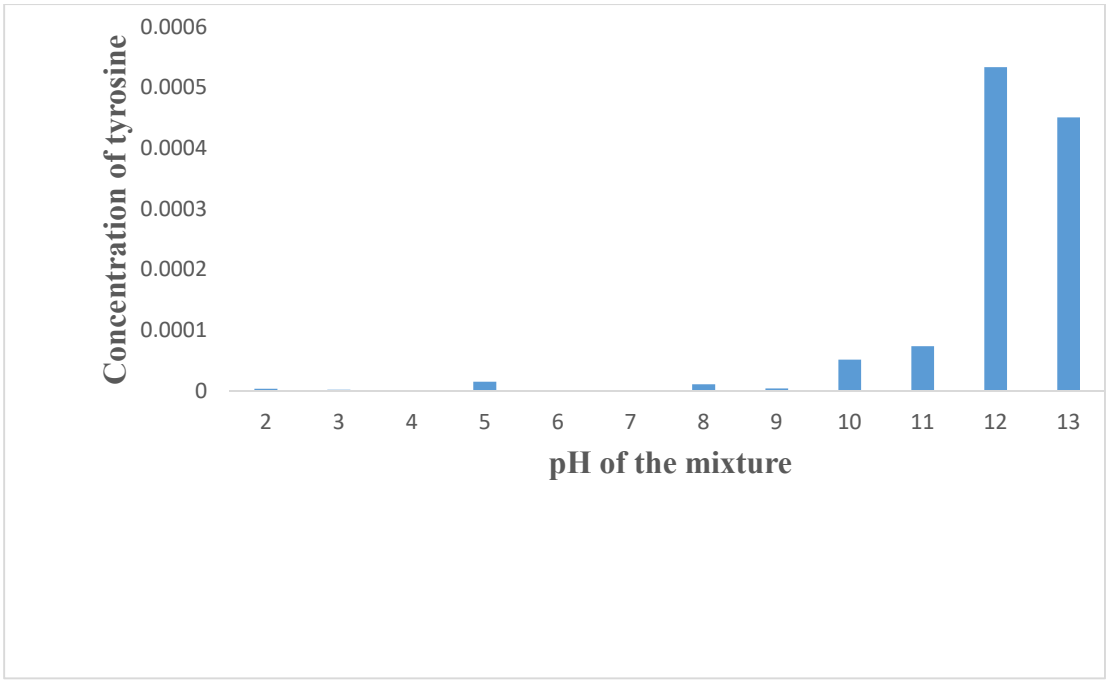

Figure 4.4: Effect of pH on hydrolysis of keratin.

From the figure 4.4, there is an increase in absorbance with increase in pH from pH 2 to pH 13. This indicates an increase in concentration of hydrolysates released during hydrolysis.

4.2.5 Effect of Temperature on Hydrolysis of Keratin.

The effect of temperature on hydrolysis of keratin was investigated and the results are presented in figure 4.5. From the graph it was observed that the amount of hydrolysates released increased with increase in temperature. Maximum yield was attained at 70 ^{o}C. Rate of hydrolysis was low at temperatures of 30 ^{o}C and 40 ^{o}C. At the temperatures of 60 ^{o}C -80 ^{o}C, the amount of hydrolysates released was high. This findings was similar to the findings by Wang et al., who investigated the dissolution of rabbit hair and reported a linear increase in concentration of aromatic amino acid released with increase in temperature (Wang et al., 2018). As the temperature is increased, more energy which is required to speed up chemical and physical breaking of peptide bonds of the keratin from the hooves is supplied. Increase in temperature, increases the rate of movement of the solvent into the inner parts of the hooves which in turn will speed the dissolution of the hooves. Also increasing the temperature causes ionization of basic amino acid order and deteriorate interaction between molecules of protein (Wang et al., 2018).

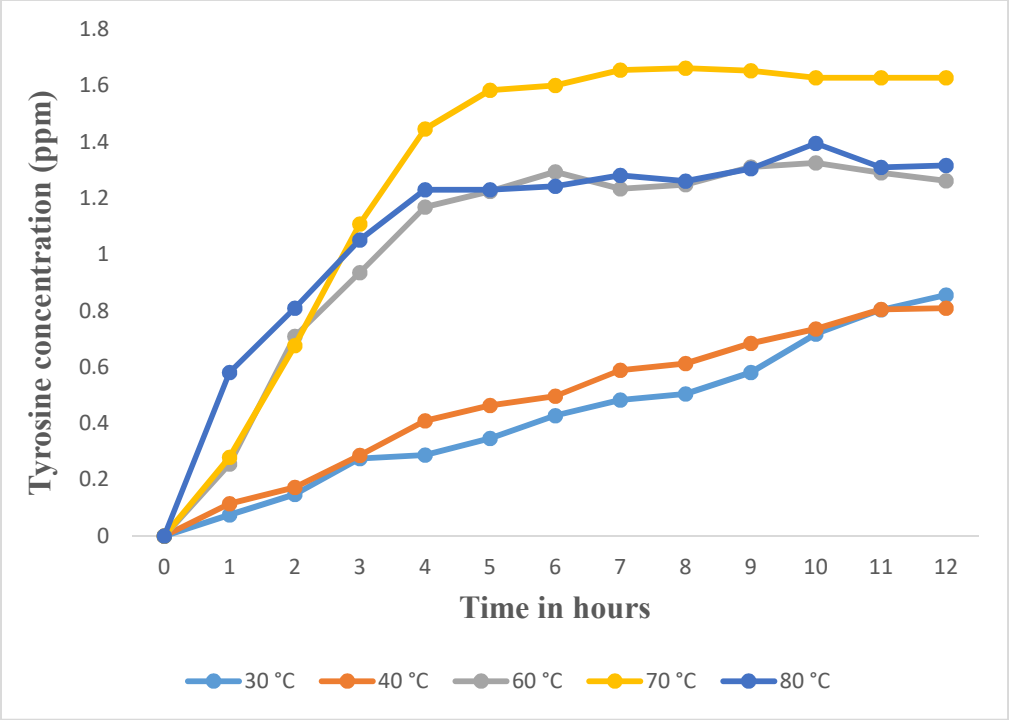

Figure 4. 5: Effect of temperature on hydrolysis of keratin

4.2.6 Effect of Mass of Hooves on Hydrolysis of Keratin

The concentration of hydrolysates obtained at equilibrium increased with increase in mass of the hooves used, the results are presented in figure 4.6. Similar results have been reported by Admassu during hydrolysis of chicken feathers in which the keratin yield increased when the chicken feathers used was increased from 20 g/l to 25 g/l (Admassu, 2020).

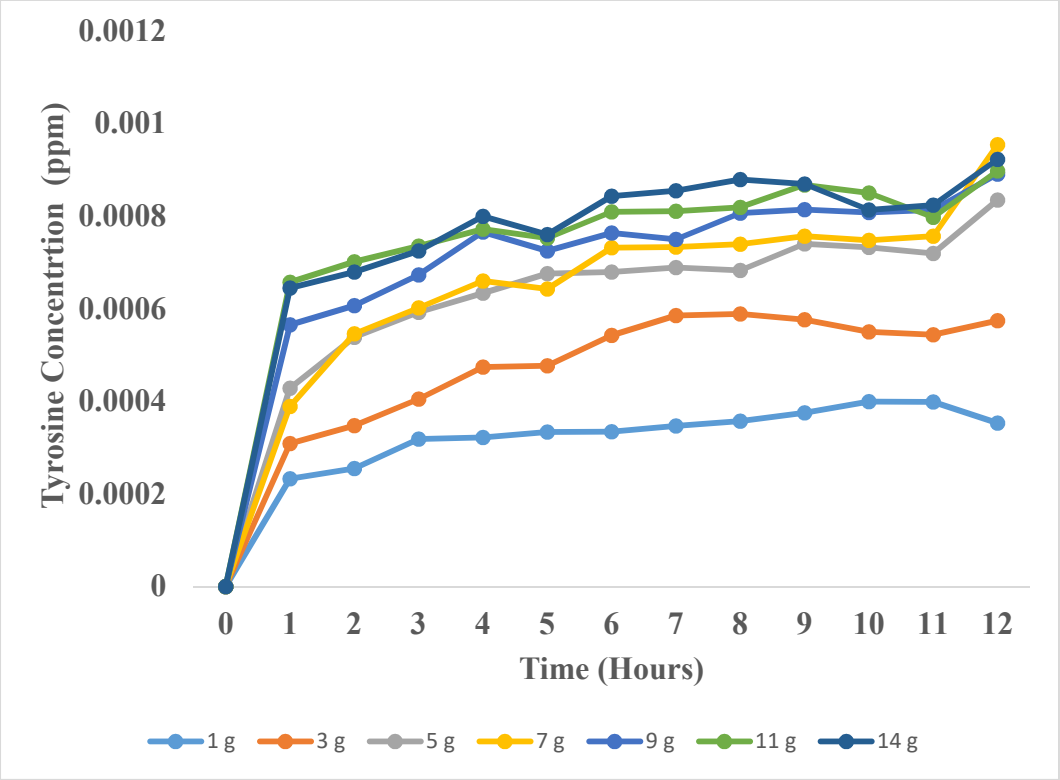

Figure 4. 6: Effect of mass of hooves on hydrolysis of keratin

4.2.7 Changes in Solution pH during Hydrolysis of Keratin

Changes in solution pH during hydrolysis of keratin is reported in figure 4.7, it was noted that there was a decrease in pH of the solution from 12.69 to 11.315 with a mass of 11.0 grams of hooves and a change in pH from 12.69 to 11.19 when the experiment carried out using 14.0 grams of hooves. There was a small decrease in pH with time during hydrolysis could be attributed to interaction between amino acid hydrolysates and hydroxide ions from sodium hydroxide (Kamarudin et al., 2017). The same trend was noted by Mokrejs et al during hydrolysis of chicken feathers using 1 % potassium hydroxide in which a small change in pH of the reacting mixture from 12.8 to 10.6 was reported (Mokrejs et al., 2011). On cooling the solution of hydrolysates, the pH rose to 12.10.

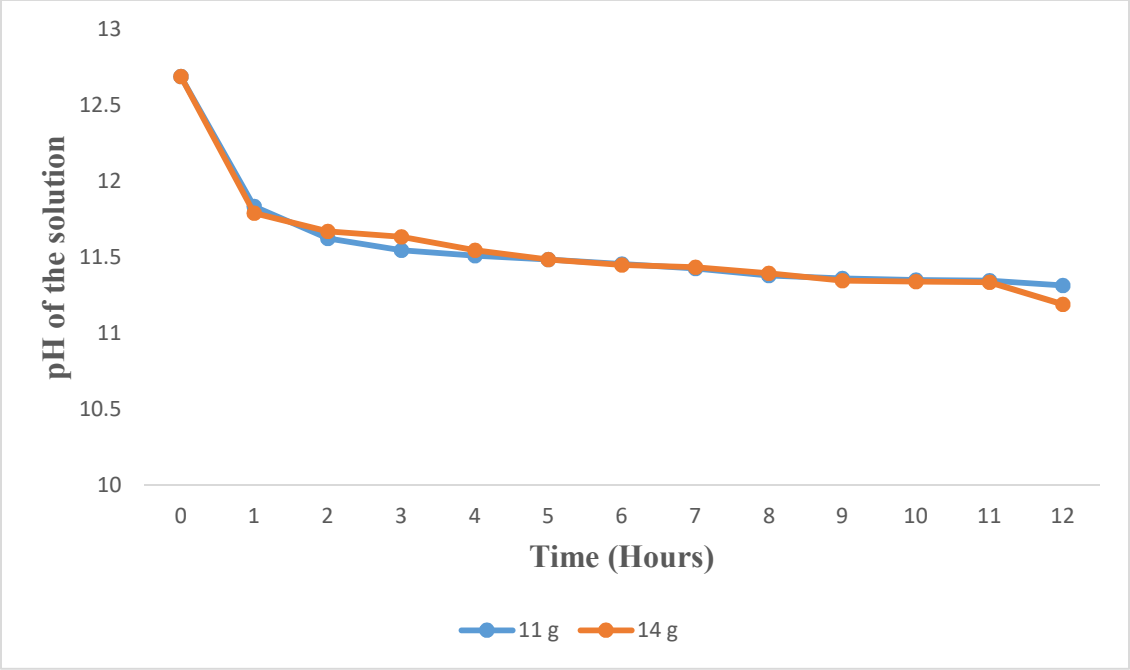

Figure 4. 7: Changes in pH of hydrolysates with time during hydrolysis of keratin

4.2.8 Extraction of Keratin

Completely solubilized keratin solution obtained after 9 hours was precipitated at a pH of 3.2 to obtain a white keratin precipitate (figure 4.8). The pH 3.2 is close to the isoelectronic point of keratin (4.9-5.4), hence the keratin is aggregation of polypeptides occur at pH values close to or at the isoelectronic point (Wang et al., 2016). The isoelectronic point fluctuates due to existence of mixed polypeptides with varied molecular weights (Dąbrowska et al., 2022). The mass of keratin obtained was 21.2 g which translates to 42.4 % percentage yield. Similar results have been reported by other researchers for example Kamarudin et al reported a percentage yield of 43.8 % keratin obtained from chicken feathers when 2 % of NaOH was used at a temperature of 80 °C (Kamarudin et al.,2017). Dąbrowska et al reported a yield of 41 % using chicken feathers and 1 M NaOH after 32 hours at room temperature (Dąbrowska et al., 2022).

(a) (b)

(c) (d)

Figure 4. 8: Images of (a) Clean hooves placed on a container after drying (b) Hooves powder (c) Keratin Hydrolysates after 9 hours of hydrolysis (d) Keratin precipitate on a petri dish.

The precipitate obtained was used as a reducing and capping agent in synthesis of nanoparticles.

4.3 Synthesis of Nanoparticles using Keratin Extracted from Sheep Hooves

4.3.1 Synthesis of Silver Nanoparticles

Silver nanoparticles were synthesized using method by Agarwal (Agarwal et al., 2014). Presence of silver nanoparticles was marked by appearance of brown color. The levels of AgNps synthesized under different conditions of reaction time, temperature, quantity of keratin and concentration of Ag^{+} were determined using UV-VIS analysis.

4.3.1.1 Effect of Time on Synthesis of Silver Nanoparticles

It was observed that the yield of silver nanoparticles increased with increase in time up to 90 minutes that is there was a direct relationship between yield and time. Further heating resulted in a decrease in the yield of silver nanoparticle. Therefore for investigation of other parameters, an optimum time of 90 minutes was selected. The results on the effect of time on synthesis of silver nanoparticles are presented in Figure 4.9. During the synthesis of the nanoparticles, more and more ions are reduced to silver nanoparticles, hence the levels of silver nanoparticles increase with increase in time until saturation time is attained (90 mins). Amount of silver nanoparticles decreases with further increase in time due to growth of larger particles or aggregation of smaller particles (Lukman et al., 2011). Other reports indicate that, different optimum incubation time for synthesis of AgNps has been reported using plant extracts. Singh et al reported an optimum time of 30 minutes during AgNps synthesis using 5 mM $AgNO_3$ and hibiscus leaf extract (Singh et al., 2020). Liaqat et al., 2022 reported an optimum time of 60 minutes during synthesis of AgNps using *Terminalia arjuna* and *Eucalyptus camaldulensis* plant extract and 1 mM $AgNO_3$ solution (Liaqat et al.,2022), while Kesik et al reported an optimum time of 180 minutes in green synthesis of

silver nanoparticles using *Agrimonia eupatoria* aqueous plant extract and 5 mM $AgNO_3$ at a temperature of 70 ºC.

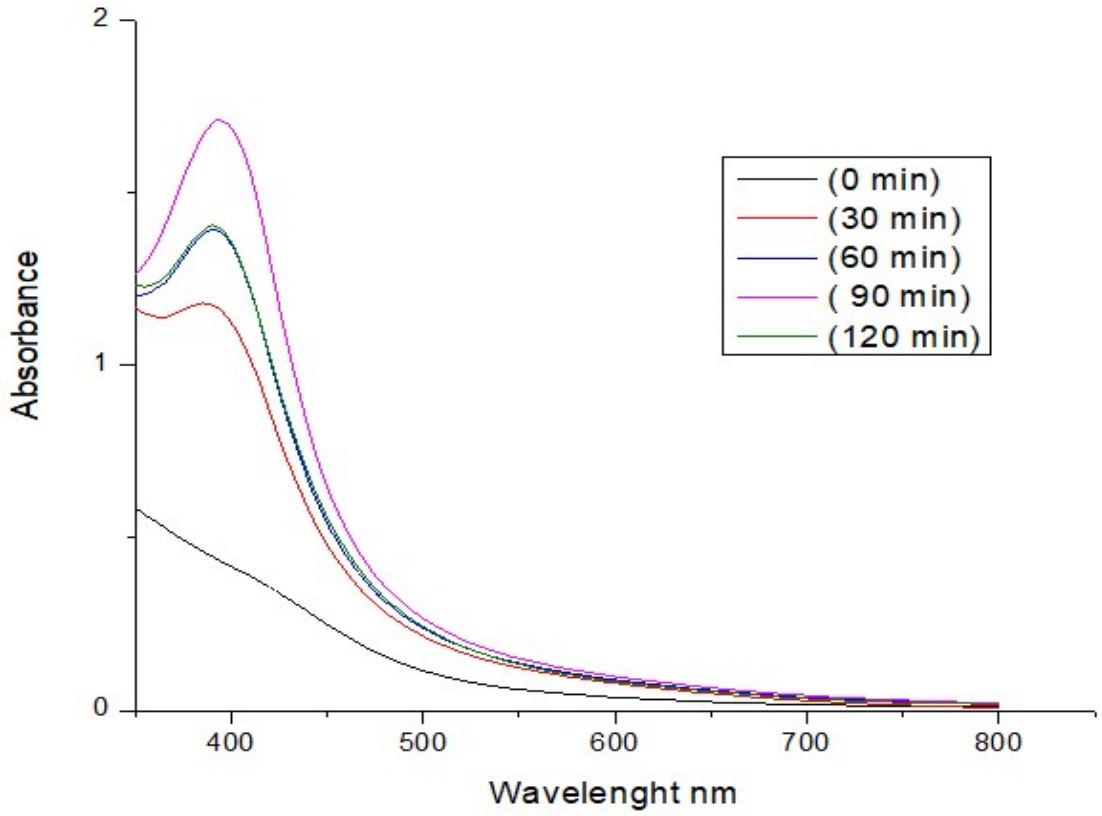

Figure 4. 9: Effect of time on synthesis of silver nanoparticles

4.3.1.2 Effect of Temperature on synthesis of Silver nanoparticles

Effect of temperature on synthesis of silver nanoparticles findings are presented in figure 4.10, the results showed that bio reduction rate of metal ions is affected by temperature. At ambient temperature the bio reduction is much higher and metabolites can reduce silver ions to silver (Keat, 2015). However the reaction must be carried out at elevated temperature (Lukman et al., 2011). Amount of silver nanoparticles obtained increased with increase in temperature. Maximum yield of AgNps was attained when the experiment was carried out at 80 ºC. Similar trend has been reported from previous results. Liaqat et al.,

2022 reported optimum temperature of 75 ºC during synthesis of AgNps using a mixture of *Terminalia arjuna* and *Eucalyptus cameldulensis* plant extracts (Liaqat et al., 2022). Kesic et al, reported a maximum yield of silver nanoparticles using at a temperature of 70 ºC using *Agrimonia eupatoria L.* plant extract and 1 mM $AgNO_3$ (Kesić etal., 2023). Sila et al, reported an optimum temperature of 90 ºC during synthesis of AgNps using *Eucalyptus corymbia* leaf extract (Sila et al., 2019). At high temperature, nanoparticles formation rate is high. The stabilizing capabilities of bio molecules increases and smaller particles are formed (Bhavyasree and Xavier, 2022). The extend of crystalinity of nanoparticles increases as temperature is increased due to increase in crystal growth rate, hence there is a shift in λ_{max} for the nanoparticles (Thomas et al., 2015).

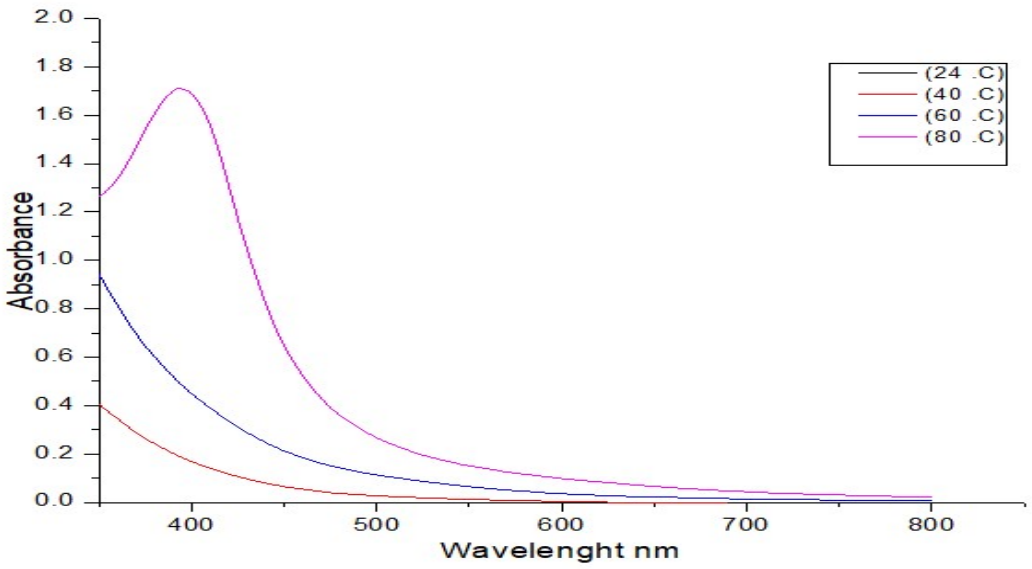

Figure 4. 10: Effect of temperature on synthesis of silver nanoparticles

4.3.1.3 Effect of amount of Keratin on Synthesis of Silver Nanoparticles

The amount of silver nanoparticles synthesized increased with increase in amount of keratin precipitate added up to 1 g as shown in figure 4.11. With further increase in quantity of keratin precipitate, the yield of silver nanoparticles decreased. When the quantity of keratin is insufficient to reduce all silver ions, lower yield of nanoparticles is obtained, when the best ratio of the reducing agent to silver ions is obtained, maximum yield of silver nanoparticles is attained. When the best ratio of reducing agent to silver ions has been obtained, maximum yield of nanoparticles is obtained. When the amount of reducing agent exceeds the amount required for the best ratio with the silver ions, there is release of ions in solution caused by excess reducing agent and nanoparticles which have a higher hydrodynamic diameter by aggregation (figure 4.11). Aggregated silver nanoparticles causes precipitation (Cardoso et al., 2014). Similar results have been reported by Agustina et al in synthesis of silver nanoparticles using *Diospyros maritima* Blume extract (Agustina et al., 2021).

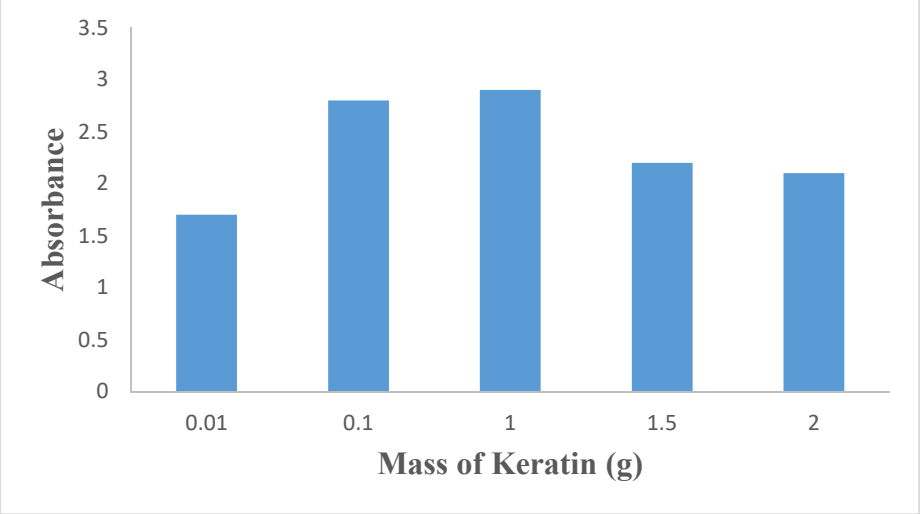

Figure 4. 11: Effect of quantity of keratin on synthesis of silver nanoparticles

4.3.1.4 Effect of Initial Concentration of Silver Ions

The results for effect of initial concentration of silver ions indicated that AgNps yields diminished with increase in concentration of $AgNO_3$ solution, these results are as shown in figure 4.12.

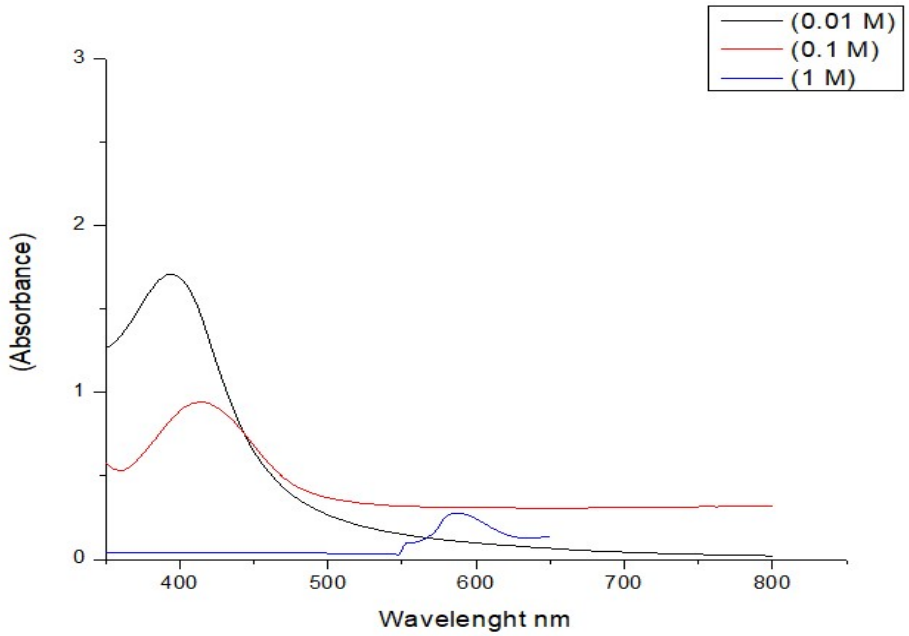

Figure 4. 12: Effect of $AgNO_3$ concentration on synthesis of silver nanoparticles

The graph shows maxima absorbance of 400nm for AgNps synthesized using 0.01M silver nitrate.There is a shift in the λ_{max} when higher concentrations of $AgNO_3$ are used. This could be ascribed to aggregation of nanoparticles resulting in precipitation (Cardoso et al., 2014). Precipitation results in bathochromatic shift to longer wavelengths (Lukman et al., 2011). Similar results have been reported by Liaqat et al during green synthesis of AgNps using *T. arjuna* and *E. camaldulensis* plant extract, in which maximum yield of AgNps was attained using 1mM $AgNO_3$ (Liaqat et al., 2022), whereas Kesie et al on synthesis of silver nanoparticles using *Agrimonia eupatoria L.* plant extract reported a decrease in

nanoparticles yield when the concentration of $AgNO_3$ was increased. The maximum yield was attained using 0.005M $AgNO_3$ at a temperature of 70°C (Kesić et al., 2023).

4.3.2 Synthesis of Copper Nanoparticles

The synthesis of copper nanoparticles was in accordance to the method by Khan, where the presence of copper nanoparticles was marked by appearance of a violet color (Khan, 2016). UV-VIS analysis was used to determine the levels of CuNps in solution, hence the optimum conditions for synthesis of the nanoparticles was identified.

4.3.2.1 Effect of Time on Synthesis of Copper Nanoparticles

The results on the effect of time on synthesis of copper nanoparticles are presented in figure 4.13. In the graph, length of incubation time affects type and quality of nanoparticles synthesized using green methods (Patra and Baek, 2014). The yield of nanoparticles increased with increase in time until 90 minutes when saturation was attained. When time was increased further, the concentration of nanoparticles decreased. This could be attributed to further growth of nanoparticles to form larger particles or aggregation of nanoparticles to form larger particles (Lukman et al., 2011); (Patra and Baek, 2014). Similar results on increase in quantity of nanoparticles with time followed by a decrease in levels of nanoparticles beyond the optimum time has been reported by have been reported in literature (Bhavyasree and Xavier, 2022); (Qomariyah and Hakim, 2024).

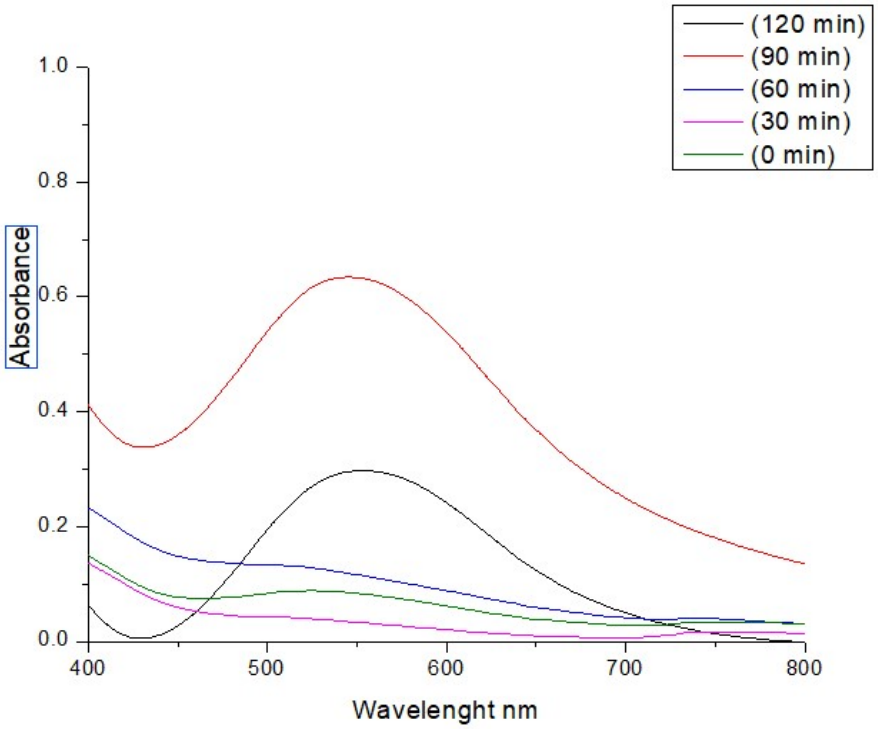

Figure 4. 13: Effect of time on synthesis of copper nanoparticles

4.3.2.2 Effect of Quantity of Keratin on Synthesis of Copper Nanoparticle

The results on Effect of quantity of keratin on synthesis of copper nanoparticle are presented in figure 4.14, which indicate that the yield of copper nanoparticles increased with increase in amount of keratin precipitate. Maximum yield was obtained using 1 g of keratin. The yield decreased with further increase in amount of keratin used. Smaller quantities of keratin were not sufficient to reduce all Cu^{2+} to Cu^{0} this resulted in lower yield (Bhavyasree and Xavier, 2022). When larger quantity of keratin is used, there was further growth of nanoparticles or aggregation of nanoparticles to form larger nanoparticles (Cardoso *et al.,* 2014). Similar findings were reported by Bhavyasree and Xavier in biosynthesis of CuNps using plant extracts (Bhavyasree and Xavier, 2022).

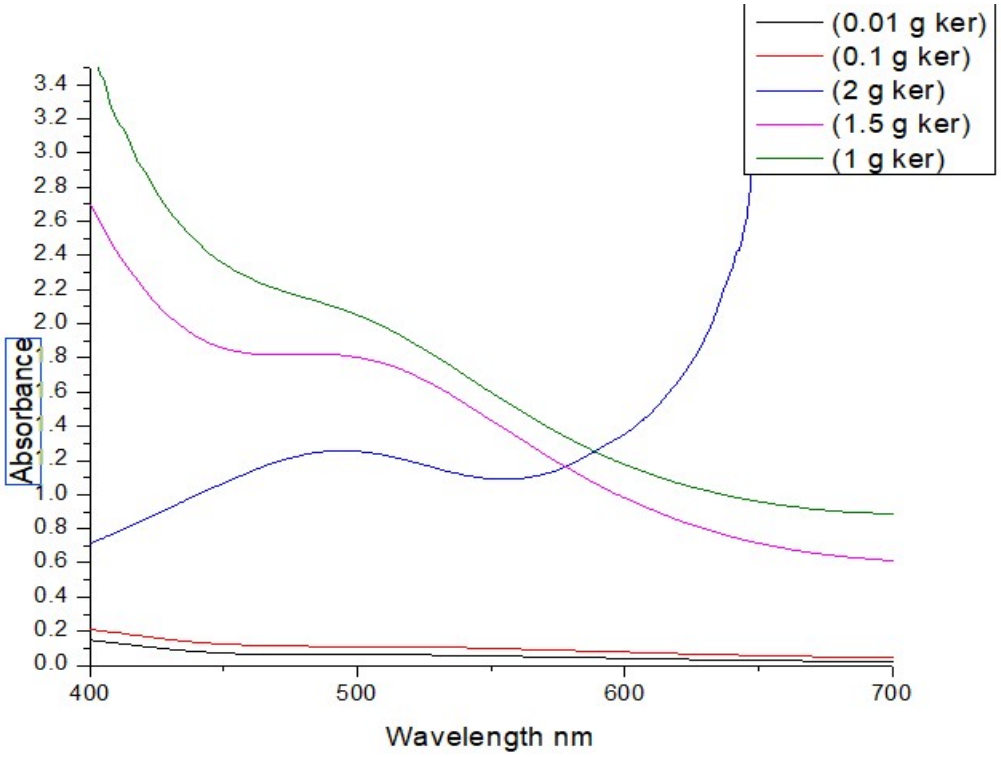

Figure 4. 14: Effect of quantity of keratin on synthesis of copper nanoparticles

4.3.2.3 Effect of Copper (II) Sulphate Concentration on Synthesis of Copper Nanoparticle

The results on effect of Copper (II) Sulphate concentration on synthesis of copper nanoparticles are shown in Figure 4.15. From the graph, it can be seen that there was decreased in the yield of Copper nanoparticles with increase in the concentration of copper sulphate, this could be attributed to the fact that when the concentration of copper (II) sulphate is increased, the nanoparticles formed aggregate to form larger particles which precipitate (Cardoso et al., 2014). Growth of nanoparticles to larger particles results in bathochromic shift to longer wavelength (Lukman et al., 2011). Similar results were reported in synthesis of collagen based silver nanoparticles for biological applications and

characterization (Cardoso et al., 2014) and in synthesis of CuNps using *Senna didymobotrya* (Sadia et al., 2021).

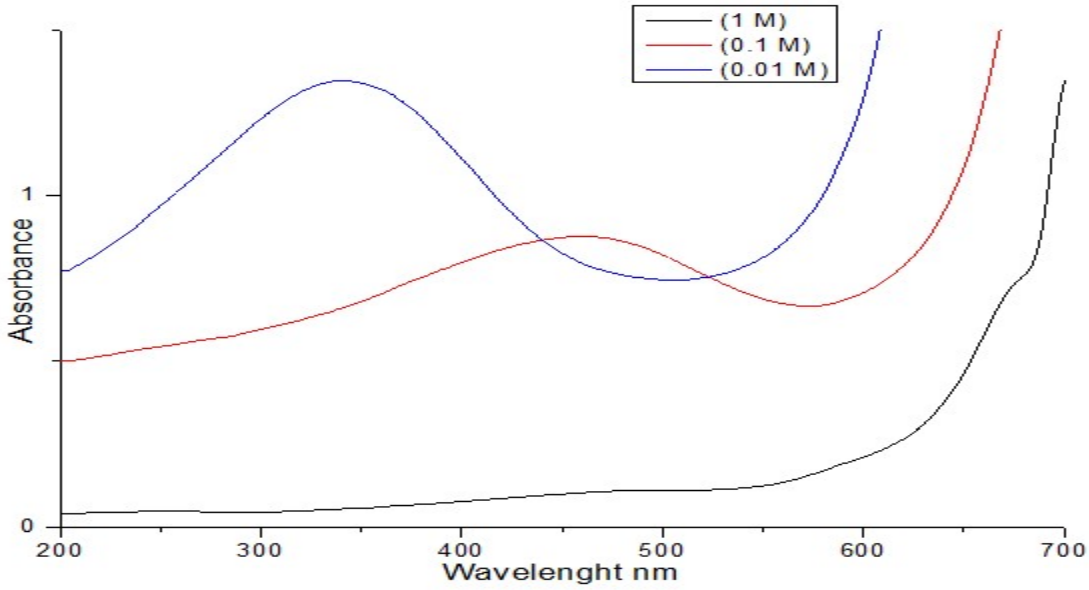

Figure 4.15: Effect of concentration of copper (II) sulphate on synthesis of copper nanoparticles.

4.3.2.4 Effect of Temperature on Synthesis of Copper Nanoparticles

Temperature affects bio reduction of metal ions. Ambient temperature is required in biosynthesis of nanoparticles to obtain a maximum yield (Keat, 2015). Some metabolites reduce metal ions at elevated temperature (Lukman et al., 2011). Figure 4.16 shows results on the effect of temperature on synthesis of copper nanoparticles using keratin. The quantity of copper nanoparticles obtained increased with increase in temperature. At lower temperature, there is agglomeration of nanoparticles (Sadia et al., 2021). At elevated temperature, crystal growth rate increases (Keat, 2015). Similar results have been reported

by Sadia et al, in synthesis of CuNps using *Senna didymobotrya* root extract (Sadia et al., 2021).

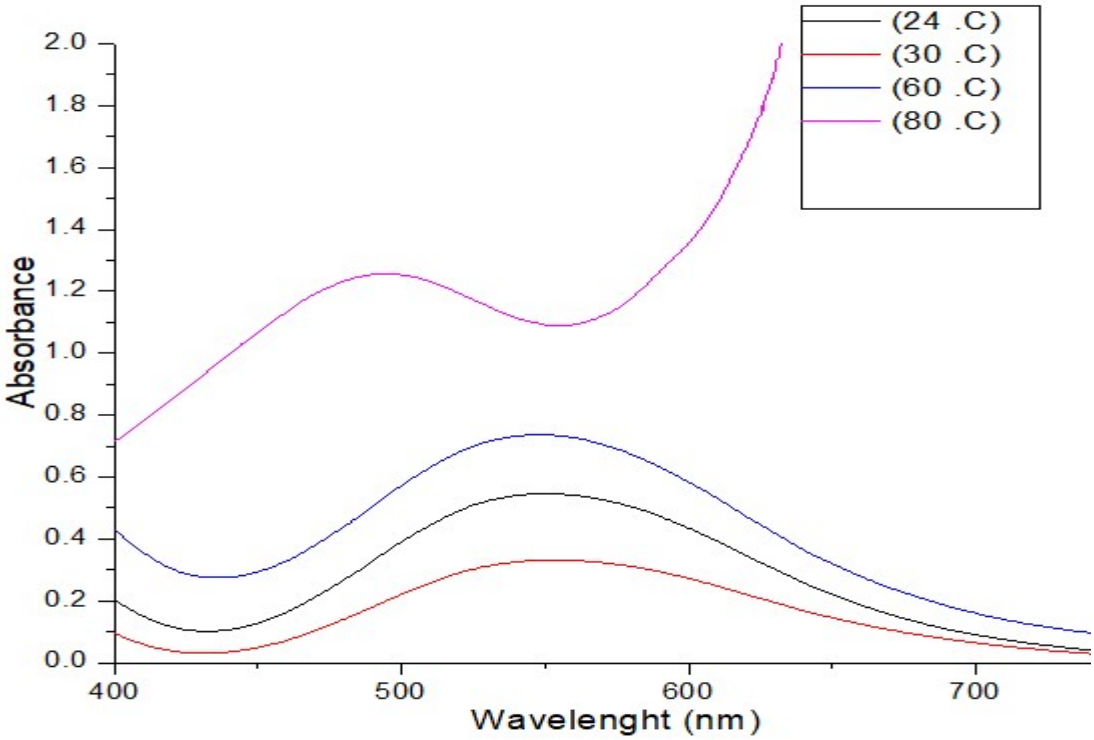

Figure 4.16: Effect of concentration of copper (II) sulphate on synthesis of copper nanoparticles.

4.3.3 Synthesis of Zinc Oxide Nanoparticles

Zinc Oxide nanoparticles were synthesized according to the method by Ezealisiji et al (Ezealisiji et al., 2019). The formation of zinc oxide nanoparticles was marked by appearance of grey suspension, which was analysed by FT- IR to determine the presence of ZnO Nps.

4.3.4 Synthesis of Magnetic Iron (III) Oxide Nanoparticles

Synthesis of magnetic iron (III) oxide was conducted in accordance with the procedure by Rashid (Rashid et al.,2020). Figure 4.17 exhibits results for the synthesis of magnetic iron

(III) Oxide nanoparticles, appearance of a black suspension marked the formation of magnetic iron (III) oxide. The nanoparticles could be seen attracted toward a magnet as black substance, indicating the presence of magnetic iron (III) oxide nanoparticles. These nanoparticles were analysed to determine the presence and properties of the nanoparticles in the resultant mixture.

Figure 4. 17: Image of magnetic iron (III) oxide placed near a magnet

4.4 Characterization of Nanoparticles prepared

4.4.1 UV-VIS Analysis

Optical properties of copper, silver and magnetic iron (III) oxide nanoparticles were determined using UV-VIS technique. Wavelength scan was carried out at a range of 200 nm-800 nm using Shimadzu UV-VIS spectrometer UV-1800 (Shimadzu, Japan).

4.4.1.1 UV-VIS Analysis of Silver Nanoparticles

The results for UV-VIS analysis of Silver nanoparticles are shown in figure 4.18. Maximum absorbance was obtained at 410 nm (Fig 4.18) confirming the presence of AgNp since it is reported that theyhave a maximum absorbance within 400 nm-475 nm (Jahan et al., 2021). AgNps with λ_{max} attained at 424 nm has been reported in green synthesis of AgNps using *Pedalium murex* leaf extract (Anandalakshmi et al., 2016). Singh et al synthesized silver nanoparticles using aqueous extracts from hibiscus leaf and attained λ_{max} attained at 416 nm (Singh et al., 2020), Liaqat et al reported a λ_{max} of 410-430 nm during green synthesis of AgNps using a mixture of plant extracts (*Terminalia arjuna and Eucalyptus camaldulensis*) (Liaqat et al., 2022).

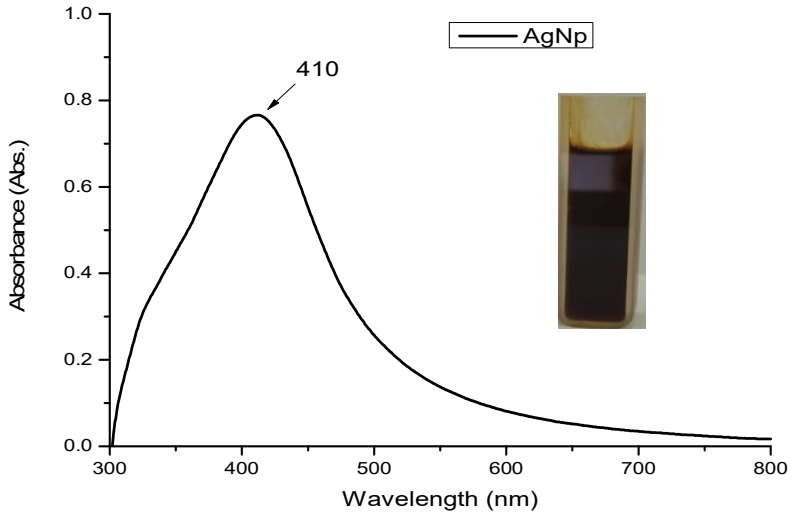

Figure 4. 18: UV-VIS wavelenght scan for silver nanoparticles (AgNp); inset shows a digital image of silver nanoparticles solution in a cuvette.

4.4.1.2 UV-VIS Analysis of Copper Nanoparticles

UV-VIS analysis of Copper nanoparticles scan 200 nm-800 nm was done using spectrometer (UV-1800 Shimadzu USA). A peak absorption band obtained in the visible region at 544 nm signified formation of copper nanoparticles. The results are presented in figure 4.19. According to Lukman, particles with a small size display single SPR band however anisotropic nanoparticles display two or more bands due to multiple excitation (Lukman et al., 2011). CuNps with SPR peak at 540 nm has been reported in synthesis of CuNps using one- pot thermal decomposition (Oscar et al., 2015).

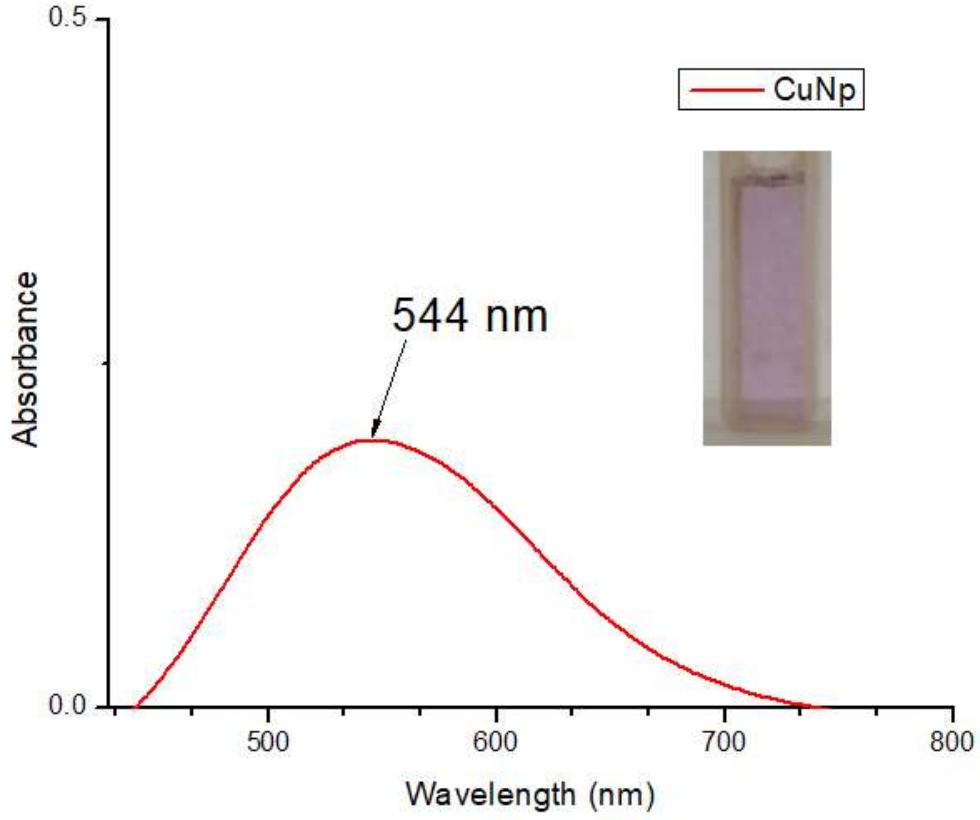

Figure 4. 19: UV-VIS wavelength scan for copper nanoparticles solution. The inset is a photograph of copper nanoparticles in a cuvette.

4.4.1.3 UV-VIS Analysis of Magnetic Iron (III) Oxide Nanoparticles

UV-Vis analysis on magnetic iron (III) oxide was carried out to determine the presence of the magnetic iron (III) oxide nanoparticles in the resultant solution at 0.5-1.5 hrs. Maximum absorbance at wavelength of 344 nm was attained after 60 minutes (Fig 4.20). The peak at 344 nm is slightly lower than the range of 350 nm-400 nm which has been reported for magnetic iron (III) oxide nanoparticle (Fatemi et al., 2018). This is attributed to the keratin capping agents which regulated the size of nanoparticles resulting in smaller particles with λ_{max} at lower wavelength due to bathochromic shift to shorter wavelength as the particle size decreases (Dang et al., 2011), (Jahan et al., 2021); (Lukman et al., 2011). When the ratio of Fe^{2+} :Fe^{3+} was increased beyond 0.02:0.01, a brown precipitate was formed, indicating that higher concentrations of Fe^{2+} and Fe^{3+} were not suitable for synthesis of magnetic iron (III) oxide nanoparticles.

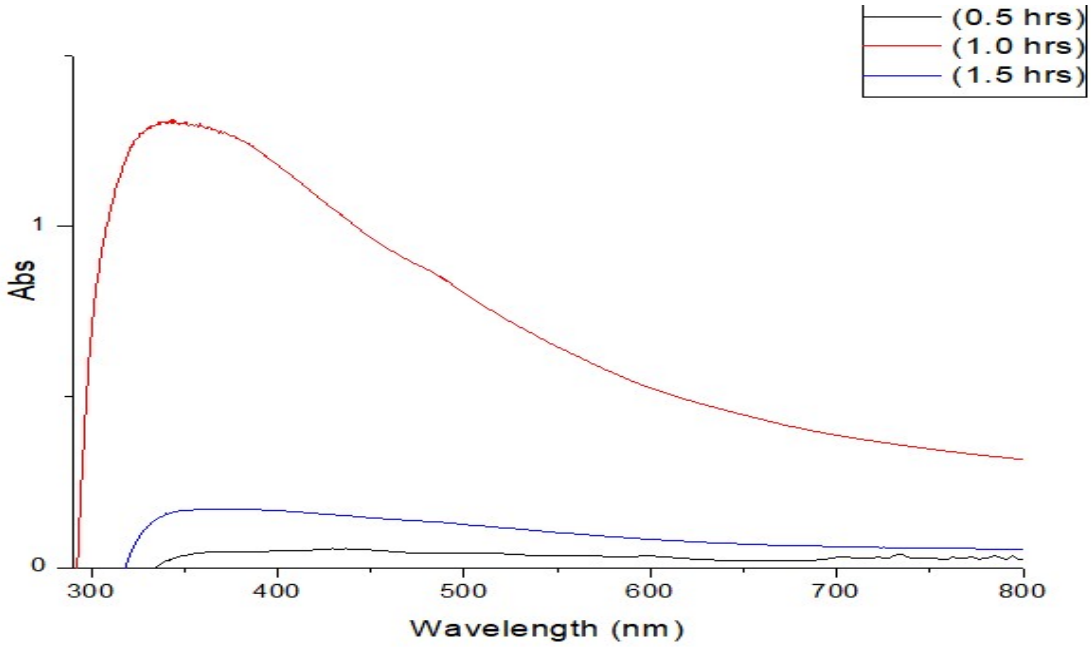

Figure 4. 20: UV-VIS analysis of magnetic iron (III) oxide at different intervals of time.

4.4.2 Fourier Transform Infrared Spectroscopy (FT-IR) Spectroscopy

Fourier Transform Infrared Spectroscopy (FT-IR) was done on the synthesized nanoparticles using IR. Affinity-1S Fourier Transform Infrared spectrophotometer was used to identify the functional groups involved in formation and stabilization of nanoparticles obtained.

4.4.2.1 Fourier-Transform Infrared Analysisof Silver Nanoparticles (FTIR).

Characterization of AgNps was done using Fourier-Transform Infrared Spectroscopy. The FT-IR spectrum in the wavenumber range 3000 cm^{-1} to 500 cm^{-1} is presented in figure 4.21. Characteristic bands of AgNps indicated the involvement of keratin biomolecules in formation of silver nanoparticles (Figure 4.21). The characteristic amide III band at 1217 cm^{-1} indicates C-O stretching (Kamarudin et al., 2017). The characteristic peak at 1369 cm^{-1} is attributed to C-H bending in keratin biomolecules. Amide II band was observed at 1533 cm^{-1} is this is attributed to C-N stretching coupled with N-H bending (Ashraf et al., 2016). Amide I band at 1739 cm^{-1} indicated C=O stretching in the carboxyl group (Cheng et al., 2016).

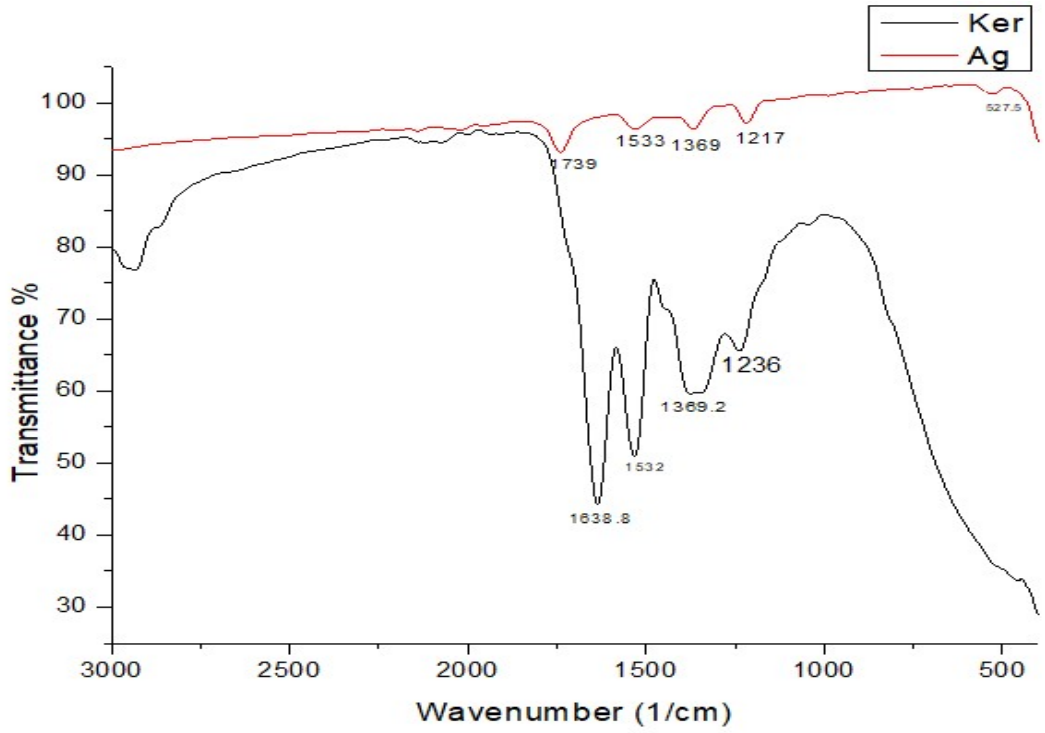

Figure 4. 21: FT-IR spectrum for Ag-Ker nanoparticles

4.4.2.2 Fourier-Transform Infrared Spectroscopy Analysis of Copper Nanoparticles

FT-IR spectrum of synthesized copper nanoparticles in the wavenumber range 4500 cm^{-1}-500 cm^{-1}(Fig 4.22) indicated the involvement of keratin biomolecules on CuNps formation. The absorption band at 574 cm^{-1} is due to copper nanoparticles formed (Thiruvengadam et al., 2019). Absorption peak observed at 1397 cm^{-1} is associated with C-H bending vibrations in the biomolecules (Amaliyah et al., 2020). Amide 1 band obtained at 1646 cm^{-1} is associated with C=O stretching(Vahur et al., 2016). While the absorption band obtained at 3150 cm^{-1} corresponds to N-H or O-H stretching (Göl et al., 2020).

Absorption band at 1397 cm^{-1} is due to O-H stretching. The absorption band obtained at 1118 cm^{-1} is associated with C-O stretching (Amaliyah et al., 2020).

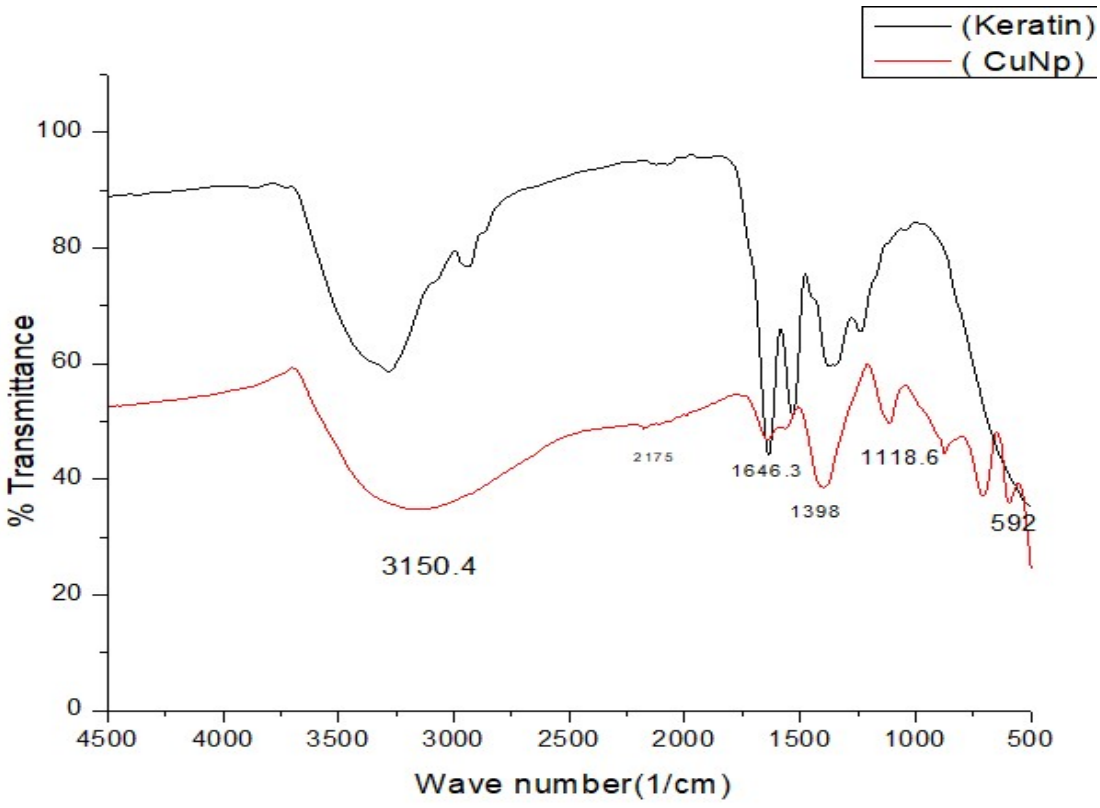

Figure 4. 22: FT-IR spectrum for copper nanoparticles

4.4.2.3 Characterization of Magnetic Iron (III) Oxide Nanoparticles using Fourier-Transform Infrared Spectroscopy (FTIR).

The FTIR spectrum for magnetic iron (III) oxide nanoparticles in the range of 4500 cm^{-1} to 500 cm^{-1} is presented in figure 4.23.

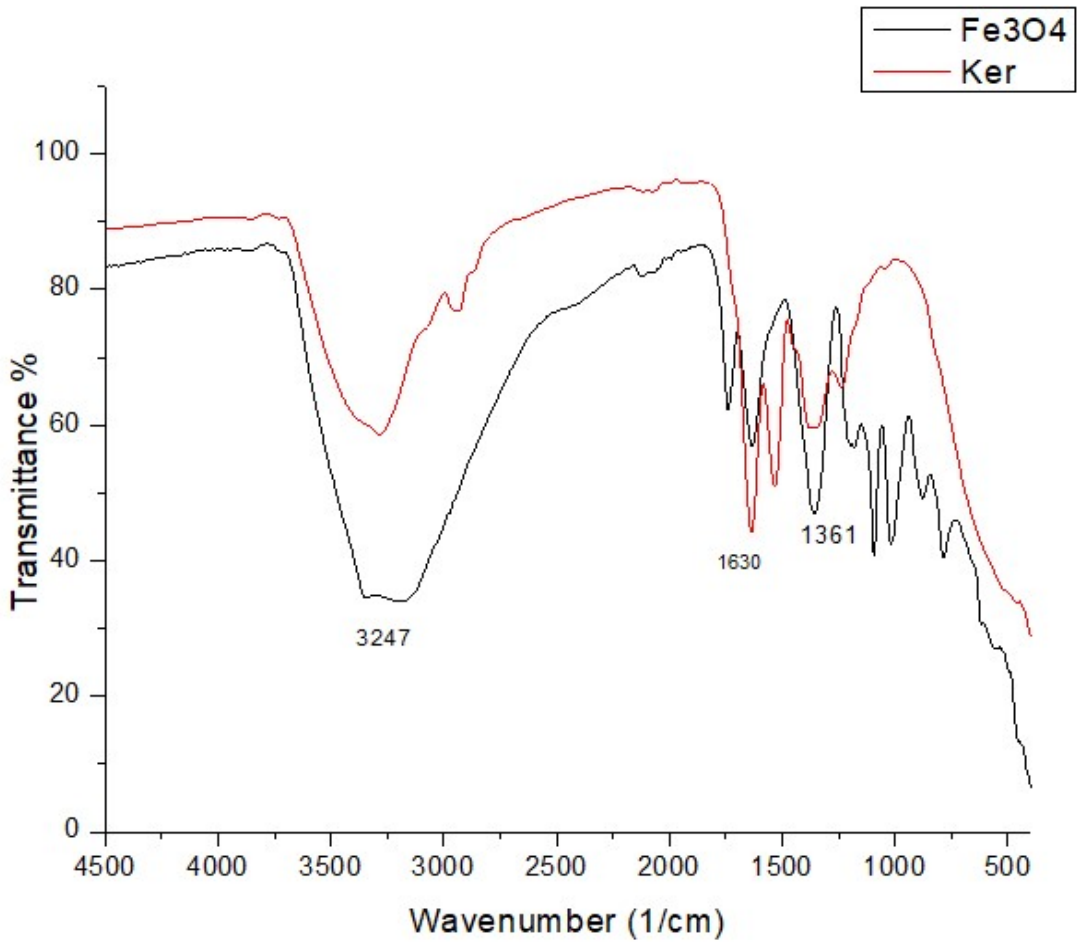

Figure 4. 23: FT-IR spectrum for Fe_3O_4-Ker nanoparticles

The FT IR spectrum of Fe_3O_4 indicates involvement of keratin biomolecules in capping of Fe_3O_4 nanoparticles. The broad band at 3247 cm^{-1} is due to O-H stretching (Amaliyah et al., 2020). Characteristic band formed at 1630 cm^{-1} is associated with C=O extension (Amide I) range (Berechet et al., 2020). The band at 1352.8 cm^{-1} is due to C-H bending (Ashraf et al., 2016).

4.4.2.4 Fourier-Transform Infrared Spectroscopy of Zinc Oxide Nanoparticles

FT-IR spectrum of ZnO nanoparticles in the wavenumber range from 4000 cm^{-1}– 500 cm^{-1} is presented in figure 4.24.

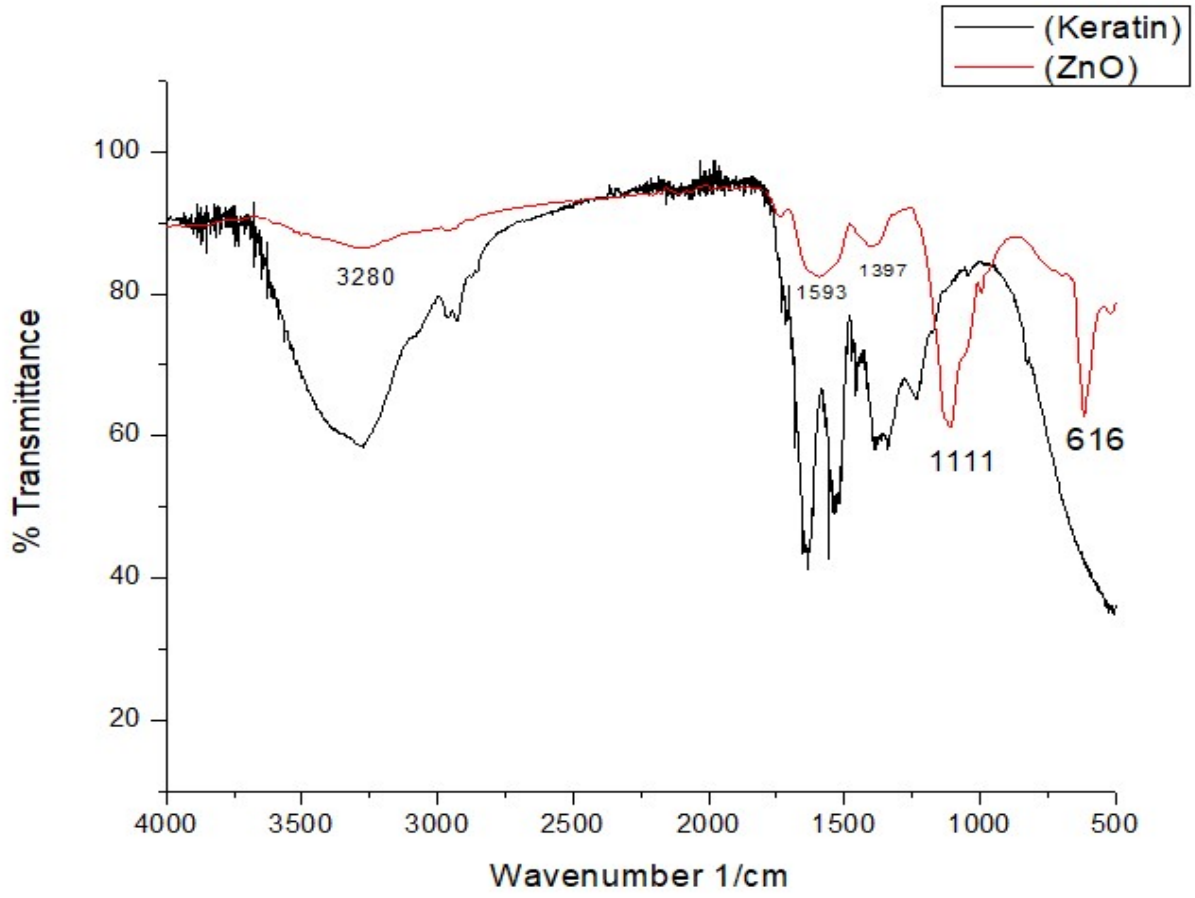

Figure 4.24: FT-IR spectrum of zinc oxide nanoparticles

The ZnO FT-IR spectrum indicates the involvement of functional groups from keratin biomolecules. The peak formed at 615 cm^{-1} is due to Zinc oxide hexagonal phase (Muhammad et al., 2019). Distinctive band formed at 1111 cm^{-1} results from C-O stretching vibration (Amaliyah et al., 2020). Distinctive band at 1397 cm^{-1} is associated with C-H bending vibration (Amaliyah et al., 2020). Absorption band at 1593 cm^{-1} is due to N-H group (Thiruvengadam et al., 2019) and the distinctive band formed at 3280 cm^{-1} is associated with O-H stretching (Singh et al., 2020).

4.4.3 XRD Analysis Results

XRD diffraction results for copper are presented in figure 4.25. The peaks were allotted in assessment with standard powder diffraction card of the joint committee on powder diffraction standards (Bhavyasree and Xavier, 2022).

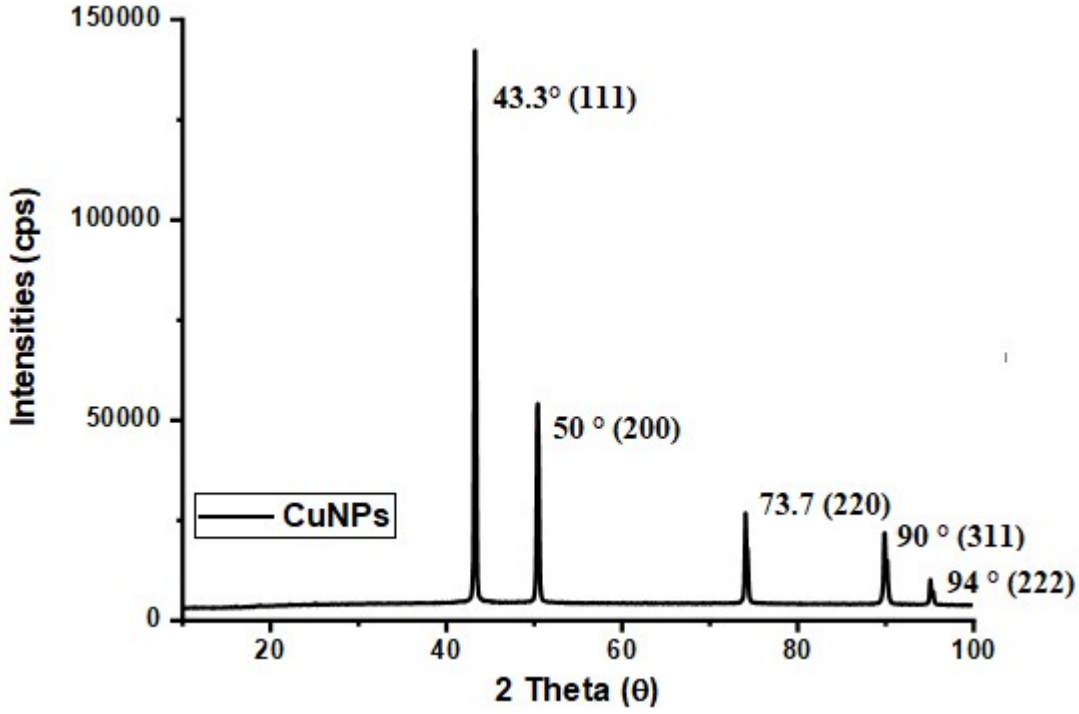

Figure 4.25: XRD pattern for copper nanoparticle**s**

The results indicate an intense peak at 43.3^{o} which corresponds to fcc plane (111). This matches fcc of bulk copper (Suramwar et al., 2016). The peak at 50^{o} corresponds to (200) fcc structure. The peak at 73.7^{o} corresponds to (220) fcc plane. Small peaks at 90^{o} and 94.7^{o} matched fcc planes (311) and (222) respectively. These peaks matched fcc structure of copper (Thiruvengadam et al., 2019).

4.4.4 SEM Analysis

SEM analysis was carried out on CuNps to determine the surface morphology and the size of nanoparticles, the results are presented in figure 4.26. SEM image for the CuNps presented at a magnification of 47700X (Fig 4.26 a) indicates non agglomerated spherical shaped CuNps.

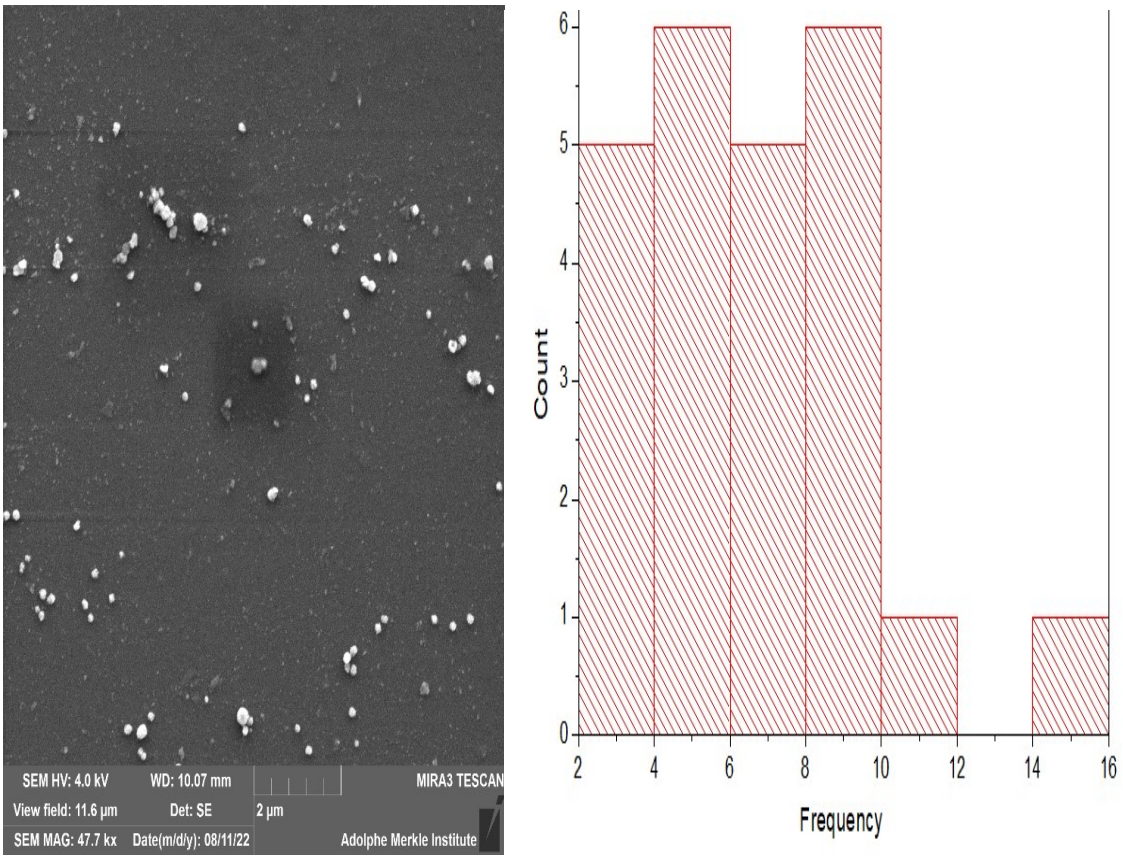

(a) (b)

Figure 4.26: (a) SEM image for CuNps at 47700 × magnification scale in the size range of 2000 nm (b) Image size distribution for CuNps

The dimensions dispersal analysis displays that the dimensions range for copper nanoparticles attained was within the range of 2 nm-16 nm.

4.5 Application of Nanoparticles in Removal of Dyes in Aqueous Solution

4.5.1 Maximum Absorbance Wavelength for Dyes

The wavelength at which maximum absorbance in UV-VIS analysis of the dye was attained through a wavelength scan of the working solution of the dyes from 300 nm-700 nm using UV-VIS spectrometer UV-1800 Shimadzu model. The wavelength at which maximum absorbance of the dye was attained (λ_{max}) was used in determining absorbance of the dyes during quantification of colorant removed by nanoparticles from aqueous medium. Plots of absorbance against optical wavelength in the visible region for methylene blue are presented in figure 4.27. Maximum peak absorbance of methylene blue was attained at wavelength of 664 nm, hence the UV-VIS spectrophotometer was set at 664 nm for absorbance measurements during adsorption process. The peak is formed due to n – π* transition with –N=N− in the is due to MB^+ monomer of the MB dye (Mrunal et al., 2019). The λ_{max} value was comparable with 665 nm reported in literature (Li etal., 2022).

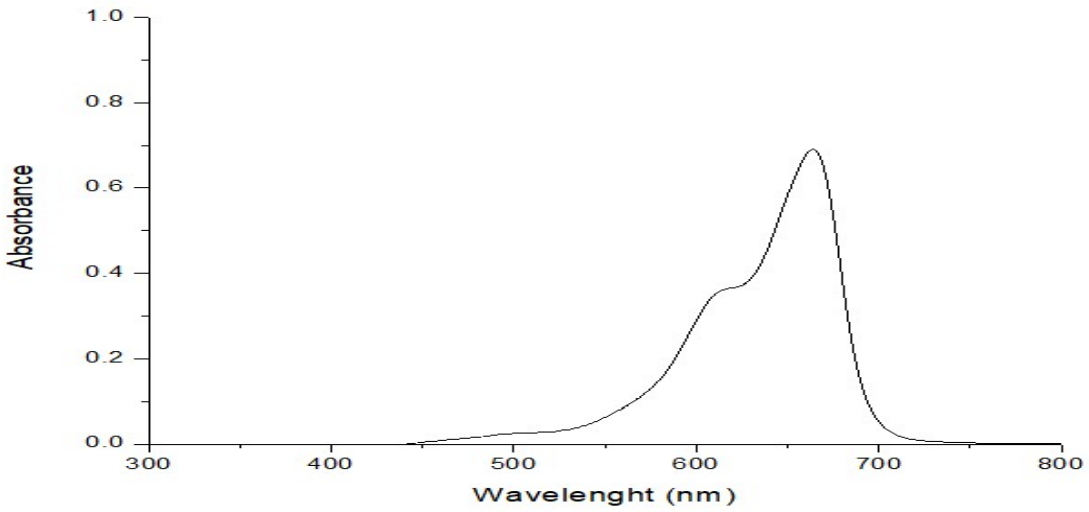

Figure 4. 27: UV-VIS wavelength scan for methylene blue dye

A smaller peak formed at wavelength between 600 nm and 625 nm is due to absorption of visible light by (MB_2^{2+}) dimer (Zubrik et al., 2023).

The procedure was repeated to determine the UV-VIS maximum absorbance for crystal violet colorant. The results are presented in figure 4.28. The maximum absorbance was attained at 588 nm due to symmetric monomer and a shoulder peak at 550 nm due to distorted monomer. The peaks were due to π –π * in the crystal violet molecules (Noimark et al., 2013). Azo dyes contains an azo group (–N=N−) joining C atoms which are SP^2 hybridised in the visible region due to π–π* transitions. The electron transitions results in maximum aabsorbance (Sıdır et al., 2011). The peaks The results were comparable with 590 nm reported during investigation of removal of crystal violet dye in aqueous solution using *Rhizophora mucronata* stem-barks (Oloo et al., 2020). The λ_{max} was used in UV-Visible light analysis of residual dye during investigation of various parameters.

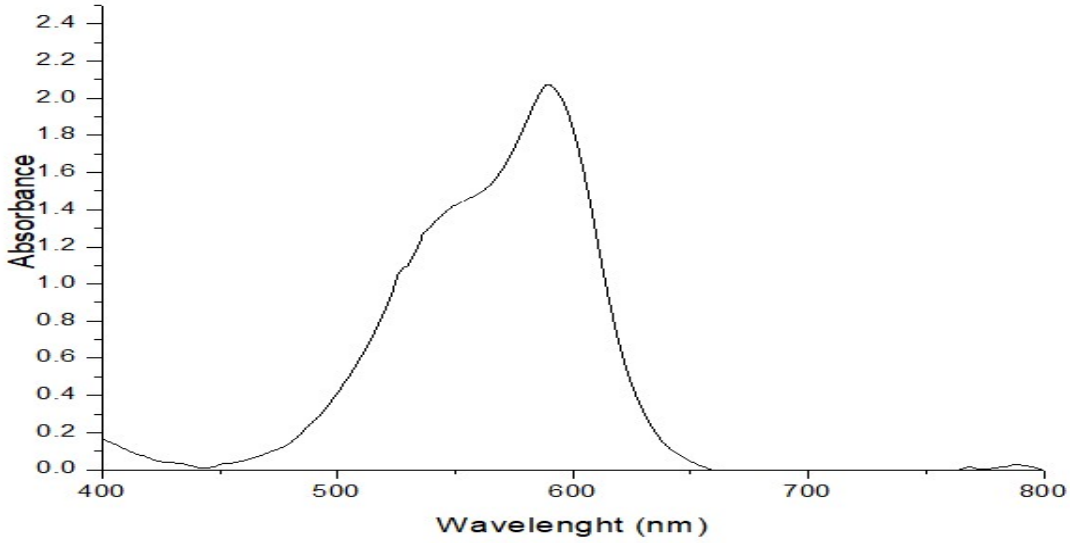

Figure 4. 28: UV-VIS wavelength scan for crystal violet colorant

4.5.2 Standardization Curves

Standardisation curves are a reference for determining the concentrations corresponding to recorded absorbance. By comparing investigational records of absorbance with the standard curve equation, the residual colorant concentrations were determined. Dilute solutions of concentrations 0.5 mgL^{-1} up to 5 mg L^{-1} prepared by diluting the stock solution of methylene blue were analysed using UV-VIS spectrophotometer set at 664 nm. The results were used to produce a standard curve presented in figure 4.29. A straight line with R^2 value of 0.999 was attained, signifying a good correlation coefficient for various methylene blue concentrations and the corresponding absorbance.

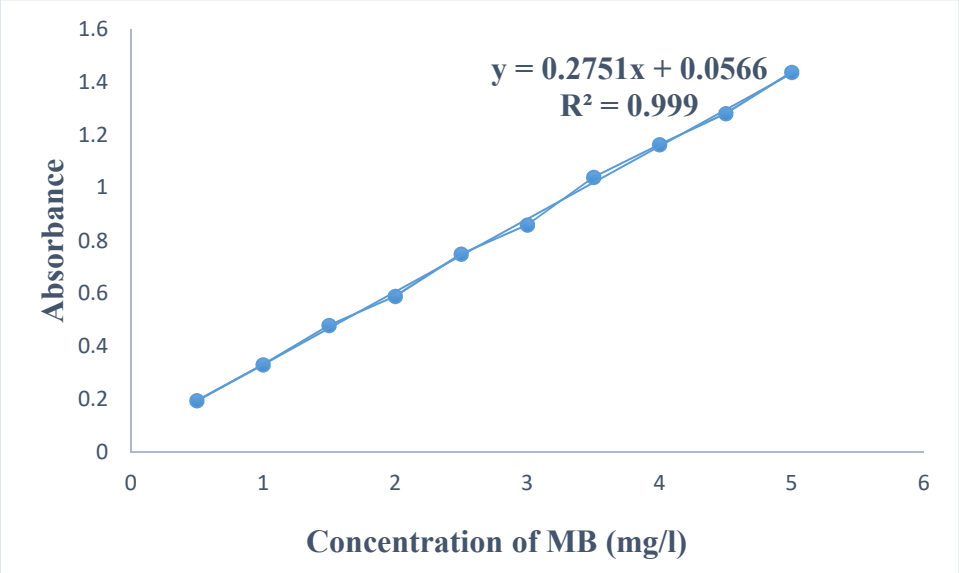

Figure 4. 29: Regulation curve for methylenebluedye

Regulation curve for crystal violet colorant was obtained by preparing dilute solution with concentration range of 5 ppm to 0.5 ppm from crystal violet stock solution and measuring the corresponding absorbance using UV- VIS spectrophotometer. The standard curve

presented in figure 4.30, was obtained by plotting a graph of absorbance against concentration of the dye.

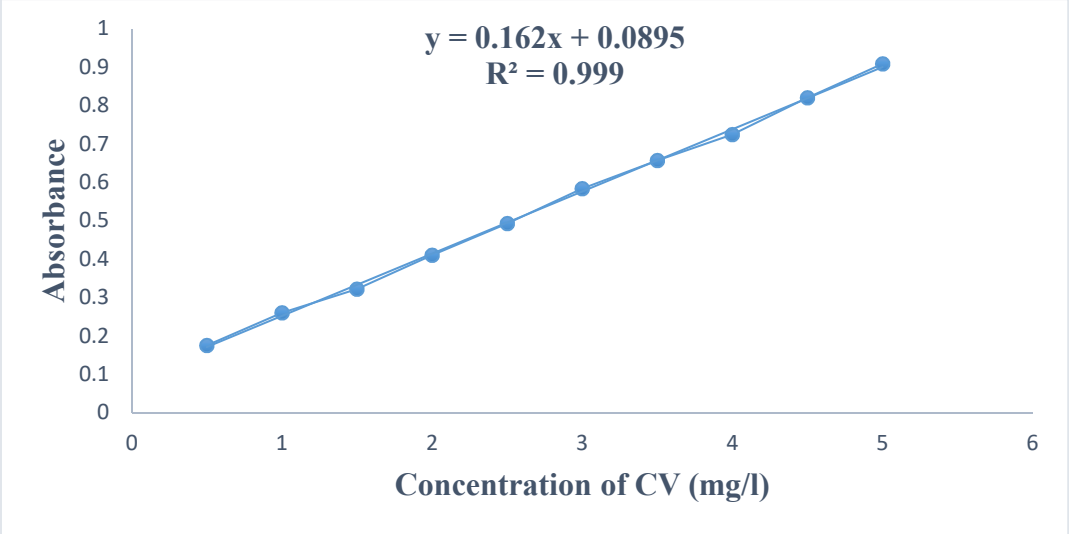

Figure 4. 30: Regulation curve for crystal violet

4.5.3 Effect of Contact Time on Adsorption of Methylene Blue and Crystal Violet Dyes using Nanoparticles

Interaction period between adsorbent and adsorbate is crucial for cost approximation in designing large scale industrial adsorption system (Cheruiyot et al., 2019). In this investigation, influence of time was explored by monitoring variations in concentration of methylene blue dye adsorbed using copper nanoparticles with time from 0 min to 390 min at 25 °C. Control experiment was conducted under similar conditions by monitoring the changes in concentration of methylene blue without copper nanoparticles. Effect of time on crystal violet dye adsorption using magnetic iron (III) nanoparticles was investigated from 0 min to 10 min at 25 °C and the influence of time on crystal violet adsorption using silver nanoparticles was examined from 0 min to 200 min. Control experiment on adsorption of crystal violet was conducted by monitoring the changes in CV dye

concentration with time due to self-degradation. Dye removal curve for methylene blue % removal with time is presented in figure 4.31.

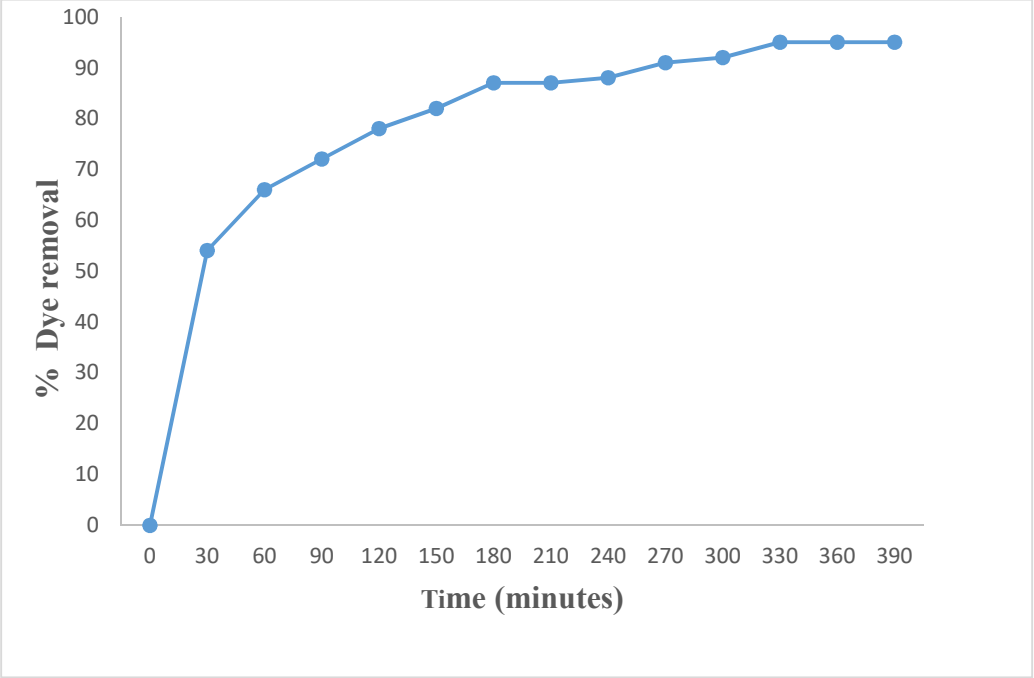

Figure 4.31: Effect of time on adsorption of methylene blue by copper nanoparticles (MB 5 ppm, CuNp 8mg/10 ml at 25°C).

Quantity of dye removed increased with increase in time. Rate of adsorption was high at the beginning of the experiment with 54 % of the methylene blue adsorbed within the first 30 minutes. Equilibrium was attained after 330 minutes with 95 % of the dye removal attained. Higher adsorption rate at the beginning of adsorption process is due to large surface area on the nanoparticles. At equilibrium, the adsorbent surface became saturated. At this point, the remaining unoccupied adsorption sites can't be occupied due to electrostatic repulsion between colorant molecules on adsorbent surface and the residual dye molecules in solution (Wanyonyi et al., 2014). The results were similar to other research reports on changes in adsorption rates for various dyes using nanoparticles (Zhang

et al., 2020). From the previous results the percentage dye removal and the time taken to attain equilibrium varied due to the difference in nanoparticles used and the functional groups on nanoparticles which influence interaction between nanoparticles and the colorant molecules (Mohammad and Atassi, 2020). Igwebe et al reported equilibrium time of 15 min with 71.17 % removal of methylene blue using Ho-CaWO4 nanoparticles (Igwegbe et al., 2019). In other findings, Zeebare et al reported an optimum adsorption time of 20 minutes with 92 % removal efficiency of methylene blue using copper nanoparticles bio engineered using *Malva sylvestris* plant extract (Zeebaree et al., 2021). Control experiment conducted to determine the rate of self-degradation of MB without addition of CuNps (figure 4.32).

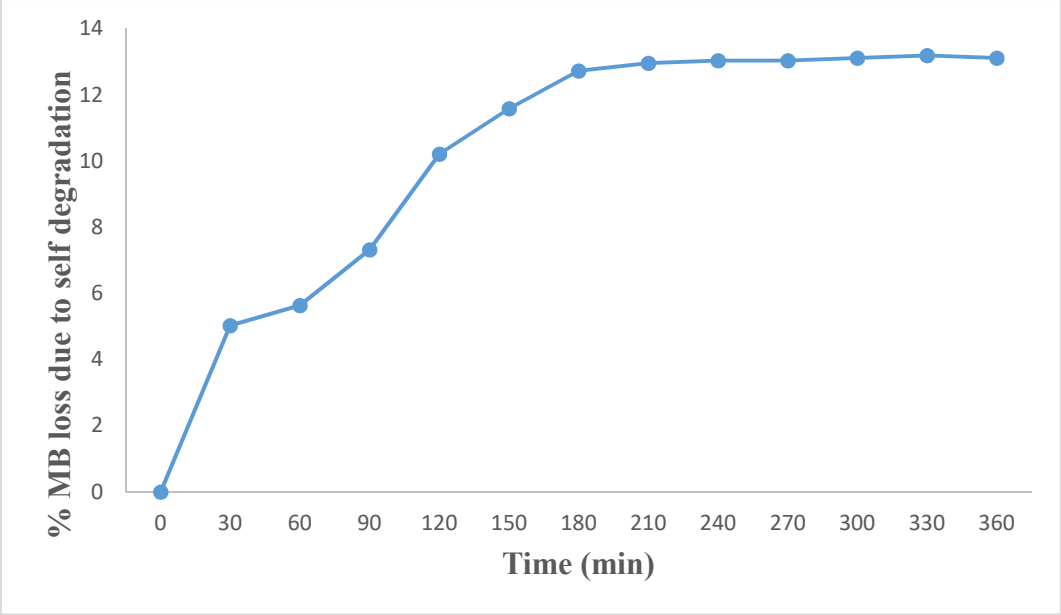

Figure 4. 32: Effect of time on self degradation of methylene blue without copper nanoparticles (MB 5 ppm at 25 °C).

The results indicated 13.1 % loss of methylene blue after 360 min. From other studies, Sinha and Ahmaruzzaman reported that there was no self-degradation of methylene blue when investigating adsorption of MB using CuNps after monitoring the dye for 135 min (Sinha and Ahmaruzzaman, 2015). Zuo et al., reported a small self-degradation of MB in absence of nano-TiO_2after 150 minutes (Zuo et al., 2014). Sutanto et al., reported self-degradation of 13 % on MB after 45 minutes in presence of sunlight (Sutanto et al., 2020). The self-degradation rate for MB is influenced by intensity of UV or Visible light radiations and presence of radicals such as hydroxyl radicals (Cabrera et al., 2020).

The contact time influence on adsorption of crystal violet using silver nanoparticles is presented in figure 4.33. The amount of dye removed from the dye solution increased with increase in contact time. The rate of adsorption was large at the start of the experiment, with 77 % of the dye removed within the first 20 minutes. Adsorption progression attained equilibrium after 60 minutes, with 97.9 % dye removal efficiency.

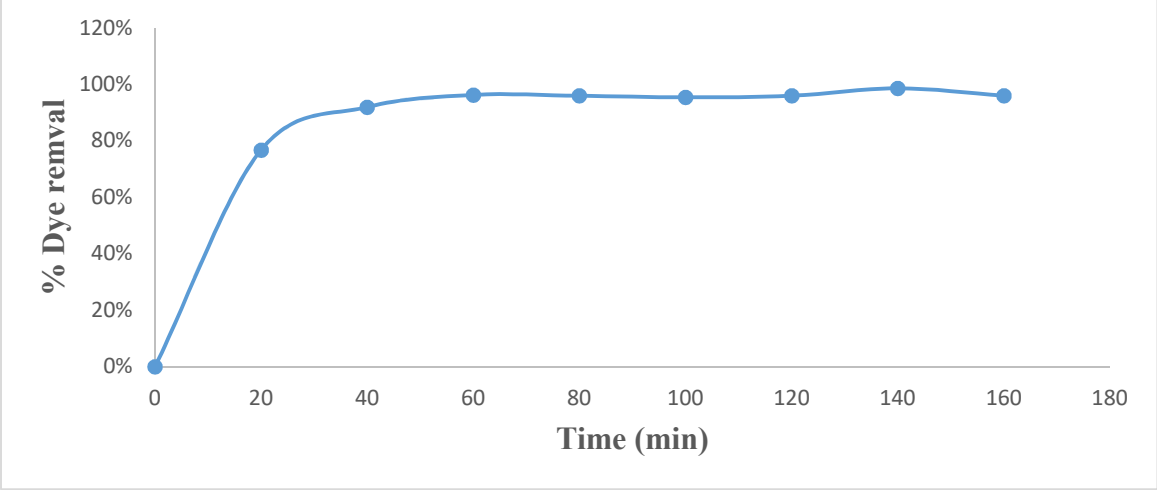

Figure 4.33: Effect of time on adsorption of crystal violet using silver nanoparticles (Crystal Violet 10 ppm, AgNp 8 mg/10 ml at 25°C).

Similar results were reported on other by other researchers (Cheruiyot et al., 2019).

Generally, a high rate of adsorption at the onset of the experiments was due to a large surface area of the nanoparticles and many adsorption sites (Sabna et al., 2016). More and more dye molecules get attached to the nanoparticles adsorbents until equilibrium point is attained when the adsorption sites on the nanoparticles became saturated (Kuang et al., 2020). Control experiment results indicated a loss of 30.3 % in crystal violet concentration due to self-degradation (figure 4.34).

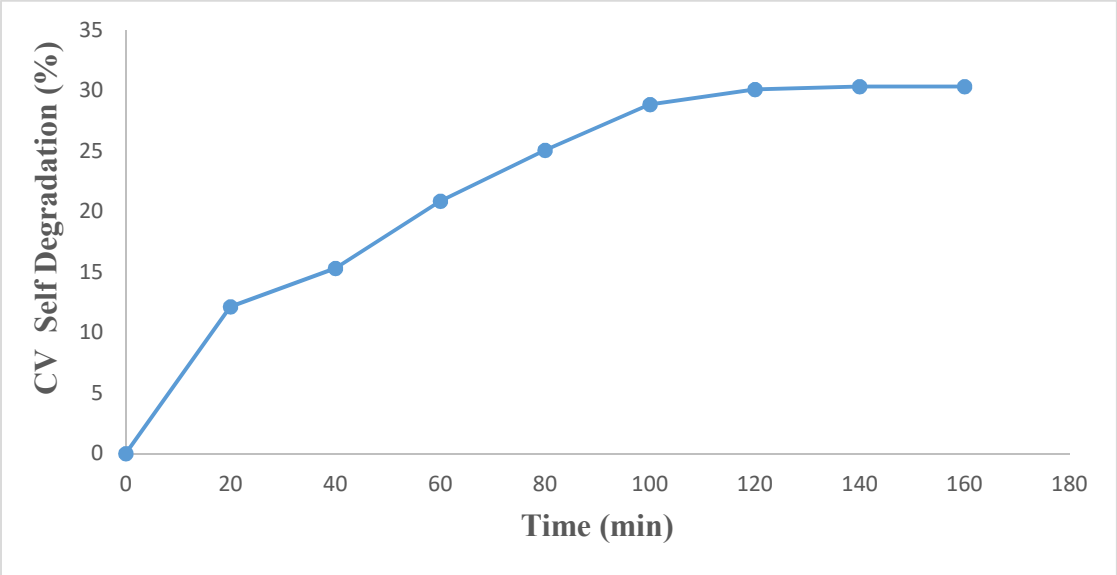

Figure 4.34: Effect of time on self degradation of crystal violet without silver nanoparticles (CV 10 ppm at 25 °C).

Influence of contact time on adsorption of crystal violet colorant using magnetic iron (III) oxide is presented in figure 4.35. Quantity of crystal violet dye adsorbed increase with increase in contact time. Equilibrium was attained after 8 minutes, when the adsorption capacity of the nanoparticles q_e is 12.39 mg/g.

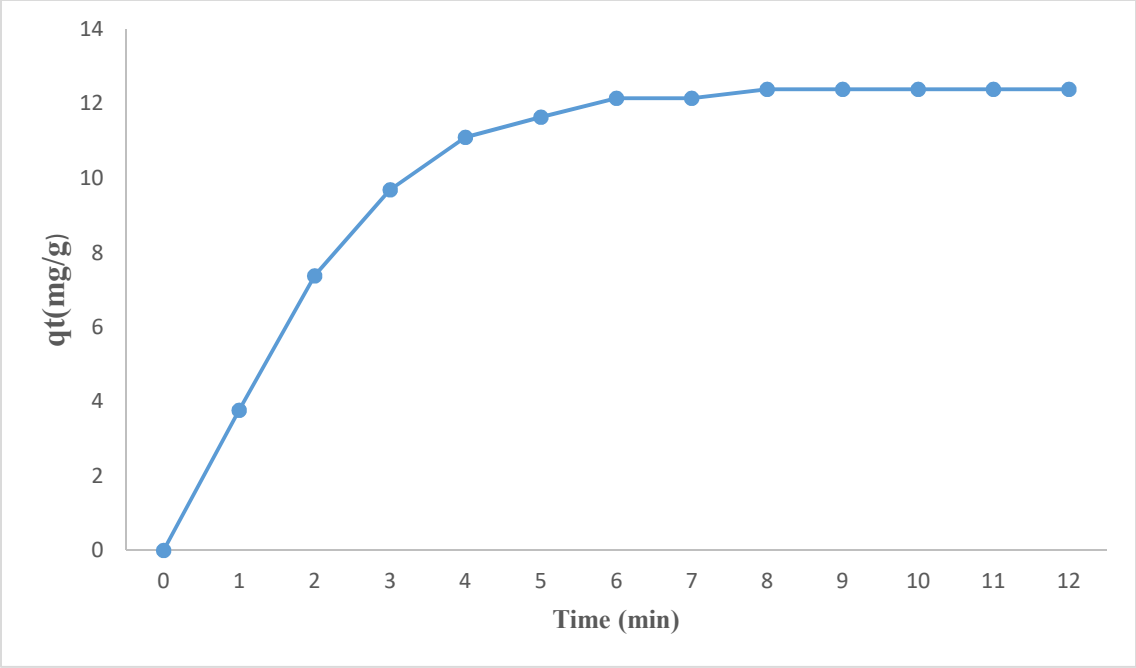

Figure 4.35: Effect of time on adsorption of crystal violet by magnetic iron (III) oxide nanoparticles (Crystal Violet 10 ppm, magnetic iron (III) oxide nanoparticles 6 mg/10 ml at 25 °C).

Efficiency of the crystal violet dye removal was 99.2 %. At this point the nanoparticles surface becomes saturated, hence no more dye molecules will be removed from colorant solution (Cheruiyot et al., 2019). A larger quantity of dye was removed at the beginning of the experiment, with 59 % of the dye adsorbed within the first 2 minutes. This substantiates a greater number of attachment sites on the nanoparticles (Sabna et al., 2016). When equilibrium has been attained, any remaining adsorption sites will no longer take any dye molecules due to electrostatic forces of repulsion between molecules bound on occupied binding sites on the surface of nanoparticles and the dye molecules within the dye solution (Wanyonyi et al., 2014). This is similar to results which have been reported on adsorption of various dyes (Kuang, et al., 2020).

4.5.4 Effect of Adsorbent Dose

Dosage of the adsorbent influences the quantity of accessible attachment sites on adsorbent surface, thus affecting adsorption rates and capacity. Effect of dosage was investigated on adsorption of methylene blue dye using copper (1mg/10 ml-10 mg/10 ml) and the results are presented in figure 4:36.

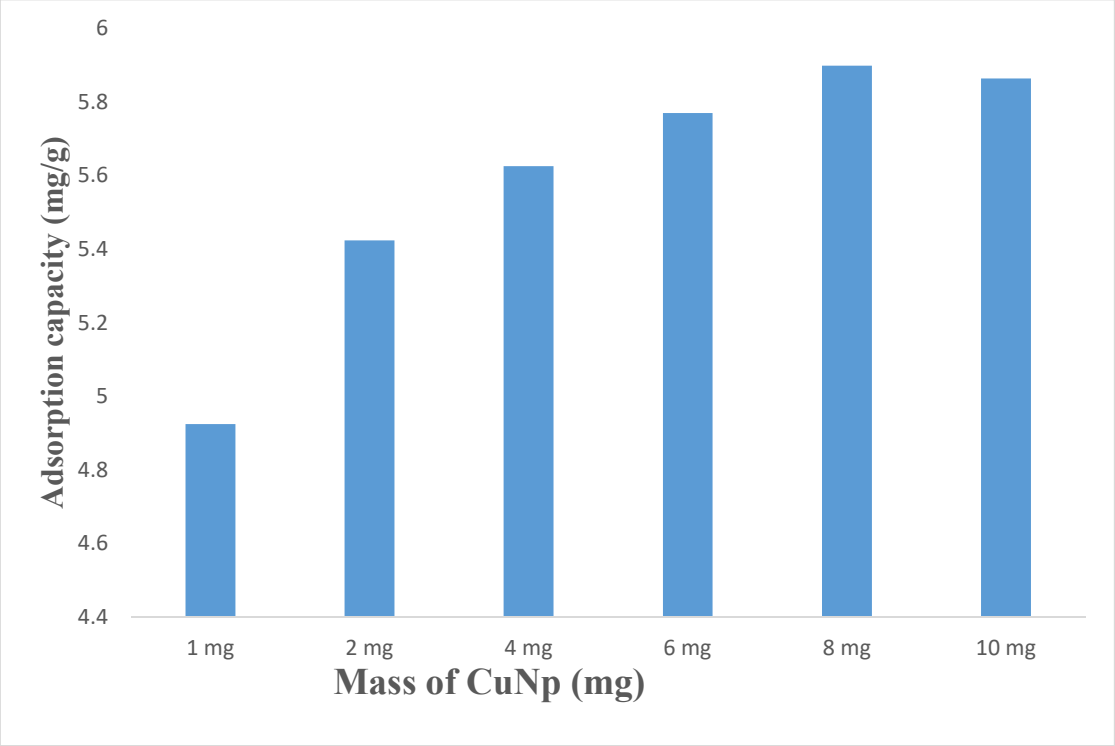

Figure 4. 36: Effect of amount of copper nanoparticles on adsorption of methylene blue dye (MB 5ppm, 10 ml at 25 °C).

Efficiency of methylene blue removal increased with increase in quantity of copper nanoparticles used. The efficiency of the dye removal at equilibrium increased from 4.925 mg/g to 5.899 mg/g when the quantity of copper nanoparticles was increased from 1 mg/10 ml to 8 mg/10 ml. Efficiency of dye removal decreased with further increase in amount of nanoparticles to 5.864 mg/g when 10 mg/10 ml of CuNp was used. Effect of quantity of

AgNps on adsorption of crystal violet colorant was investigated using silver nanoparticles (2 mg/10 ml-12 mg/10 ml), the findings are presented in figure 4:37.

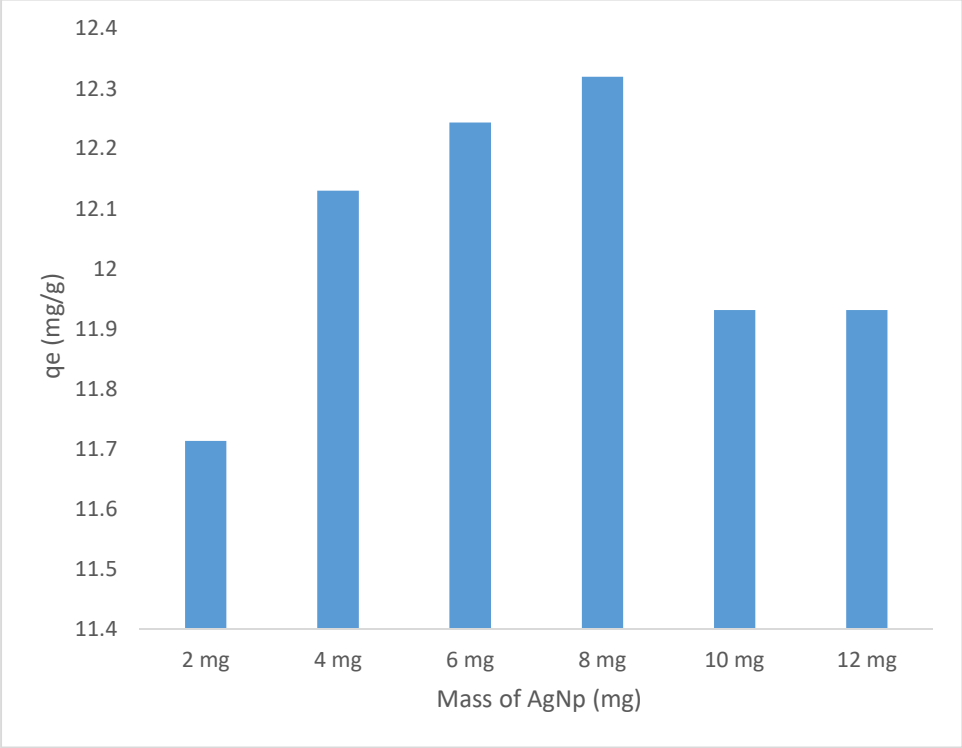

Figure 4. 37: Effect of dosage on adsorption of crystal violet by silver nanoparticles (Crystal violet 10 ppm, 10 ml at 25 °C).

Amount of dye removed first increased with increase in amount of nanoparticles used, followed by a decrease in adsorption capacity when dosage used exceeded 8 mg (figure 4.33). A rise in amount of dye removed with increase in amount of nanoparticles could be due to increase in surface area which provides sufficient adsorption sites (Wu, 2017). Effect of quantity of Fe_3O_4 on adsorption of crystal violet using magnetic iron (III) oxide (1 mg/10 ml-8 mg/10ml) was investigated; the results are presented in figure 4.38.

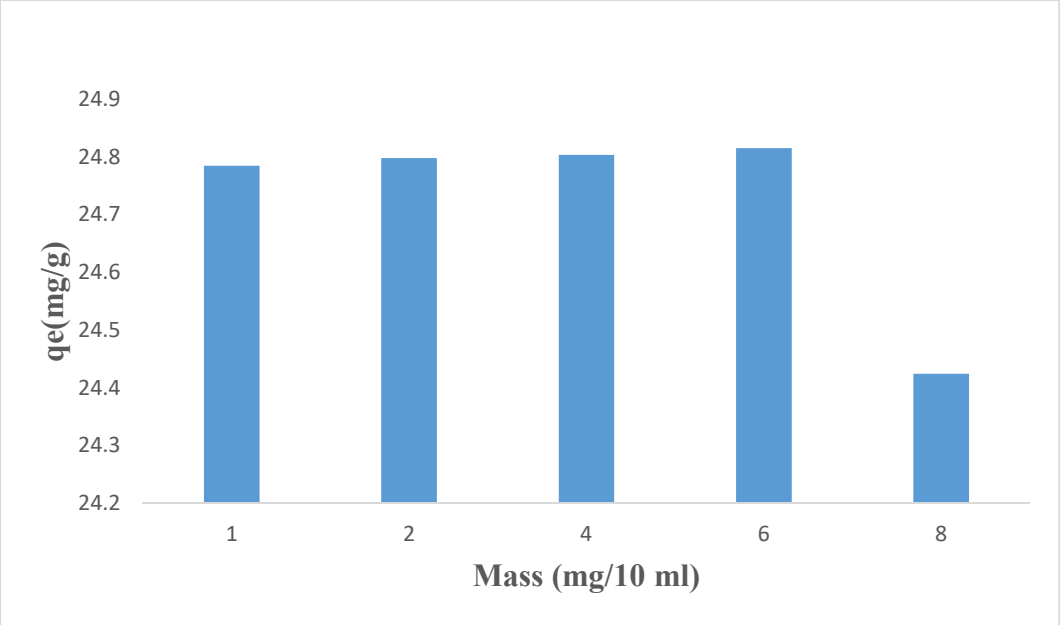

Figure 4.38: Effect of dosage on adsorption of crystal violet by magnetic iron (III) nanoparticles (Crystal violet 20 ppm, 10 ml at 25 °C).

A slight increase in adsorption capacity from 24.78 mg/g to 24.815 mg/g was observed when the dosage of Fe_3O_4 was increased from 1 mg/10 ml to 6 mg/10 ml. A decrease in adsorption capacity was observed with further increase in dosage of the nanoparticles. Adsorption capacity of the nanoparticles increased with increase in quantity of nanoparticles until saturation is attained. This is due to increased number of adsorption sites and adsorption bores as the quantity of adsorbent is increased (Kuang, et al., 2020). Adsorption capacity decreased with further increase in dosage due to aggregation of adsorbent particles, decreasing surface area of the adsorbent. Aggregation results in overlying of binding sites lowering the number of adsorption sites and increased length of diffusion path (Sabna et al., 2016).

4.5.5 Effect of Preliminary Dye Concentration

Preliminary dye concentration affects the extent of driving force for mass transfer of dye molecules to adsorbent binding sites influencing the quantity of dye removed (Srivastava and Choubey, 2021). Preliminary concentration influence on adsorption of methylene blue and crystal violet dyes using nanoparticles was explored by varying preliminary methylene blue dye and crystal concentration. The preliminary colorant concentrations of 0.625 ppm, 1.25 ppm, 2.5 ppm, 5 ppm, 10 ppm and 20 ppm of crystal violet were used to examine the influence on adsorption using silver nanoparticles. Quantity of the crystal violet colorant adsorbed by AgNp increased with increase in initial preliminary dye concentration (figure 4.39).

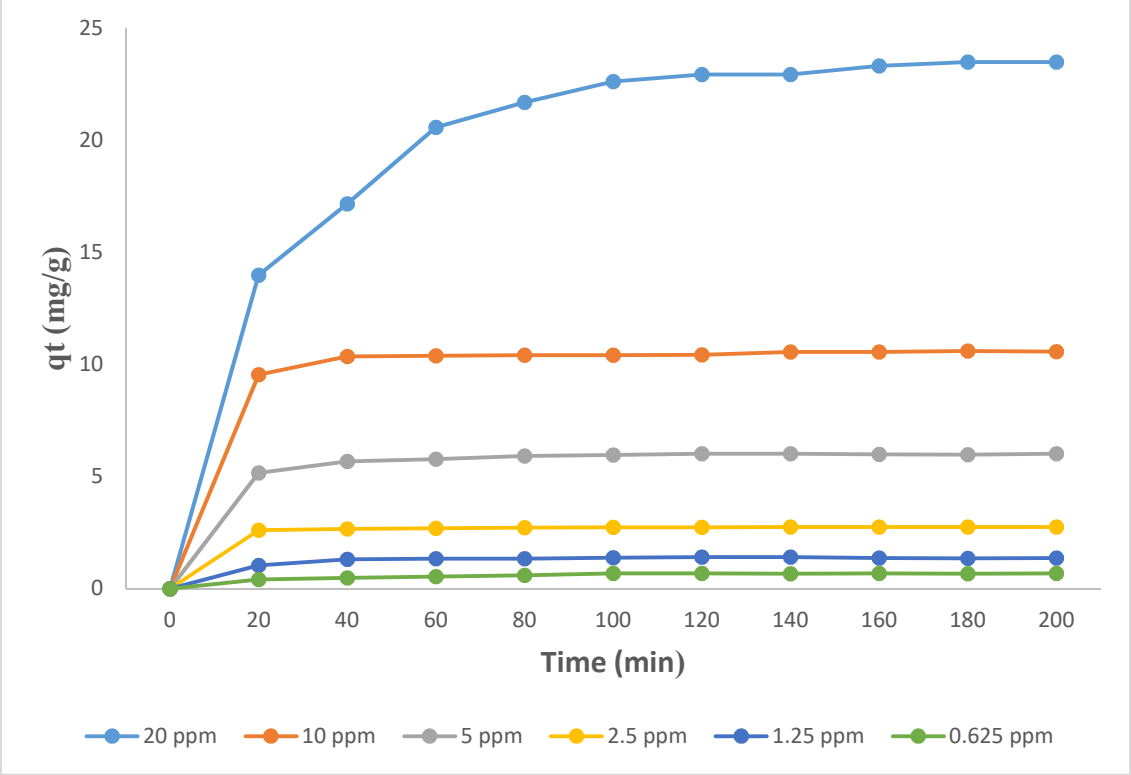

Figure 4.39: Effect of initial concentration on adsorption of crystal violet by silver nanoparticles (Silver nanoparticles 8 mg/10 ml at 25 °C)

From the results quantity of crystal violet adsorbed per unit mass of AgNp at equilibrium q_e increased from 0.6867 to 23.50 mg/g when the concentration of crystal violet was raised up from 0.625 ppm to 20 ppm. Exploration on adsorption of methylene blue using CuNp was carried out using preliminary methylene blue colorant concentration of 0.625 ppm, 1.25 ppm, 2.5 ppm, 5 ppm and 10 ppm, the findings are presented in figure 4.40.

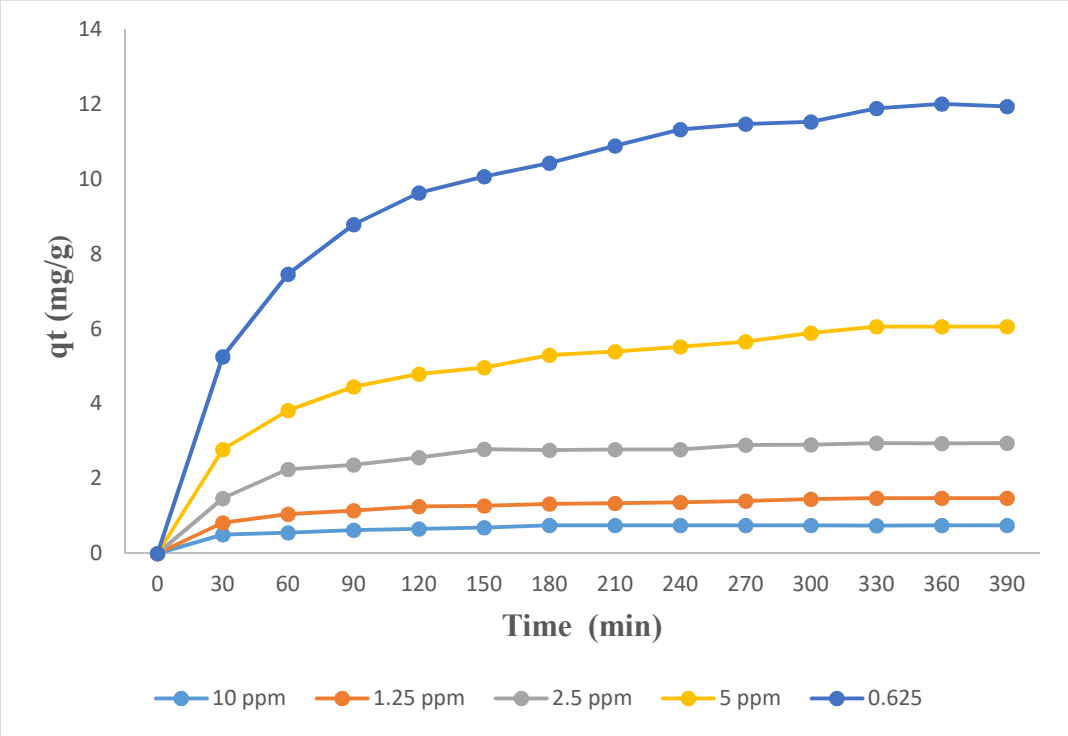

Figure 4. 40: Effect of initial dye concentration on removal of methylene blue by copper nanoparticles (Copper nanoparticles 8 mg/10 ml of the dye at 25°C).

Quantity of methylene blue adsorbed per unit mass of CuNp at equilibrium increased from 0.75217 mg/g to 12.01 mg/g when the initial concentration of methylene blue was increased from 0.625 ppm to 10 ppm. When lower initial concentration was used,

equilibrium was attained within a shorter time. For instance when 0.625 ppm was used, equilibrium was attained after 180 minutes, while adsorption process attained equilibrium after 360 minutes when 10 ppm was used. Similar results have been reported on removal of methylene blue using activated carbon (Kuang et al., 2020).

Studies on adsorption of crystal violet using magnetic iron (III) oxide was explored using initial concentrations of 0.625 ppm, 1.25 ppm, 2.5 ppm, 10 ppm and 20 ppm. The results are accessible in figure 4.41. From the results, maximum adsorbed crystal violet molecules per unit mass of Fe_3O_4 increased from 1.302 mg g^{-1} to 24.81 mg g^{-1}, when the crystal violet initial concentration was raised from 0.625 ppm to 20 ppm.

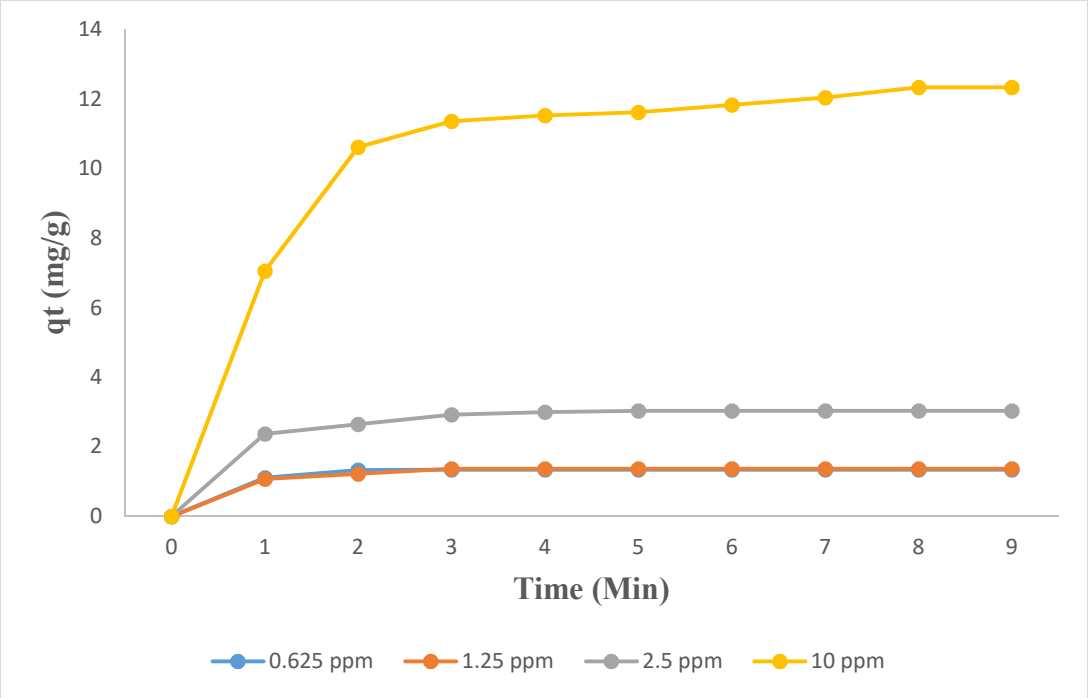

Figure 4. 41: Effect of initial concentration on adsorption of crystal violet by magnetic iron (III) oxide nanoparticles (Fe_3O_4 Nanoparticles 6 mg/10 ml at 25 °C)

For both methylene blue and crystal violet colorants, it was observed that quantity of dye adsorbed increase with increase in preliminary concentration used. This is because of a rise in concentration gradient as preliminary concentration of the colorant rises increasing the driving force. Opposition to mass transfer of the dye molecules from the bulk to the surface of nanoparticles is overcome by the driving force hence more molecules are adsorbed (Wanyonyi et al., 2014). These results are similar to previous reports on adsorption of crystal violet using coffee husks (Cheruiyot et al., 2019) and adsorption dye using olive leaves (Elsherif et al.,2021) and adsorption of methylene blue using activated carbon (Zhang et al., 2020).

4.5.6 Effect of Initial pH on Adsorption of Crystal Violet and Methylene Blue Dyes

The pH of colorant solution is one of the parameters which influence adsorption progression. Changes incolorant solution pH influence the surface characteristics of colorant molecules and the adsorbent surface augmenting or hindering interaction between them (Wu, 2017). The pH affects the level of ionization of basic and acidic compounds (Kuang, et al., 2020). The effect of pH on adsorption of crystal violet by AgNp was explored by varying the preliminary pH of the crystal violet solution from pH 3 to pH 10 and the results are presented in figure 4.42. The pH 2 was omitted due color change of crystal violet from purple to blue, at pH 11-13 the dye solution was colorless hence these pH values were also omitted. There was a small increase in q_e from 12.34 at pH 3 to 12.48 at pH 6. Maximum adsorption was attained with a pH of 6-8. At lower pH, there is a high number of hydrogen ions in solution which compete for adsorption sites with crystal violet molecules which are cationic in nature. Hydrogen ions are preferentially attached to the sites due to their higher mobility rate (Sabna et al., 2016).

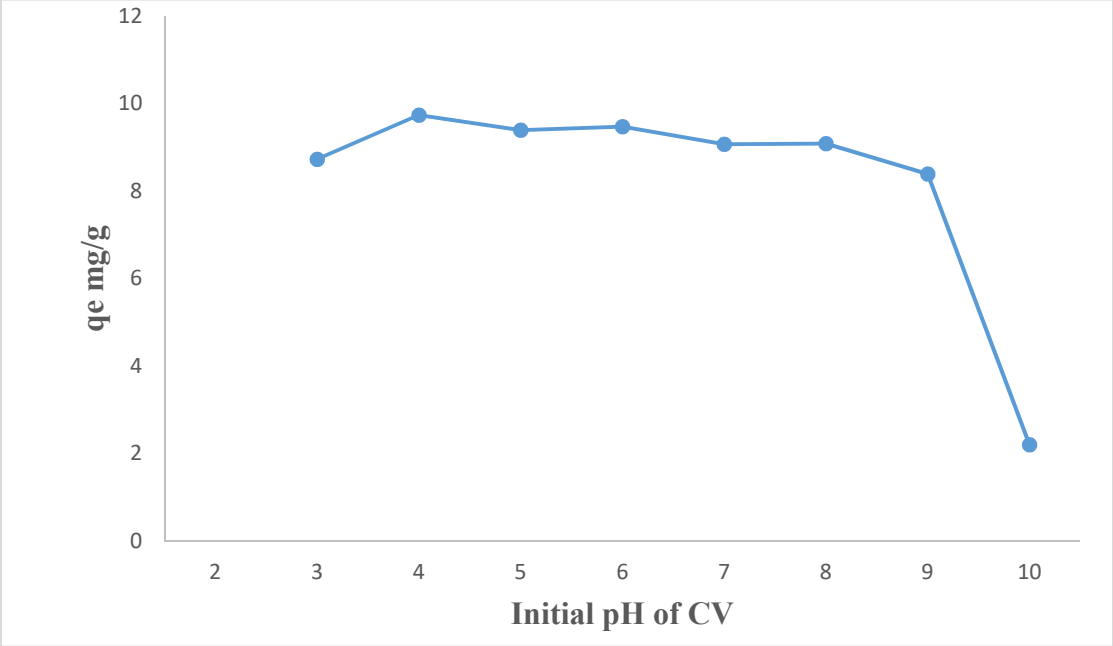

Figure 4.42: Influence of pH on removal of crystal violet by silver nanoparticles (Crystal violet 10 ppm, silver nanoparticles 8 mg/10 ml at 25 °C).

Effect of pH on adsorption of methylene blue by copper nanoparticles was investigated by varying primary pH of methylene blue dye from 2-13 at 25°C. Change in adsorption capacity of CuNp was not pronounced over the selected pH range. High adsorption of 96 % was attained in acidic conditions with a pH range of 2-5 (Fig 4.43). Similar results were reported on methylene blue removal using activated carbon from lemon and orange peels in which maximum removal was attained at pH 5 (Ramutshatsha-Makhwedzha et al., 2022).

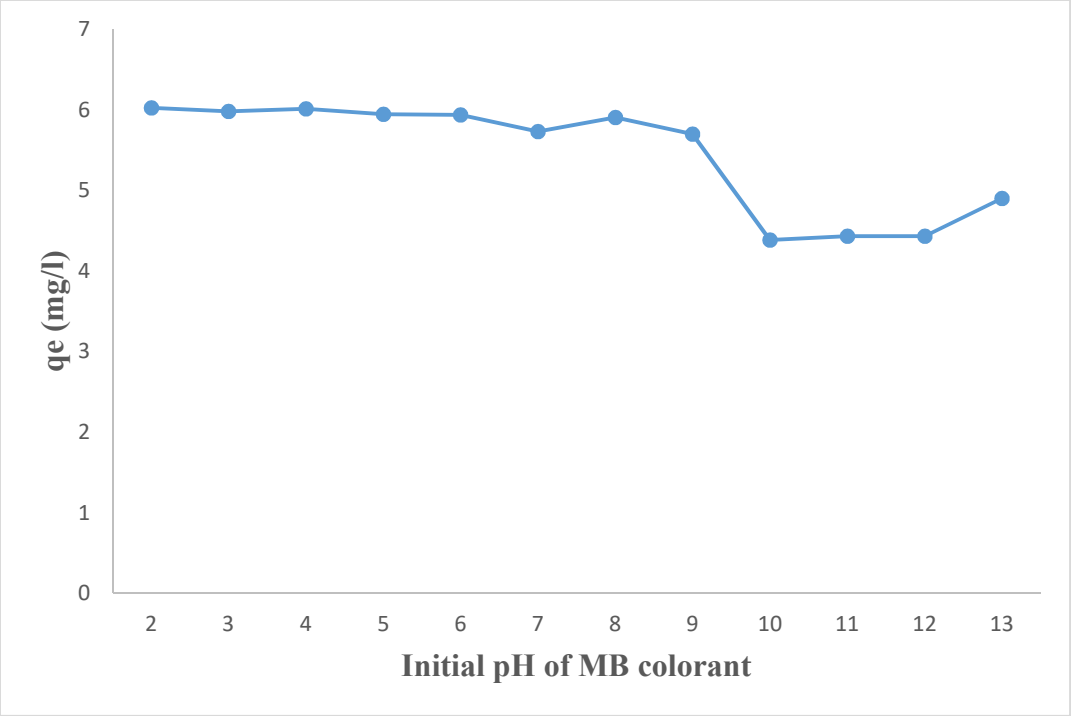

Figure 4.43: Effect of pH on adsorption of methylene blue by CuNPs (Methylene blue 5 ppm, CuNPs 8 mg/10 ml, at 25 °C)

4.5.7 Temperature Influence on Adsorption of Dyes

Temperature affects the properties of the surface of the adsorbent, solubility of the colorant, viscosity, flow of adsorbate molecules across boundary layers of the adsorbent particles and mobility of the dye molecules (Cheruiyot et al., 2019). Adsorption of crystal violet was investigated at varying temperature of adsorption from 25 °C to 60 °C and the findings are presented in figure 4.44. A small increase in amount of crystal violet adsorbed in mg/g from 12.02 mg/g to 12.10 mg/g was observed when the temperature was raised from 25 °C to 40 °C. This is associated with improved colorant mobility as the temperature rises up to 40 °C. As the temperature was increased further, the adsorption capacity decreased to 9.56 mg/g at 50 °C and 9.418 mg/g at 60 °C. This could be attributed to decrease in the strength

of the binding forces hence some of the crystal violet colorant molecules are detached from silver nanoparticles (Cheruiyot et al., 2019), crystal violet colorant solubility upgraded amid the rise in temperature (Chakraborty et al., 2020).

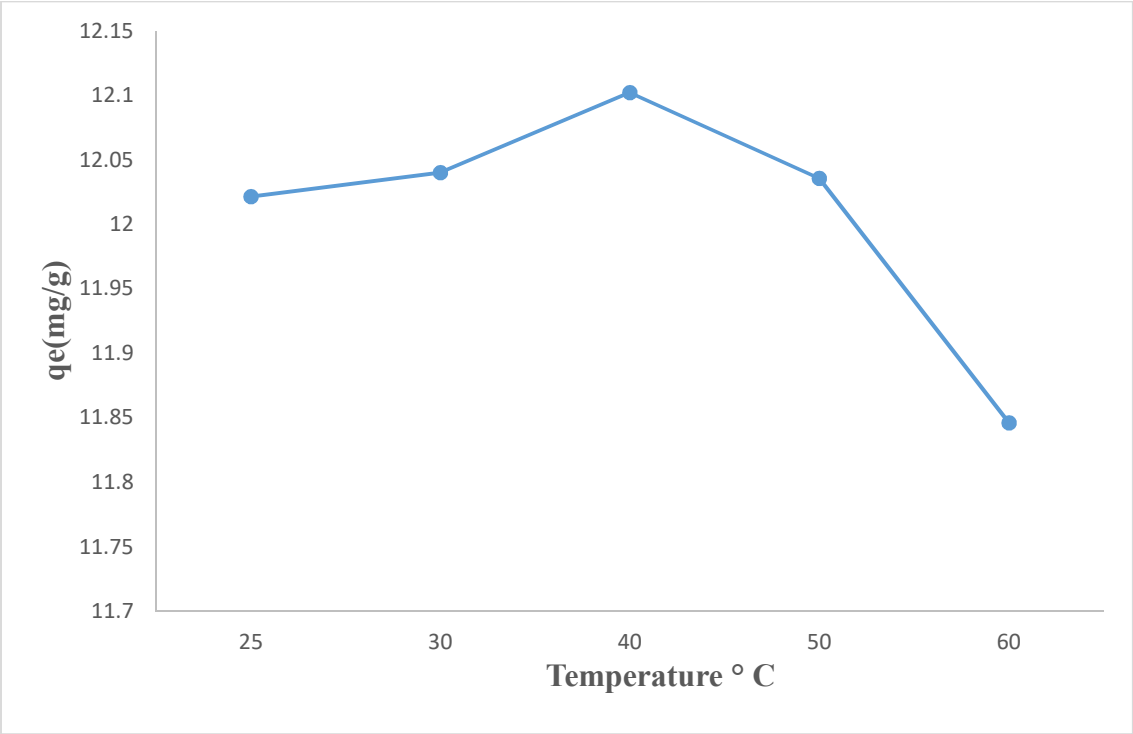

Figure 4. 44: Effect of temperature on adsorption of crystal violet by silver nanoparticles (Crystal violet 10ppm, AgNps 8 mg/10 ml at 25 °C)

Influence of temperature on adsorption of methylene blue by CuNps was explored under the same range of temperature, the findings obtained are presented in figure 4.45.

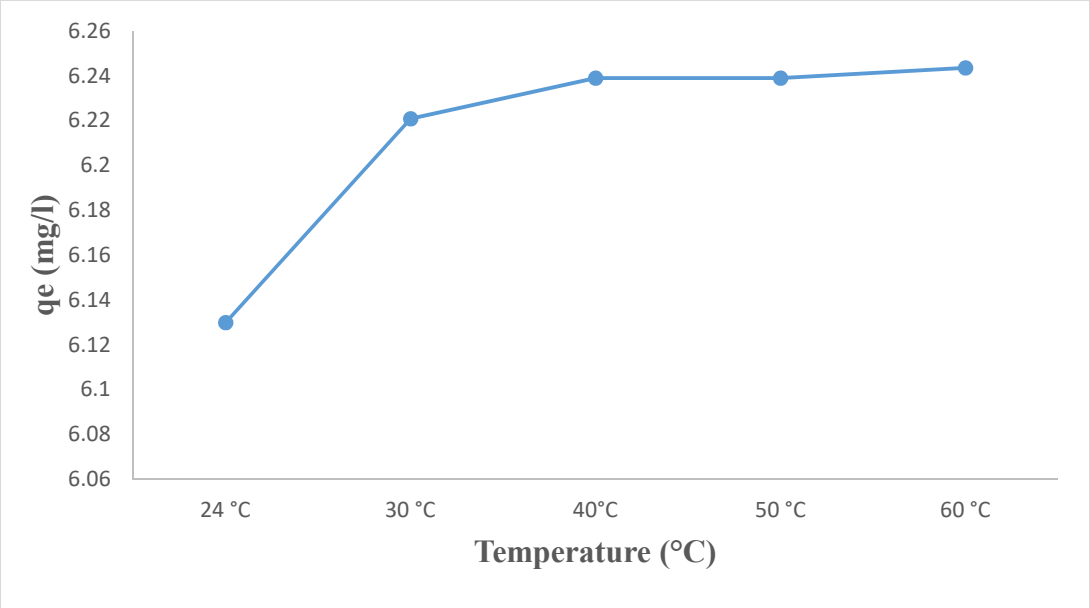

Figure 4. 45: Plots for effect of temperature on removal of methylene blue by CuNP (CuNp 8mg/10 ml of the dye, methylene blue initial concentration 5 ppm)

There was a slight increase in adsorption capacity from 6.13 to 6.2436 mg/g when temperature was raised from 25 °C to 60 °C. This indicates that adsorption of methylene blue by copper nanoparticles is an endothermic process (Liu et al., 2017). Similar results have been reported on adsorption of methylene blue using activated carbon (Kuang et al., 2020).

4.6 Adsorption Isotherms and Kinetics analysis

4.6.1 Isotherm Analysis of the Findings

In this research, Langmuir isotherm (equation 2.1 and 2.2), Freundlich isotherm (equations 2.3 and 2.4) and Tempkins isotherm (equations 2.5 and 2.6) were used to describe the sorption of crystal violet using AgNPs. Langmuir isotherm and Freundlich isotherms were used to describe the sorption of MB using CuNps and sorption of crystal violet using Fe_3O_4.

Adsorption data on adsorption of crystal violet with concentrations from 0.625 ppm to 20 ppm using silver nanoparticles were used to describe the sorption progression. Figure 4.46 represents the plots for Freundlich figure 4.47 represents the plots Langmuir and figure 4.48 represents the plots Temkin isotherms.

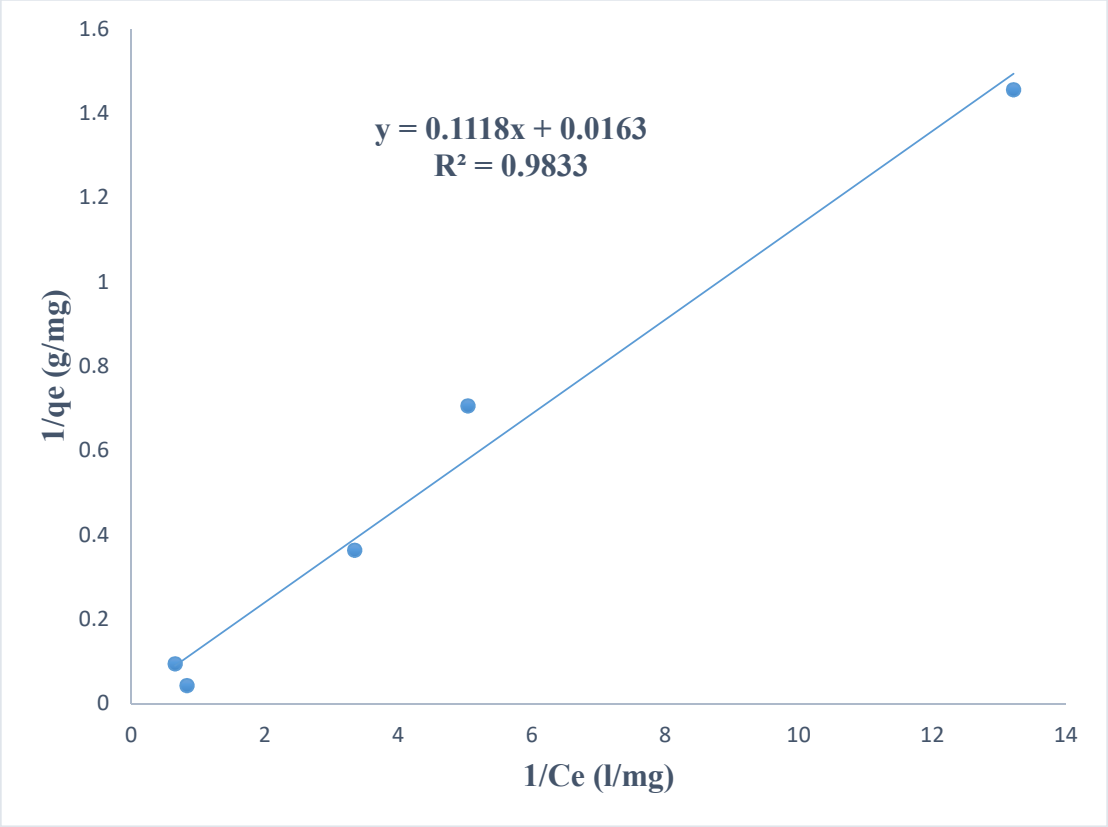

Figure 4. 46: Langmuir isotherm curve for removal of crystal violet by AgNps

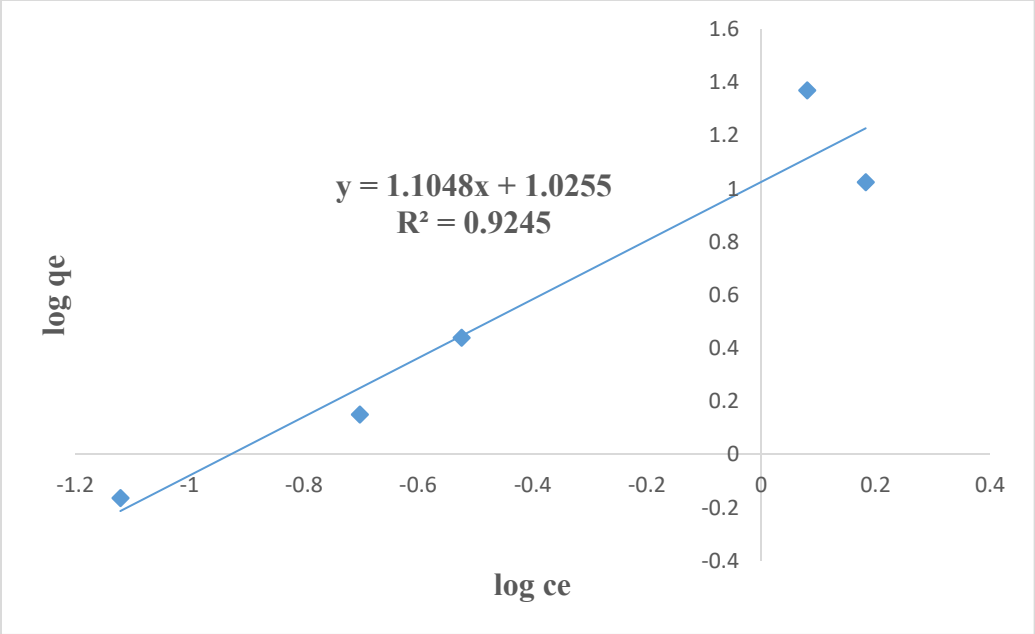

Figure 4.47: Freundlich isotherm curve for removal of crystal violet by AgNps

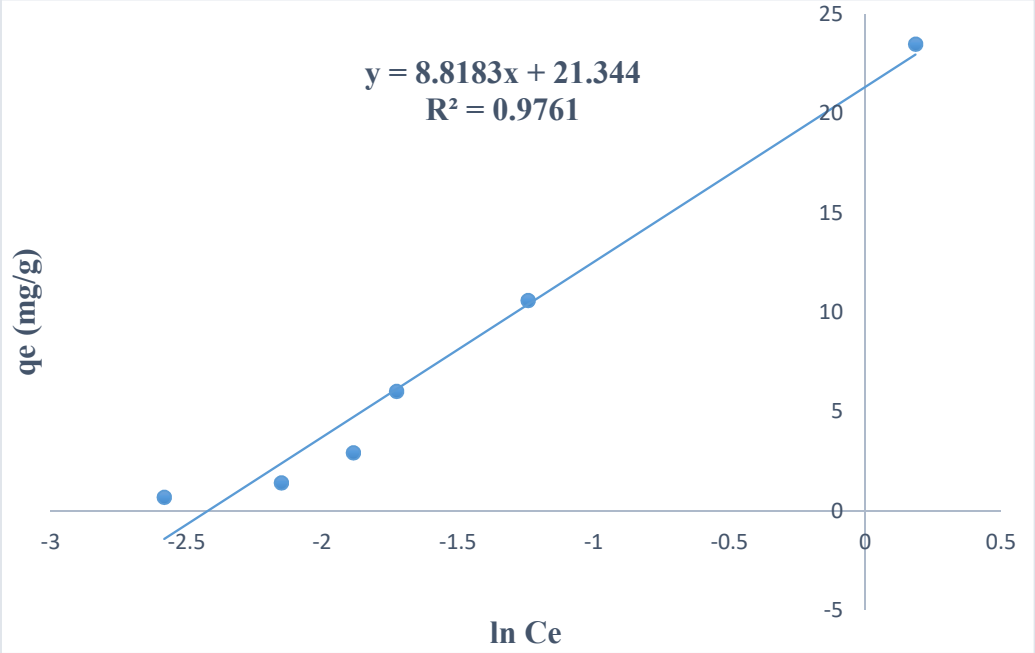

Figure 4. 48: Temkin isotherm curves for removal of crystal violet by AgNps

The higher R^2 value obtained for Langmuir isotherm indicates that it was more fitting for describing the adsorption isotherm behavior.

Table 4.1

Isotherms for Adsorption of Crystal Violet using AgNps.

Isotherm	**Parameters for the Isotherm**	**R^2**
Freundlich	n =0.9051, K_{Fr}= 10.60 g^{-1}mg	0.9245
Langmuir	q_{ax}= 61.35 g^{-1}mg R_L=0.2554 b_o = 0.1458 mg^{-1}L	0.9833
Temkin	A=11.25 L/g B=8.818 J/mol b=280.02 mg L^{-1}	0.9761

C_e (mgL^{-1}) and q_e (g^{-1} mg) are equilibrium colorant concentration and adsorption capacity correspondingly;

q_{ax} represents the maximum adsorption capacity of silver nanoparticles.

K_L (L/mg) is Langmuir constant which relates to free energy for adsorption.

K_{Fr} (mg/g)(L/mg) is the Freundlich isotherm constant relating to adsorption capacity.

$\frac{1}{n}$ is the heterogeneity factor describing divergence from sorption linearity.

b_o affinity for binding sites.

The value of $\frac{1}{n}$ should be between 0.1and 1 for a favorable adsorption process.

In this study, the value was above 1 indicating that Freundlich model was not suitable for unfolding the procedure. R_L Values shows whether the adsorption is linear (R_L =1), unfavorable (R_L>1) or favorable (0<R_L<1). From the findings, (0<R_L<1) indicating that Freundlich isotherm was more suitable for explanation of crystal violet adsorption using silver nanoparticles.

Adsorption data for adsorption of methylene blue with concentrations from 0.625 ppm to 10 ppm using CuNps were used to describe the sorption progression. Figures 4.49 and 4.50 (a) represents the plots for Freundlich and Langmuir representations.

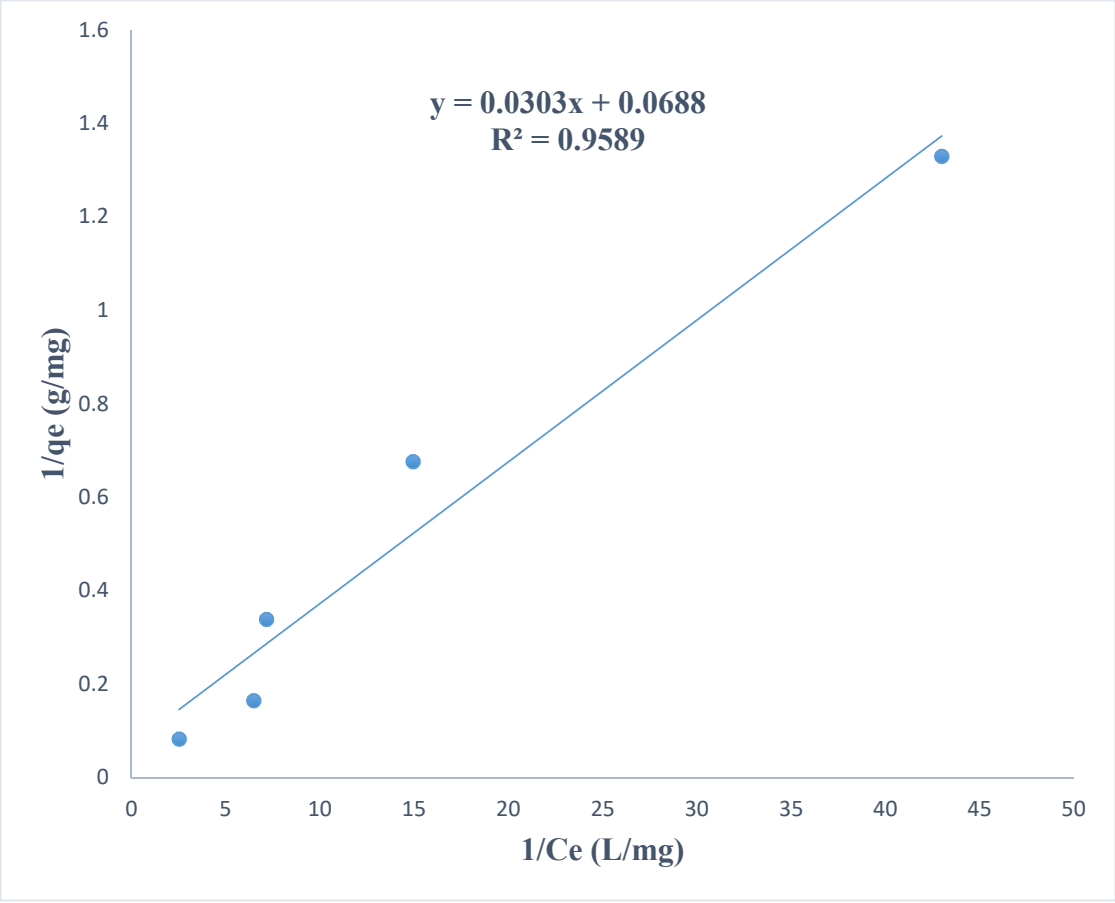

Figure 4. 49: Langmuir curve for removal of methylene blue by CuNps

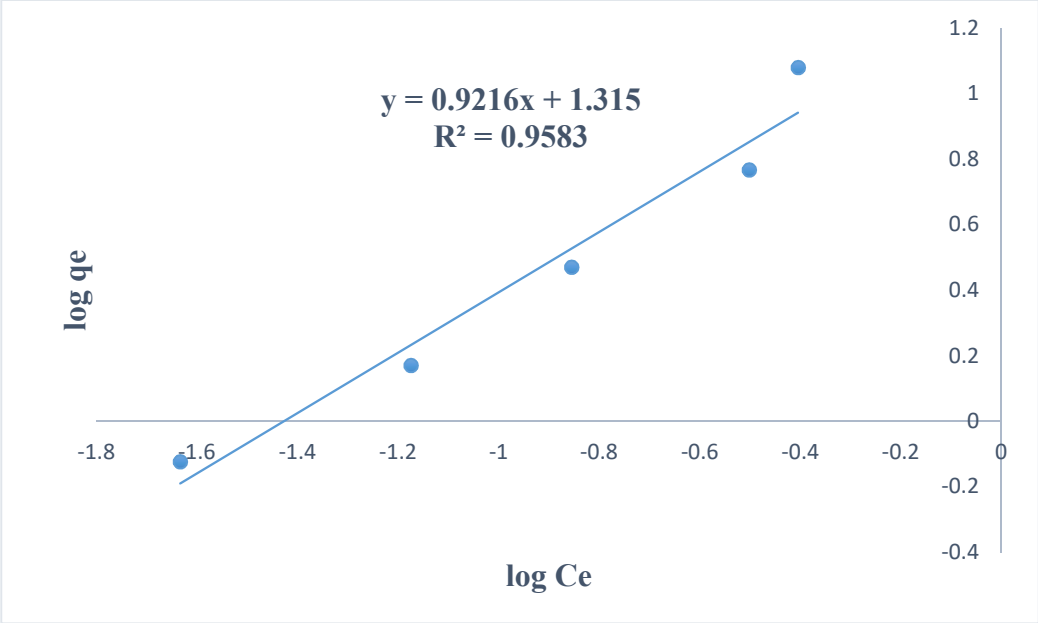

Figure 4. 50 (a): Freundlich curve for removal of methylene blue by CuNps

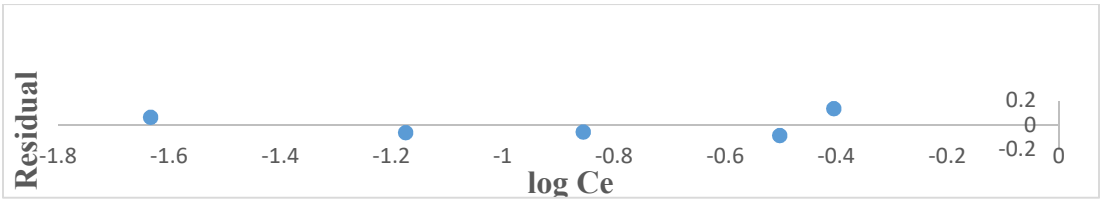

Figure 4. 50 (b): Residual plots for Freundlich curve for removal of methylene blue by CuNps

The value of n is more than 1, an indication of a satisfactory progression of adsorption. From the results R^2 value for Langmuir isotherm is higher than R^2 obtained using Freundlich isotherm, this indicates that the model was more suitable for describing the adsorption process. The constants for Langmuir and Freundlich parameters are presented in table 4.2. The residual plots for Freundlich isotherm (Figure 4.50 b) do not have a trend, and the values are close to the log C_e axis. This indicates that the linear curve is a good model for the data.

Table 4.2:

Langmuir and Freundlich Parameters for Adsorption of Methylene Blue using CuNps

Isotherm	Parameters	R^2 Value
Langmuir Isotherm	q_{ax}= 14.53 mgg^{-1} b_o = 0.4404 $mg^{-1}L$ R_L=0.1850	0.9589
Freundlich Isotherm	n= 1.085 K_{Fr} =20.6538 (mg/g)(L/mg)	0.9585

Adsorption results on removal of crystal violet by magnetic iron (III) oxide were fitted to Langmuir isotherm (Figure 4.51) and Freundlich isotherm (figure 4.52).

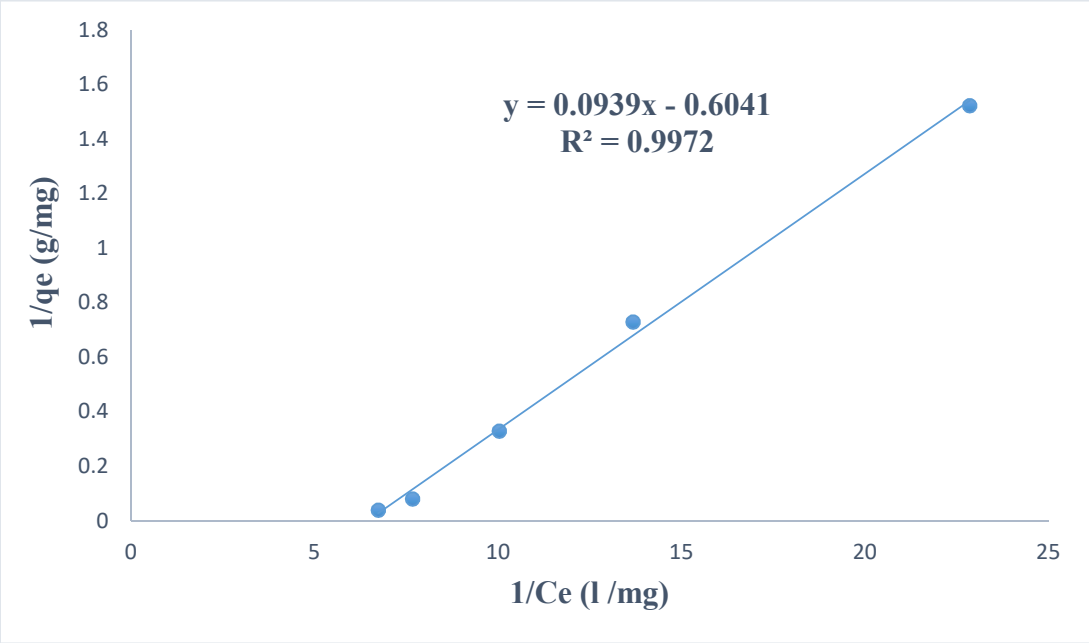

Figure 4. 51: Langmuir isotherm for adsorption of crystal violet using Fe_3O_4

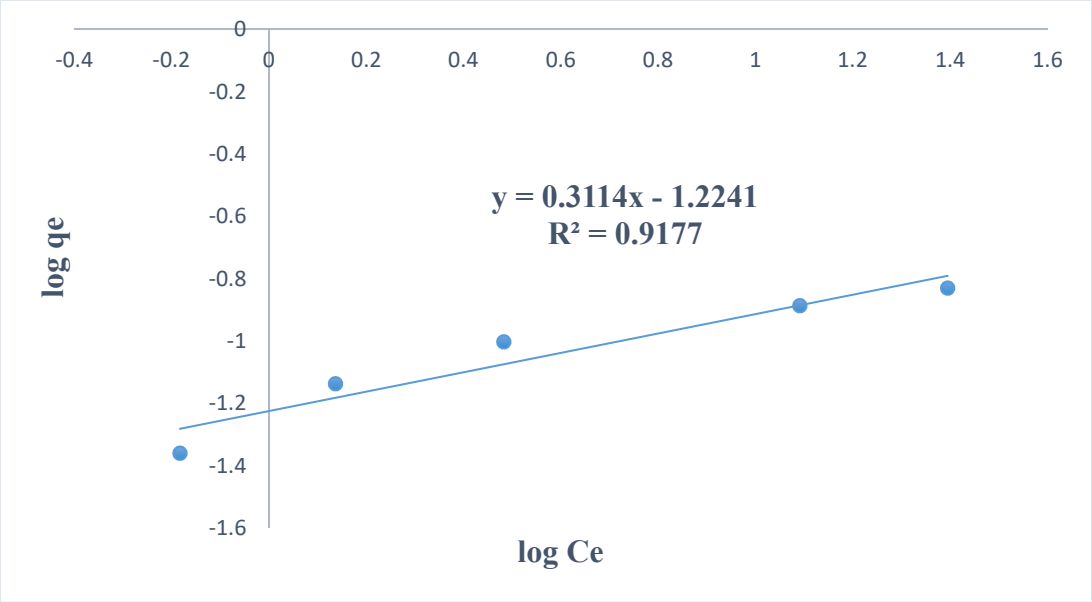

Figure 4.52: Freundlich isotherm for adsorption of crystal violet using Fe_3O_4

The isotherm parameters for Langmuir and Freundlich isotherms for adsorption of crystal violet using magnetic iron (III) oxide are presented in table 4.3. From the table the parameters for Freundlich indicate a favourable adsorption process.

Table 4.3:

Langmuir and Freundlich Isotherm Parameters for Adsorption of Crystal Violet using Fe_3O_4)

Isotherm	**Parameters**	**R^2 Value**
Langmuir Isotherm	q_{ax}= -1.655 mgg^{-1} b_o = -6.433 $mg^{-1}L$ R_L=(0.1992-0.007125)	0.9972
Freundlich Isotherm	n= 3.214 K_{Fr}=0.05969 (mg/g)(L/mg)	0.9177

From the findings, Langmuir isotherm results had a higher R^2 value however negative values of b_o and q_{ax} makes the model unsuitable. The value of n which is above 1 for Freundlich isotherm indicates a favourable process.

4.6.2 Kinetics Studies

Adsorption kinetics are commonly applied to find out mechanism of adsorption in a system. A linear curve with correlation coefficient close or equal to one indicates that the kinetic model suits the adsorption process. In this study, pseudo first (Equation 3.9) and second order (Equations 3.10 and 3.11) kinetic models were applied to describe the colorants adsorption process using the nanoparticles. For adsorption of crystal violet using AgNps, a graph of log $(q_e - q_t)$ against t (Figure 4.53) produced curves with low R^2 values ($R^2 < 0.77$) hence the model was not suitable for explaining the rate process, the graph of $\frac{t}{q_t}$ against t is presented in fig (4.52). From the gradient of the graph and $\frac{t}{q_t}$ intercept q_e and k_2 the rate constant for pseudo second order adsorption in g/mg/min can be determined. From the graph, higher values of correlation efficient ($R^2 > 0.9$) were obtained. This shows that the experimental results fit pseudo second order model. The equilibrium capacities anticipated, rate constants and the R^2 values for the selected concentrations are presented in table 4.4. High consensus between experimental values and the calculated values indicated that the removal of crystal violet dye from aqueous solution by silver nanoparticles followed pseudo second order kinetics. The results shows that the adsorption process is controlled by the quantity of silver nanoparticles and the number of unoccupied adsorption sites on AgNp (Dahri et al., 2013). Comparable results on kinetic modelling were attained for adsorption of crystal violet colorant using coffee husks

(Cheruiyot et al., 2019) and adsorption of crystal violet onto carbon nanotubes (Sabna et al., 2016).

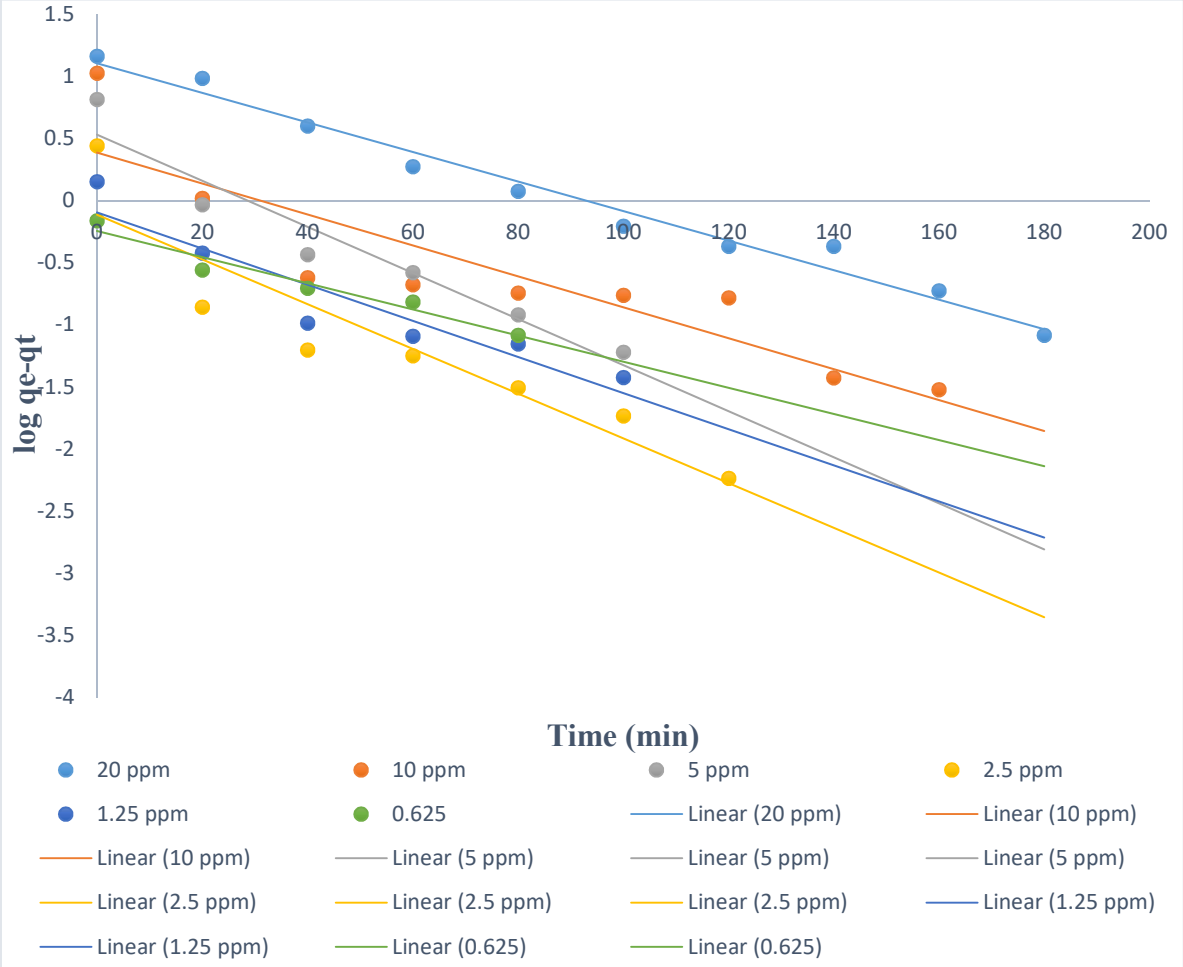

Figure 4.53: Pseudo first order kinetics for adsorption of crystal violet using AgNps.

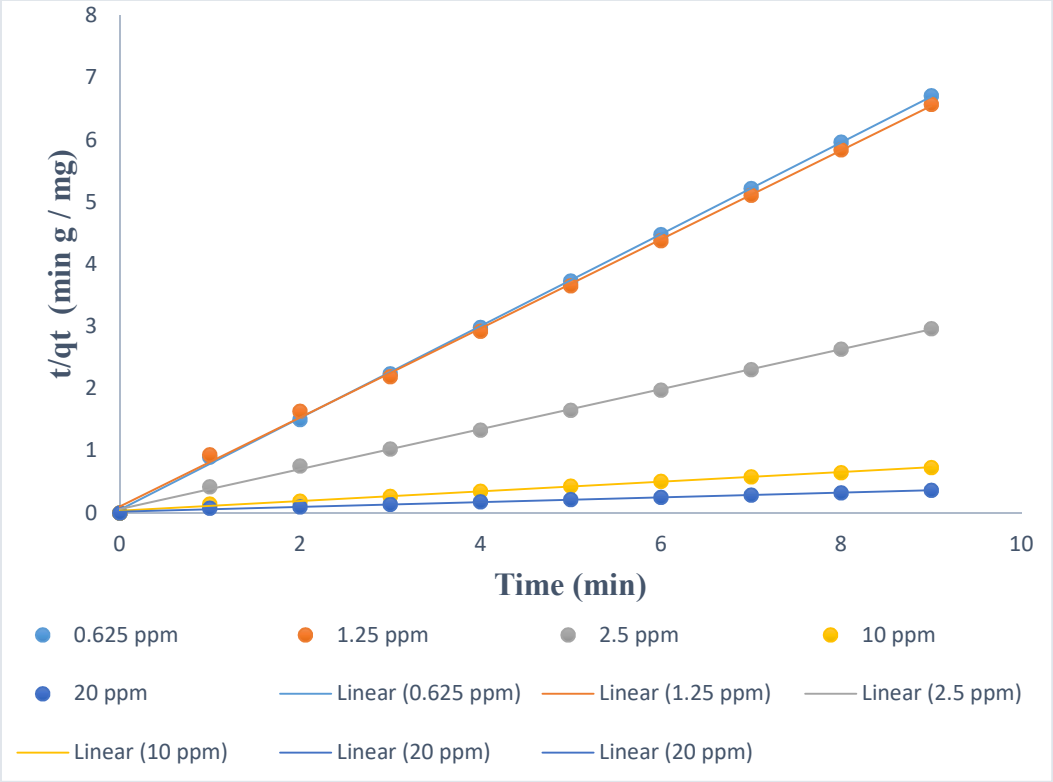

Figure 4.54: Pseudo second order kinetics for adsorption of crystal violet using silver nanoparticles

The parameters for the adsorption kinetics of adsorption of crystal violet using AgNps are presented in table 4.4. From the table, the R^2 values for Pseudo second order kinetics were in the range 0.9912- 0.999. The q_e calc values were comparable to q_e exp values. The R^2values for Pseudo First order Kinetics were in the range 0.8006-0.9792. This was lower than R^2 values for Pseudo second order kinetics. The q_e calc values for pseudo first order kinetics was not comparable to q_e exp. This indicates that Pseudo second order kinetics model was more suitable for describing adsorption of crystal violet colorant using AgNps.

Table 4.4:

Parameters on Pseudo First and Second Order Kinetics on Adsorption of Crystal Violet using AgNps.

		Pseudo First Order Parameters			**Pseudo Second Order Parameters**		
Conc of CV (ppm)	$q_e$exp (g^{-1}mg)	q_e calc (g^{-1}mg)	k_1 (gmg^{-1} min^{-1})	R^2	q_e calc (mg/g)	k_2(g mg^{-1} min^{-1})	R^2
0.625	0.6867	0.5678	0.02418	0.9515	0.7277	0.11207	0.9912
1.25	1.417	0.8041	0.03339	0.8809	1.398	0.3109	0.9983
2.5	2.935	1.263	0.02810	0.555	2.813	0.79937	0.9976
5	6.028	3.391	0.0426055	0.9307	6.083	0.07947	0.9998
10	10.60	2.428	0.0285572	0.8006	10.65	0.06710	0.9999
20	23.50	12.69	0.0274057	0.9792	24.69	0.0038758	0.9957

Experimental data on adsorption of methylene blue using CuNps were fitted to pseudo first order kinetics (Fig 4.55) and pseudo second order kinetics (Fig 4.56).

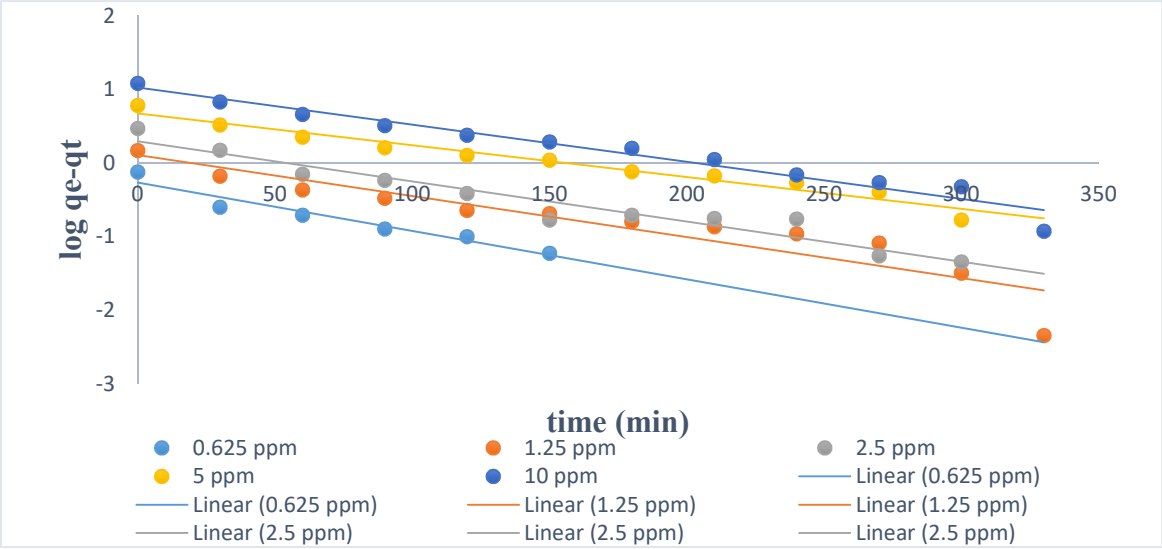

Figure 4.55: Pseudo first order kinetics for adsorption of methylene blue dye using CuNps.

The parameters of pseudo first order kinetics that is the R^2 values, the calculated adsorption capacity and the pseudo first order kinetics constant are presented in table 4.5.

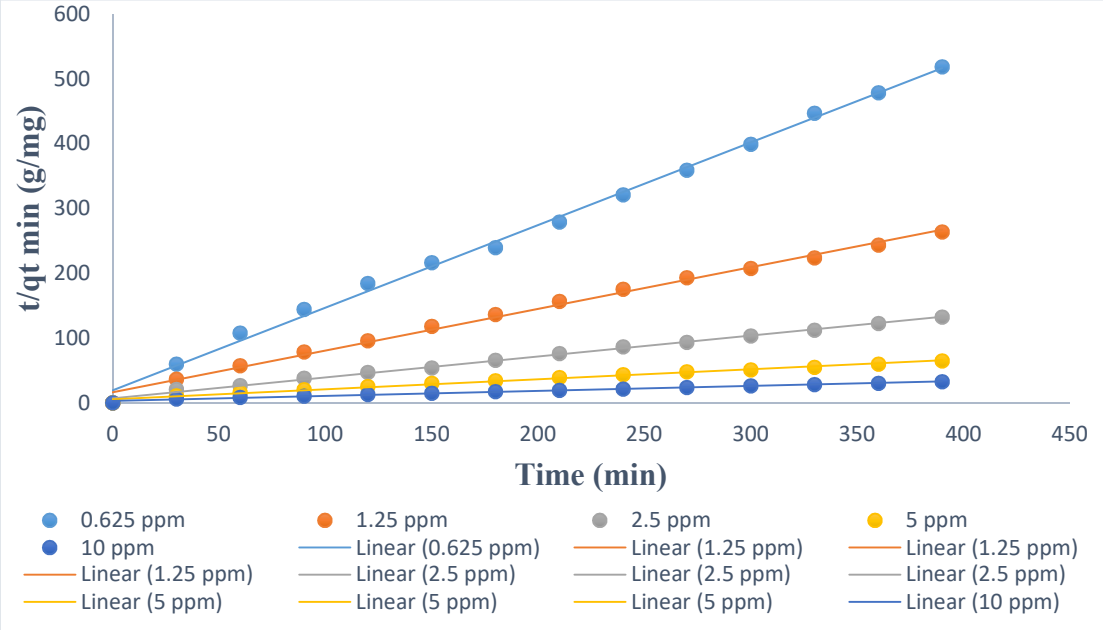

Figure 4.56: Pseudo second order kinetics for adsorption of MB using CuNps

The parameters for the pseudo second order kinetics such as the R^2, calculated equilibrium capacity, the experimental adsorption capacity and pseudo second order kinetics constant are obtainable in table 4.5

Table 4.5:

Pseudo First and Second Order Kinetics for Adsorption of Methylene Blue using CuNps.

		Factors for Pseudo First Order Kinetics			**Factors for Pseudo Second Order Kinetics**		
Conc of MB(ppm)	q_e exp (mg/g	q_e calc (mg/g)	k_1 (g mg^{-1} min^{-1})	R^2	q_e calc (mg/g)	k_2(g mg^{-1} min^{-1})	R^2
0.625	0.7522	0.5411	0.001520	0.9356	0.7839	0.08414	0.9969
1.25	1.479	1.276	0.01290	0.8602	1.554	0.02535	0.9947
2.5	2.951	1.960	0.01244	0.9377	3.0989	0.01529	0.9963
5	6.057	4.699	0.009903	0.9625	6.519	0.004304	0.9904
10	12.01	10.60	0.01175	0.9577	12.94	0.002208	0.9971

Pseudo first order and Pseudo second order adsorption kinetic models were used to describe the adsorption of crystal violet colorant using Fe_3O_4. The Pseudo first order kinetics curve (Fig 4.57) and the Pseudo second order kinetics curves (Fig 4.58) were plotted.

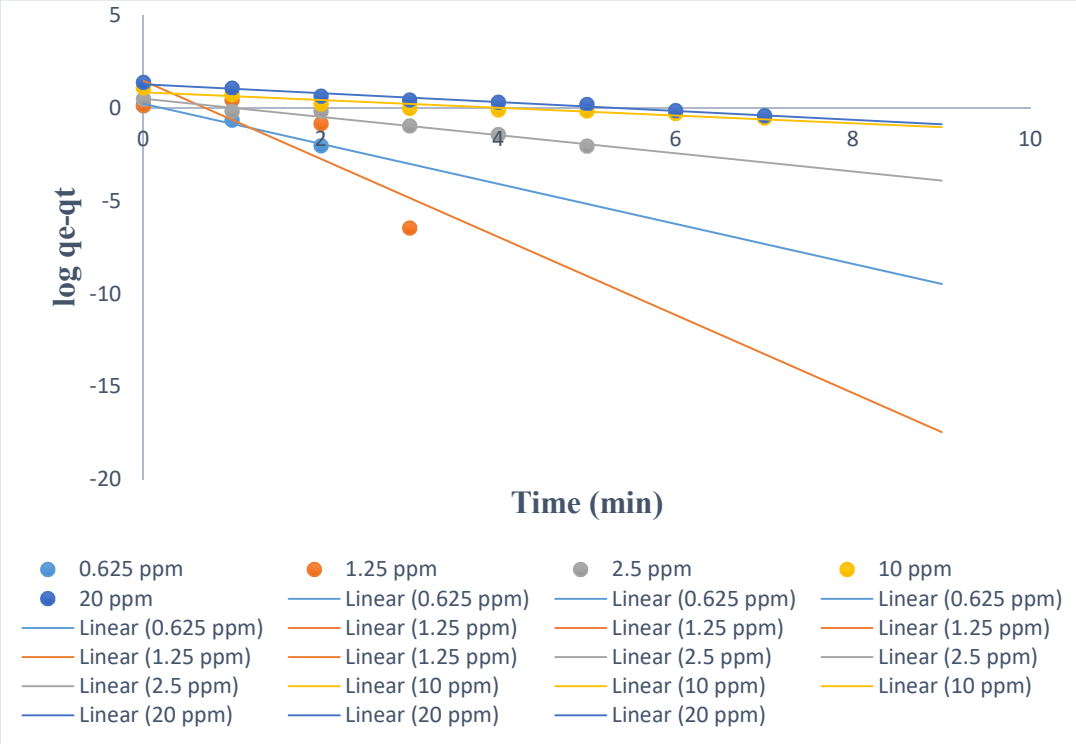

Figure 4.57: Pseudo first order kinetics for adsorption of crystal violet colorant using magnetic iron (III) oxide.

The Pseudo first order kinetics parameters: The R^2, calculated qe and the Pseudo first order kinetics constant k_1 are presented in table 4.6. The pseudo second order kinetics are obtainable in figure 4.58.

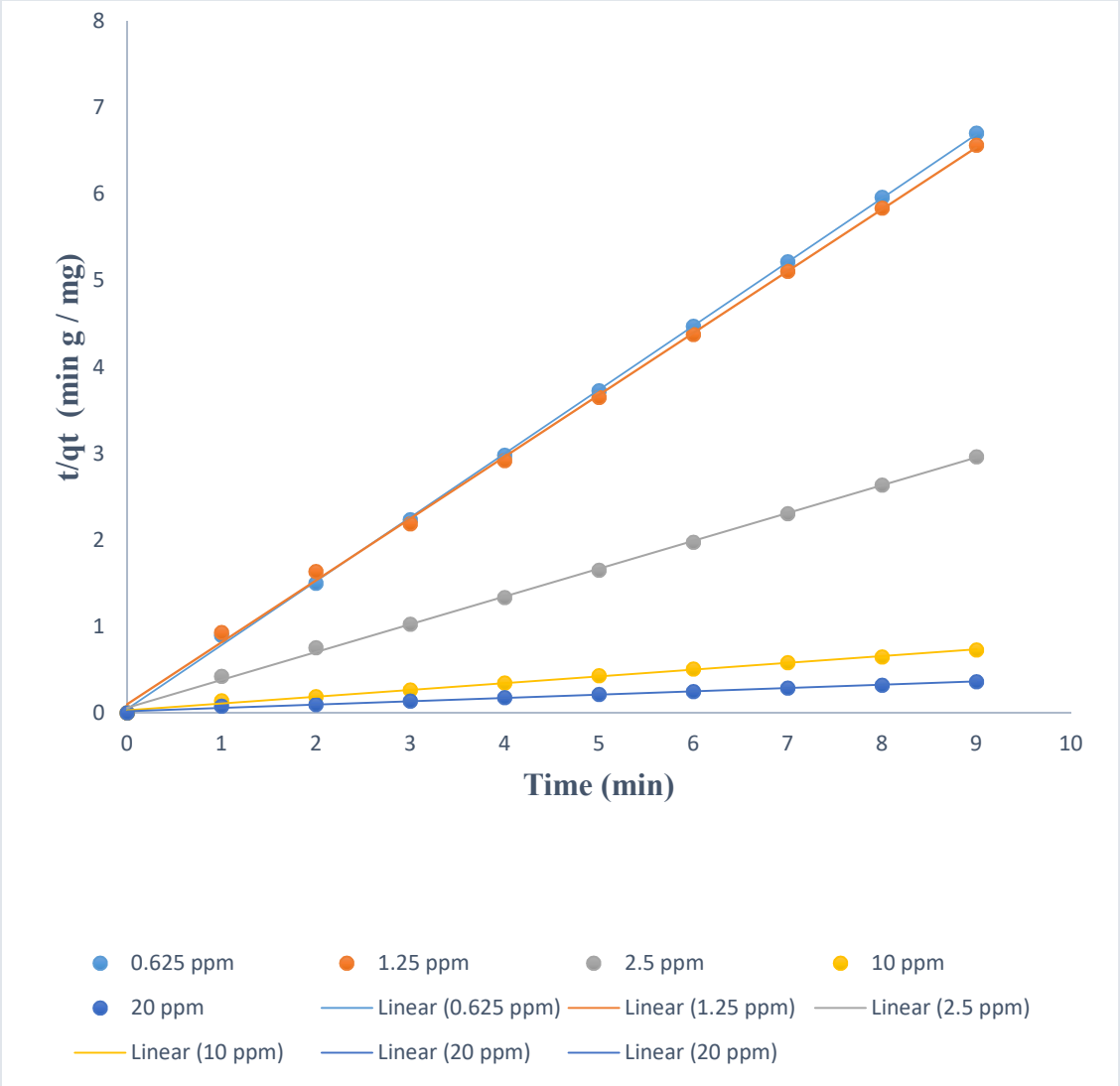

Figure 4.58: Pseudo second order kinetics for adsorption of crystal violet using magnetic iron (III) oxide

The R^2 values, calculated equilibrium adsorption capacities and the Pseudo kinetic model constants are presented in table 4.6. The higher R^2 values and q_e calc values close to the q_e exp values for pseudo second order kinetics indicate that the model suits the adsorption of crystal violet using magnetic iron (III) oxide more than Pseudo first order kinetics model which had lower R^2 values and larger deviation between q_e exp and q_e calc values. This

shows that the adsorption process is controlled by the quantity of magnetic iron (III) oxide nanoparticles and the number of unoccupied adsorption sites on Fe_3O_4 Nps (Dahri et al., 2013).

Table 4.6:

Pseudo First and Second Order Kinetics for Adsorption of Crystal Violet using Fe_3O_4 Nps.

		Factors for Pseudo First Order Kinetics			**Factors for Pseudo Second Order Kinetics**		
Conc of CV(ppm)	$q_e$exp (mg/g	q_e calc (mg/g)	k_1 (g mg^{-1} min^{-1})	R^2	q_e calc (mg/g)	k_2(g mg^{-1} min^{-1})	R^2
0.625	0.6567	1.696	2.482	0.9725	1.354	11.55	0.9996
1.25	1.370	3.003	4.843	0.7026	1.397	5.103	0.9990
2.5	3.038	3.249	1.131	0.9685	3.109	1.747	0.9990
10	12.34	7.219	0.4834	0.9072	12.69	0.2023	0.9956
20	24.81	19.00	0.5513	0.9724	26.18	0.07153	0.9934

From the table, higher values of R^2 were recorded for pseudo second order kinetics compared to pseudo first order kinetics.

4.6.3 Thermodynamics Studies on Adsorption of Methylene Blue using CuNps

Study of thermodynamic behavior on adsorption of methylene blue using CuNps was examined. Experimental data on adsorption of methylene blue at various temperatures from 297 K- 333K were used to generate graphical plots for ln K against 1/T (K^{-1}) (Figure 4.59 a). Thermodynamic variables which include entropy change ΔS° (J/kg/mol) and enthalpy change (ΔH°) (kJ/mol), were determined from the ln K intercept, and the slope respectively. Gibbs free energy change ΔG° (kJ/mol) at various temperatures according to equation 3.16.

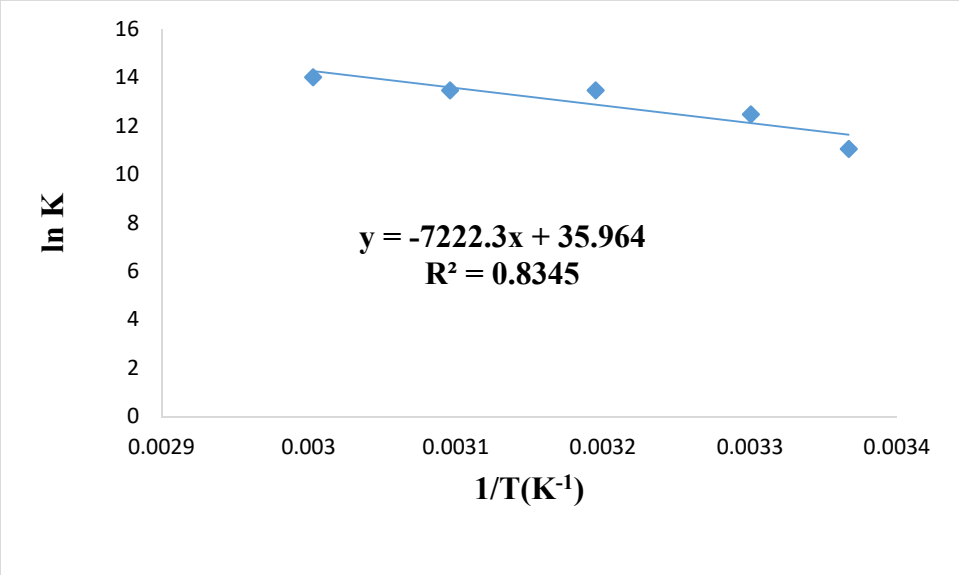

Figure 4. 59 (a): Thermodynamic studies on adsorption of methylene blue using CuNps

A residual curve was plotted to determine the suitability of the linear curve for the data. The results are presented in figure 4. 59 b.

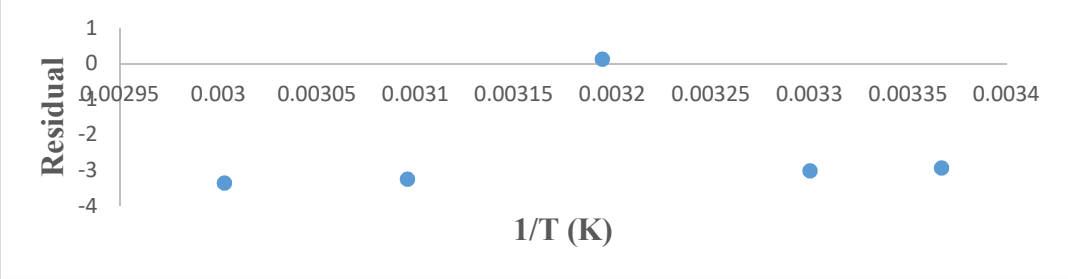

Figure 4. 59 (b): Residual plots for thermodynamic studies on adsorption of methylene blue using CuNps

The residual plotted values are close to zero, and did not have a trend. This indicates a linear relationship between ln K and 1/T (K^{-1}).

Thermodynamic parameters determined from the graph are presented in table 4.7.

Table 4. 7:

Thermodynamic parameters for adsorption of methylene blue using CuNps

T (K)	ΔG°(KJ/mol)	ΔH°(KJ/mol)	ΔS° (kJ mol $^{-1}$K^{-1})
297	-28.76	+60.05	+ 0.2990
303	-30.56		
313	-33.54		
323	-36.53		
333	-39.52		

From the table, negative values of ΔG° specify impulsiveness and feasibility of adsorption of MB by CuNp. Positive ΔS° specifies that the randomness of solution/solid interface augmented all through sorption progression (Zhang et al., 2020). ΔH° is positive, indicating that the adsorption process is endothermic (Piri et al., 2019). The magnitude of ΔH° is lower than 80 (KJ/mol) signifying a physisorption procedure governed by van der waals forces (Cheruiyot et al., 2019).

4.7 Reusability of the nanoparticles

Sorbent retrieval, desorption and regeneration is vital for commercial adsorbents since it enables adsorbate reuse, reduces toxicity, secondary pollution regulation and ease on cost of treatment (Fouda-Mbanga et al., 2021).

4.7.1 Reusability of AgNps

There was a small decrease in CV dye removal by AgNps from 97.9 % to 95 % after 4 cycles (Figure 4.60). The findings indicated that AgNps can be recycled in CV adsorption.

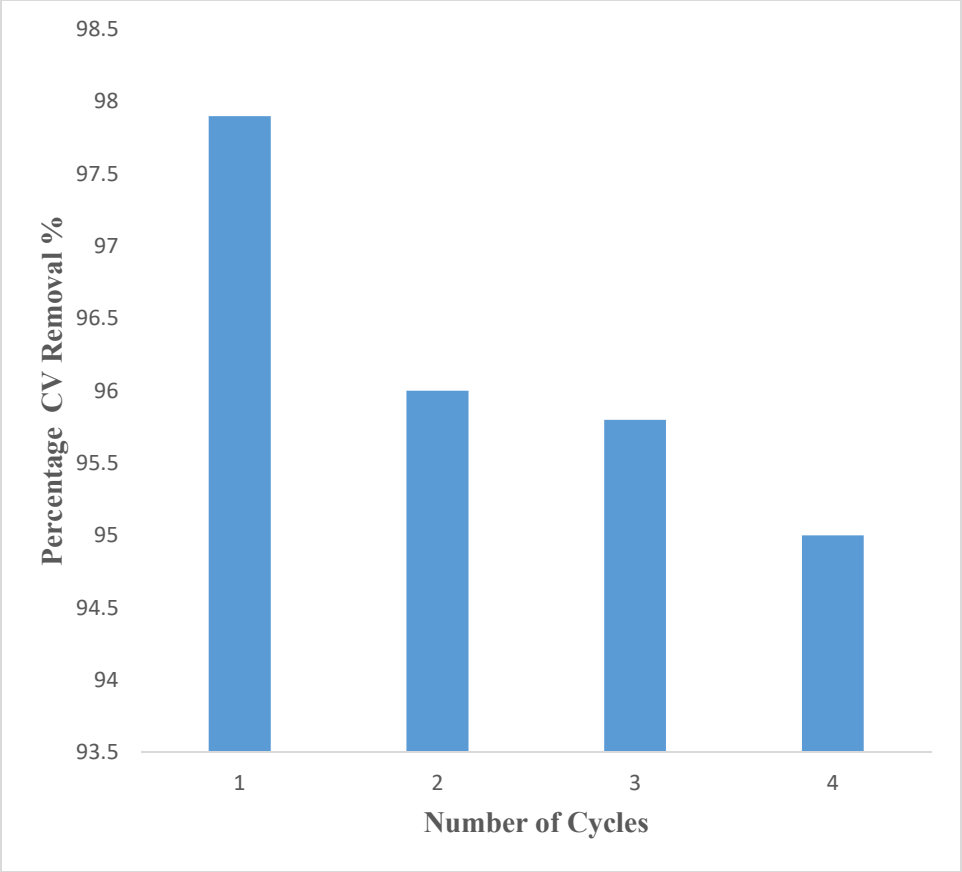

Figure 4.60: Reusability of AgNps in Removal of Crystal Violet

4.7.2 Desorption of Methylene Blue from CuNps

MB desorption from CuNps was performed using different eluents including distilled water, HNO_3, HCl, NaOH, NH_3 and CH_3COOH. The results (Fig. 4.61) revealed that, distilled water, dilute HNO_3, HCl showed a significant MB dye desorption while NH_3 and CH_3COOH displayed a better desorption capability of >1.6788 mg/g at 40°C. Temperature increase resulted in improved desorption indicating that adsorption of MB on CuNPs may have been controlled by weak van der Waals attractive forces which diminished with temperature rise liberating dye molecules to the solution. The results further showed the inefficiency of dilute NaOH in desorption MB dye. Due to miniature size of the

nanoparticle, it was difficult to recover and recycle all used nanoparticle after adsorption and hence immobilization of CuNps could facilitate effective regeneration (Cai et al., 2017).

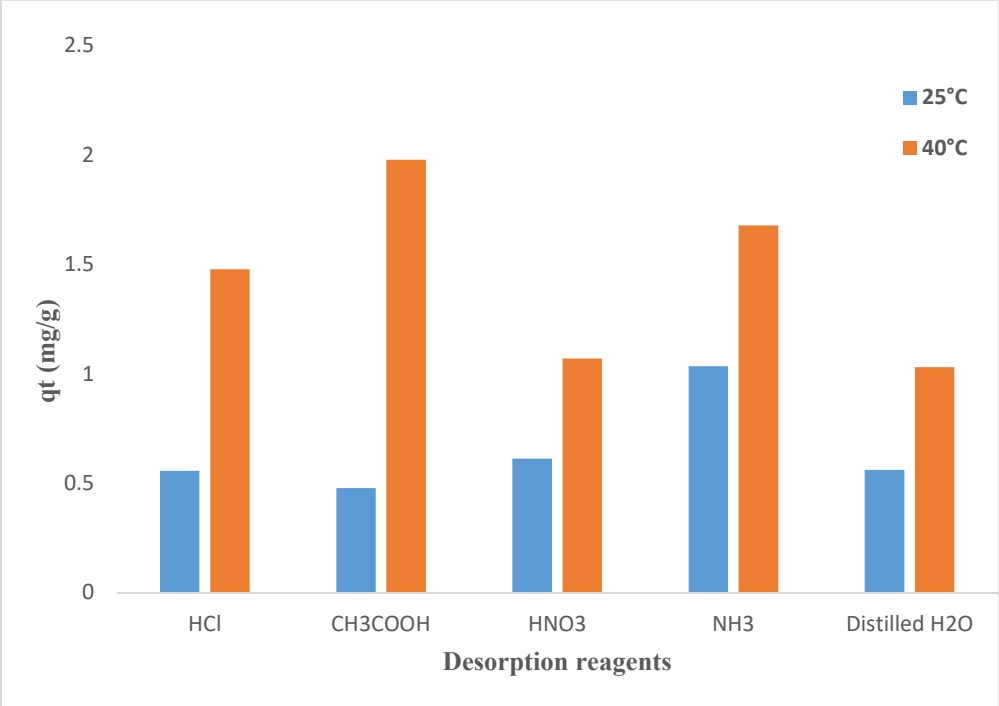

Figure 4.61: Amount of MB desorbed from CuNps using different desorbing eluents at 25 °C and 40 °C.

CHAPTER FIVE

SUMMARY, CONCLUSIONS AND RECOMMENDATIONS

5.1 Introduction

This section presents the summary and recommendations from the results on hydrolysis of extraction and hydrolysis of keratin, preparation of nanoparticles using keratin as reducing and capping agent, characterisation of the nanoparticles and application of nanoparticles for dye removal from aqueous solution.

5.2 Summary of the Findings

This study focused on synthesis and characterisation of nanoparticles using keratin obtained from sheep hooves and its application for the removal of dyes from waste. Sheep hooves were collected from slaughters house which are usually disposed as biomass. Clean water is a requisite for human as per the SDG goal number 6.

Hydrolysis of keratin using sodium hydroxide was optimized. In order to achieve this Hydrolysis of keratin using NaOH was carried out under different conditions of time, temperature, concentration of sodium hydroxide, initial pH and quantity of keratin. One parameter was varied, while others were kept constant during optimization. It was found that hydrolysis of keratin is dependent on time, temperature, concentration of NaOH, pH and quantity of hooves used. Keratin extracted was suitable for use as a reducing and capping agent in synthesis of copper and silver nanoparticles. It is suitable for use as a capping agent in synthesis of magnetic iron (III) oxide and zinc oxide nanoparticles.

UV-VIS analysis was carried out to determine optical properties of fused nanoparticles. FT-IR technique was used to determine the involvement of keratin biomolecules in

reduction and capping of the nanoparticles. SEM analysis was carried out to determine size distribution and XRD technique was used to determine the crystallinity of synthesized CuNps.

The keratin capped copper nanoparticles were suitable for adsorption of methylene blue dye in water. Adsorption of methylene blue colorant was optimized by conducting experiment under different conditions of time, quantity of CuNps, colorant concentration, temperature and initial colorant concentration. The findings indicate that adsorption of methylene blue using keratin-capped copper nanoparticles is dependent on time, colorant concentration, temperature and quantity of CuNps used and initial pH of the colorant solution.

Synthesized silver nanoparticles were used for adsorption of crystal violet dye in water. Optimum conditions for adsorption was determined by investigating adsorption process under varied conditions of contact time, quantity of AgNps, temperature, crystal violet concentration and preliminary colorant concentration. It was found that adsorption of crystal violet using AgNps was dependent on contact time, preliminary colorant concentration, quantity of AgNps used, temperature and the preliminary colorant concentration.

Keratin capped magnetic iron (III) oxide nanoparticles were found to be suitable for adsorption of crystal violet dye. The adsorption process was optimized by conducting adsorption process under varied conditions of contact time, quantity of nanoparticles used and preliminary colorant condition. It was found that adsorption of crystal violet using

keratin capped magnetic iron (III) oxide is influenced by contact time, quantity of nanoparticles used and preliminary colorant.

5.3 Conclusions

Optimization of hydrolysis of keratin from sheep hooves.

In this study, sodium hydroxide was used in hydrolysis of keratin. It was observed that hydrolysis process was dependent on hydrolysis time, w/v percentage of aqueous NaOH, temperature of hydrolysis, pH of the process and the mass of hooves used, hence the null hypothesis stated that there are no optimum conditions for chemical hydrolysis and extraction of keratin from sheep hooves was rejected. The ideal situation for hydrolysis of keratin was found to be 9 hours, NaOH 1 % (w/v) concentration pH of 12 and a temperature of 70 °C.

Synthesis of nanoparticles

From the findings, keratin was found to be a suitable reducing and capping agent for synthesis of nanoparticles. The optimum conditions for synthesis of copper and silver nanoparticles was found to be 90 minutes at a temperature of 80 ^{o}C and salt solution containing 0.01 M of metal ions. The null hypothesis stated that keratin extracted from sheep hooves cannot be used as reducing and capping agents in fusion of nanoparticles was rejected. The optimum time for synthesis of magnetic iron (III) oxide using keratin was found to be 60 minutes, using 100 ml of solution containing 0.02 moles of Fe^{3+} and 0.01 Fe^{2+}. Using solutions containing higher amount of moles of Fe^{3+} and Fe^{2+} resulted in precipitation.

Characterization of nanoparticles

Changes in color of the reacting mixture marked the formation of nanoparticles. Optical properties of nanoparticles were determined using UV-VIS spectroscopy. Maximum absorbance for synthesized silver nanoparticles was attained at a wavelength of 410 nm. Maximum absorbance for copper nanoparticles was attained at 544 nm. Synthesized magnetic iron (III) nanoparticles had a maximum absorbance at 344 nm. The optical properties confirmed the presence of nanoparticles in the resulting solution. Functional groups found on the surface of nanoparticles were C-H, C-O, C=O and C-N. The bio groups indicated the involvement of keratin bio molecules as reducing and capping agent during formation of nanoparticles. SEM analysis of copper nanoparticles indicated mono-dispersed nanoparticles with particle size in the range of 2 nm-16 nm. XRD analysis report for CuNps indicated the fcc crystal planes that correspond to copper nanoparticles.

Removal of organic dyes using nanoparticles

In this study, adsorption of methylene blue dye using copper nanoparticles and adsorption of crystal violet dye using silver and magnetic iron (III) oxide nanoparticles was investigated nanoparticles. Copper nanoparticles adsorbed up to 95 % of methylene blue dye at equilibrium which was attained after 330 min. AgNps removed 96 % of crystal violet after 60 minutes at room temperature. Adsorption of crystal violet using magnetic iron (III) oxide attained equilibrium after 4 minutes with 99 % efficiency of the dye removal. Therefore the null hypothesis stated: Keratin capped nanoparticles are not efficient in removal of organic colorants such as methylene blue and crystal violet from water was rejected. Adsorption of dyes was affected by time, quantity of nanoparticles used, preliminary colorant concentration, pH and temperature. The optimum conditions for

removal of crystal violet by silver were a pH of 5-6, 60 minutes of contact time and a temperature of 45 °C. The best conditions for the adsorption of methylene blue dye by copper nanoparticles were a pH range of 2-5 and adsorbent dose of 8 mg/10 ml of the colorant and a temperature of 60 °C. The finest settings for adsorption of crystal violet using magnetic iron (III) oxide were a time of 8 minutes and a dosage of 6 mg/10 ml of nanoparticles. The nanoparticles are eco-friendly, can be reused, do not generate toxic sludge and don't consume high energy during adsorption of dyes from water.

5.4 Recommendations

(i) It is also necessary to employ efficient green methods in synthesis of nanoparticles to reduce environmental degradation and energy consumption during the process.

(ii) It is necessary to collect keratin bio wastes from slaughter houses for use in extraction of keratin which will be stored in a small space to prevent accumulation of bio waste in the environment. Keratin collected can be used in synthesis of nanoparticles, to reduce nanoparticles production cost.

(iii) The waste water released in leather industries when removing hair from leather through solvation can be treated with acids to adjust the pH to 3.2 which is close to the isoelectronic point of keratin to obtain keratin precipitate which can be used for synthesis of nanoparticles for industrial applications.

(iv) Industries releasing effluents containing methylene blue and crystal violet dyes can design waste treatment basins where copper and silver nanoparticles respectively can be used to treat the waste water before recycling or releasing into water bodies.

5.5 Suggestion for Further Research

Further research can be done on the following areas:

i. Extraction of keratin using other alkalis for example KOH in order to determine the efficient hydrolysis technique for hydrolysis of keratin.

ii. Optimization of hydrolysis of keratin should also be investigated using KOH in place of NaOH in order to determine a more suitable alkali.

iii. Find out the suitability of other bio waste which contains keratin such as wool and horns from various animals for industrial application in synthesis of nanoparticles.

iv. Investigate on how keratin extracted from different parts of the animals affects the yield of the nanoparticles

v. Investigate how the % yield of keratin extracted varies from one part of an animal to another or from one part of an animal to a similar part of another animal e.g the yield obtained using sheep hooves compared to the yield obtained using goats hooves.

vi. Find out the suitability of other proteins found in bio wastes in the synthesis of metal and metal oxide nanoparticles for various industrial applications.

vii. Explore the suitability of copper and silver nanoparticles in purification of effluents containing other dyes not investigated in this study and other impurities such as heavy metal ions, polyphenol and antibiotic impurities.

viii. There is need for additional characterization using other methods such as TGA and TEM.

ix. Research on suitability of copper and silver nanoparticles in adsorption of multi constituent colorants should be carried out to determine suitability of the nanoparticles in adsorption of industrial effluents containing a mixture of dyes.

x. Investigation on suitability of copper and silver nanoparticles in removal of heavy metals from water

REFERENCES

Abdi, M., Balagabri, M., Karimi, H., Hossini, H., & Rastegar, S. O. (2020). Degradation of crystal violet (CV) from aqueous solutions using ozone, peroxone, electroperoxone, and electrolysis processes: A comparison study. *Applied Water Science*, *10*(7), 168. https://doi.org/10.1007/s13201-020-01252-w

Abdolkarimi-Mahabadi, M., Bayat, A., & Mohammadi, A. (2021). Use of UV-Vis Spectrophotometry for Characterization of Carbon Nanostructures: A Review. *Theoretical and Experimental Chemistry*, *57*(3), 191–198. https://doi.org/10.1007/s11237-021-09687-1

Adeola, A. O., & Forbes, P. B. C. (2021). Advances in water treatment technologies for removal of polycyclic aromatic hydrocarbons: Existing concepts, emerging trends, and future prospects. *Water Environment Research*, *93*(3), 343–359. https://doi.org/10.1002/wer.1420

Admassu, H. (2020). Chicken Feathers Based Keratin Extraction Process Data Analysis Using Response Surface—Box-Behnken Design Method and Characterization of Keratin Product. *Current Applied Science and Technology*, *20*(2), 163177. https://doi.org/10.14456/CAST.2020.6

Agarwal, P., Bairwa, V. K., Kachhwaha, S., & Kothari, S. L. (2014). Green synthesis of silver nanoparticles using callus extract of capsicum annuum l. And their activity against microorganisms. *International Journal of Nanotechnology and Application (IJNA)*, *4*(5), 1–8.

Agustina, T. E., Handayani, W., & Imawan, C. (2021). *The UV-VIS Spectrum Analysis From Silver Nanoparticles Synthesized Using* Diospyros maritima *Blume. Leaves Extract:* 3rd KOBI Congress, International and National Conferences (KOBICINC2020), Bengkulu, Indonesia. https://doi.org/10.2991/absr.k.210621.070

Ajith, M.P., & Rajamani, P. (2021). Nanotechnology for Water Purification – Current Trends and Challenges. *Journal of Nanotechnology and Nanomaterials*, *2*(2). 88-91 https://doi.org/10.33696/Nanotechnol.2.025

Akhtar, K., Khan, S. A., Khan, S. B., & Asiri, A. M. (2018). Scanning Electron Microscopy: Principle and Applications in Nanomaterials Characterization. In S. K. Sharma (Ed.), *Handbook of Materials Characterization* (pp. 113–145). Springer International Publishing. https://doi.org/10.1007/978-3-319-92955-2_4

Almatroudi, A. (2020). Silver nanoparticles: Synthesis, characterisation and biomedical applications. *Open Life Sciences*, *15*(1), 819–839. https://doi.org/10.1515/biol-2020-0094

Al-Tohamy, R., Ali, S. S., Li, F., Okasha, K. M., Mahmoud, Y. A.-G., Elsamahy, T., Jiao, H., Fu, Y., & Sun, J. (2022). A critical review on the treatment of dye-containing wastewater: Ecotoxicological and health concerns of textile dyes and possible remediation approaches for environmental safety. *Ecotoxicology and Environmental Safety*, *231*, 113160. https://doi.org/10.1016/j.ecoenv.2021.113160

Amaliyah, S., Pangesti, D. P., Masruri, M., Sabarudin, A., & Sumitro, S. B. (2020). Green synthesis and characterization of copper nanoparticles using Piper retrofractum Vahl extract as bioreductor and capping agent. *Heliyon*, *6*(8), e04636. https://doi.org/10.1016/j.heliyon.2020.e04636

Anandalakshmi, K., Venugobal, J., & Ramasamy, V. (2016). Characterization of silver nanoparticles by green synthesis method using Pedalium murex leaf extract and their antibacterial activity. *Applied Nanoscience*, *6*(3), 399–408. https://doi.org/10.1007/s13204-015-0449-z

Annesi, F., Pane, A., Pezzi, L., Pagliusi, P., Losso, M. A., Stamile, B., Qualtieri, A., Desiderio, G., Contardi, M., Athanassiou, A., Perotto, G., & De Sio, L. (2021). Biocompatible and biomimetic keratin capped Au nanoparticles enable the inactivation of mesophilic bacteria via photo-thermal therapy. *Colloids and Surfaces A: Physicochemical and Engineering Aspects*, *625*, 126950. https://doi.org/10.1016/j.colsurfa.2021.126950

Antosiewicz, J. M., & Shugar, D. (2016). UV–Vis spectroscopy of tyrosine side-groups in studies of protein structure. Part 1: Basic principles and properties of tyrosine chromophore. *Biophysical Reviews*, *8*(2), 151–161. https://doi.org/10.1007/s12551-016-0198-6

Ashraf, J. M., Ansari, M. A., Khan, H. M., Alzohairy, M. A., & Choi, I. (2016). Green synthesis of silver nanoparticles and characterization of their inhibitory effects on AGEs formation using biophysical techniques. *Scientific Reports*, *6*(1), 20414. https://doi.org/10.1038/srep20414

Aygün, A., Özdemir, S., Gülcan, M., Cellat, K., & Şen, F. (2020). Synthesis and characterization of Reishi mushroom-mediated green synthesis of silver nanoparticles for the biochemical applications. *Journal of Pharmaceutical and Biomedical Analysis*, *178*, 112970. https://doi.org/10.1016/j.jpba.2019.112970

Berechet, M. D., Simion, D., Stanca, M., Chelaru, C., Alexe, C.-A., & Rapa, M. (2020). The influence of alkaline extraction on some keratin hydrolysates properties. *Proceedings of the 8th International Conference on Advanced Materials and Systems*, 127–132. https://doi.org/10.24264/icams-2020.II.3

Bhat, A. P., Holkar, C. R., Jadhav, A. J., & Pinjari, D. V. (2021). Acoustic and hydrodynamic cavitation assisted hydrolysis and valorisation of waste human hair for the enrichment of amino acids. *Ultrasonics Sonochemistry*, *71*(2021), 105368. https://doi.org/10.1016/j.ultsonch.2020.105368

Bhati, M., & Rai, R. (2017). Nanotechnology and water purification: Indian know-how and challenges. *Environmental Science and Pollution Research*, *24*(30), 23423–23435. https://doi.org/10.1007/s11356-017-0066-3

Bhavyasree, P. G., & Xavier, T. S. (2022). Green synthesised copper and copper oxide based nanomaterials using plant extracts and their application in antimicrobial activity: Review. *Current Research in Green and Sustainable Chemistry*, *5*(2022), 100249. https://doi.org/10.1016/j.crgsc.2021.100249

Bitew, B. D., Gete, Y. K., Biks, G. A., & Adafrie, T. T. (2018). The effect of SODIS water treatment intervention at the household level in reducing diarrheal incidence among children under 5 years of age: A cluster randomized controlled trial in Dabat district, northwest Ethiopia. *Trials*, *19*(1), 412. https://doi.org/10.1186/s13063-018-2797-y

Bunaciu, A. A., Udriştioiu, E. gabriela, & Aboul-Enein, H. Y. (2015). X-Ray Diffraction: Instrumentation and Applications. *Critical Reviews in Analytical Chemistry*, *45*(4), 289–299. https://doi.org/10.1080/10408347.2014.949616

Bustillo-Lecompte, C. F., & Mehrvar, M. (2015). Slaughterhouse wastewater characteristics, treatment, and management in the meat processing industry: A review on trends and advances. *Journal of Environmental Management*, *161*, 287–302. https://doi.org/10.1016/j.jenvman.2015.07.008

Cabrera, A. F., Rodríguez Torres, C. E., Marchetti, S. G., & Stewart, S. J. (2020). Degradation of methylene blue dye under dark and visible light conditions in presence of hybrid composites of nanostructured MgFe2O4 ferrites and oxygenated organic compounds. *Journal of Environmental Chemical Engineering*, *8*(5), 104274. https://doi.org/10.1016/j.jece.2020.104274

Cai, Z., Sun, Y., Liu, W., Pan, F., Sun, P., & Fu, J. (2017). An overview of nanomaterials applied for removing dyes from wastewater. *Environmental Science and Pollution Research*, *24*(19), 15882–15904. https://doi.org/10.1007/s11356-017-9003-8

Cardoso, V. S., Quelemes, P. V., Amorin, A., Primo, F. L., Gobo, G. G., Tedesco, A. C., Mafud, A. C., Mascarenhas, Y. P., Corrêa, J. R., Kuckelhaus, S. A., Eiras, C., Leite, J. R. S., & Silva, D. (2014). *Collagen-based silver nanoparticles for biological applications: Synthesis and characterization*. 9.

Chakraborty, S., Mukherjee, A., Das, S., Raju Maddela, N., Iram, S., & Das, P. (2020). Study on isotherm, kinetics, and thermodynamics of adsorption of crystal violet dye by calcium oxide modified fly ash. *Environmental Engineering Research*, *26*(1). https://doi.org/10.4491/eer.2019.372

Cheng, S., Huang, A., Wang, S., & Zhang, Q. (2016). Effect of Different Heat Treatment Temperatures on the Chemical Composition and Structure of Chinese Fir Wood. *BioResources*, *11*(2), 4006–4016. https://doi.org/10.15376/biores.11.2.4006-4016

Cheruiyot, G. K., Wanyonyi, W. C., Kiplimo, J. J., & Maina, E. N. (2019). Adsorption of toxic crystal violet dye using coffee husks: Equilibrium, kinetics and thermodynamics study. *Scientific African*, *5*, e00116. https://doi.org/10.1016/j.sciaf.2019.e00116

Chilakamarry, C. R., Mahmood, S., Saffe, S. N. B. M., Arifin, M. A. B., Gupta, A., Sikkandar, M. Y., Begum, S. S., & Narasaiah, B. (2021). Extraction and application of keratin from natural resources: A review. *3 Biotech*, *11*(5), 220. https://doi.org/10.1007/s13205-021-02734-7

Cowie, B. E., Porley, V., & Robertson, N. (2020). Solar Disinfection (SODIS) Provides a Much Underexploited Opportunity for Researchers in Photocatalytic Water

Treatment (PWT). *ACS Catalysis*, *10*(20), 11779–11782. https://doi.org/10.1021/acscatal.0c03325

Czikkely, M., Neubauer, E., Fekete, I., Ymeri, P., & Fogarassy, C. (2018). Review of Heavy Metal Adsorption Processes by Several Organic Matters from Wastewaters. *Water*, *10*(10), 1377. https://doi.org/10.3390/w10101377

Dąbrowska, M., Sommer, A., Sinkiewicz, I., Taraszkiewicz, A., & Staroszczyk, H. (2022). An optimal designed experiment for the alkaline hydrolysis of feather keratin. *Environmental Science and Pollution Research*, *29*(16), 24145–24154. https://doi.org/10.1007/s11356-021-17649-2

Dahri, M. K., Kooh, M. R. R., & Lim, L. B. L. (2013). Removal of Methyl Violet 2B from Aqueous Solution Using *Casuarina equisetifolia* Needle. *ISRN Environmental Chemistry*, *2013*, 1–8. https://doi.org/10.1155/2013/619819

Dang, T. M. D., Le, T. T. T., Fribourg-Blanc, E., & Dang, M. C. (2011). Synthesis and optical properties of copper nanoparticles prepared by a chemical reduction method. *Advances in Natural Sciences: Nanoscience and Nanotechnology*, *2*(1), Article 1. https://doi.org/10.1088/2043-6262/2/1/015009

DeFrates, K., Markiewicz, T., Gallo, P., Rack, A., Weyhmiller, A., Jarmusik, B., & Hu, X. (2018). Protein Polymer-Based Nanoparticles: Fabrication and Medical Applications. *International Journal of Molecular Sciences*, *19*, 1–20. https://doi.org/doi:10.3390/ijms19061717

Donato, R. K., & Mija, A. (2019). Keratin Associations with Synthetic, Biosynthetic and Natural Polymers: An Extensive Review. *Polymers*, *12*(1), 32. https://doi.org/10.3390/polym12010032

Ehiomogue, P., Ahuchaogu, I. I., & Ahaneku, I. E. (2021). Review of Adsorption Isotherms Models. *ACT Corviniensis – Bulletin of Engineering*, *4*.

Elsherif, Khaled M., El-Dali, Abdelmeneim, Alkarewi, Asma A., Ewlad-Ahmed, Abdunaser M., & Treban, Abdullah. (2021). *Adsorption of crystal violet dye onto olive leaves powder: Equilibrium and kinetic studies* (Chemistry International 2; pp 79–89. Open Science Framework. https://doi.org/10.31219/osf.io/c4uqx

Ezealisiji, K. M., Siwe-Noundou, X., Maduelosi, B., Nwachukwu, N., & Krause, R. W. M. (2019). Green synthesis of zinc oxide nanoparticles using Solanum torvum (L) leaf extract and evaluation of the toxicological profile of the ZnO nanoparticles–hydrogel composite in Wistar albino rats. *International Nano Letters*, *9*(2), Article 2. https://doi.org/10.1007/s40089-018-0263-1

Fagbemi, O. D., Sithole, B., & Tesfaye, T. (2020). Optimization of keratin protein extraction from waste chicken feathers using hybrid pre-treatment techniques. *Sustainable Chemistry and Pharmacy*, *17*, 100267. https://doi.org/10.1016/j.scp.2020.100267

Fatemi, M., Mollania, N., Momeni-Moghaddam, M., & Sadeghifar, F. (2018). Extracellular biosynthesis of magnetic iron oxide nanoparticles by Bacillus cereus strain HMH1: Characterization and in vitro cytotoxicity analysis on MCF-7 and

3T3 cell lines. *Journal of Biotechnology*, *270*, 1–11. https://doi.org/10.1016/j.jbiotec.2018.01.021

Ferroni, C., & Varchi, G. (2021). Keratin-Based Nanoparticles as Drug Delivery Carriers. *Applied Sciences*, *11*(20), 9417. https://doi.org/10.3390/app11209417

Foglietta, F., Spagnoli, G. C., Muraro, M. G., Ballestri, M., Guerrini, A., Ferroni, C., Aluigi, A., Sotgiu, G., & Varchi, G. (2018). Anticancer activity of paclitaxel-loaded keratin nanoparticles in two-dimensional and perfused three-dimensional breast cancer models. *International Journal of Nanomedicine*, *13*, 4847–4867. https://doi.org/10.2147/IJN.S159942

Fouda-Mbanga, B. G., Prabakaran, E., & Pillay, K. (2021). Carbohydrate biopolymers, lignin based adsorbents for removal of heavy metals (Cd^{2+}, Pb^{2+}, Zn^{2+}) from wastewater, regeneration and reuse for spent adsorbents including latent fingerprint detection: A review. *Biotechnology Reports*, *30*, e00609. https://doi.org/10.1016/j.btre.2021.e00609

García-Gil, Á., García-Muñoz, R. A., McGuigan, K. G., & Marugán, J. (2021). Solar Water Disinfection to Produce Safe Drinking Water: A Review of Parameters, Enhancements, and Modelling Approaches to Make SODIS Faster and Safer. *Molecules*, *26*(11), 3431. https://doi.org/10.3390/molecules26113431

Göl, F., Aygün, A., Seyrankaya, A., Gür, T., Yenikaya, C., & Şen, F. (2020). Green synthesis and characterization of Camellia sinensis mediated silver nanoparticles for antibacterial ceramic applications. *Materials Chemistry and Physics*, *250*, 123037. https://doi.org/10.1016/j.matchemphys.2020.123037

Guarino, V., Benfenati, V., Cruz-Maya, I., Saracino, E., Zamboni, R., & Ambrosio, L. (2018). Instructive proteins for tissue regeneration. In *Functional 3D Tissue Engineering Scaffolds* (pp. 23–49). Elsevier. https://doi.org/10.1016/B978-0-08-100979-6.00002-1

Guo, J., Liu, J., Qie, H., Zhao, F., & Niu, C. H. (2021). Efficient synthesis strategy of folate-modified carboxymethyl chitosan/$CaCO_3$ hybrid nanospheres and their drug-carrying and sustained release properties. *Journal of Biomaterials Science, Polymer Edition*, 1–14. https://doi.org/10.1080/09205063.2020.1870258

Haleem, A., Javaid, M., Singh, R. P., Rab, S., & Suman, R. (2023). Applications of nanotechnology in medical field: A brief review. *Global Health Journal*, *7*(2), 70–77. https://doi.org/10.1016/j.glohj.2023.02.008

Ho, L., Alonso, A., Eurie Forio, M. A., Vanclooster, M., & Goethals, P. L. M. (2020). Water research in support of the Sustainable Development Goal 6: A case study in Belgium. *Journal of Cleaner Production*, *277*, 124082. https://doi.org/10.1016/j.jclepro.2020.124082

Hu, Q., Tuck, C., Wildman, R., & Hague, R. (2016). Application of Nanoparticles in Manufacturing. In M. Aliofkhazraei (Ed.), *Handbook of Nanoparticles* (pp. 1219–1278). Springer International Publishing. https://doi.org/10.1007/978-3-319-15338-4_55

Husen, A., & Siddiqi, K. S. (2014). *Plants and microbes assisted selenium nanoparticles: Characterization and application*. 10.

Igwegbe, C. A., Mohmmadi, L., Ahmadi, S., Rahdar, A., Khadkhodaiy, D., Dehghani, R., & Rahdar, S. (2019). Modeling of adsorption of Methylene Blue dye on Ho-CaWO4 nanoparticles using Response Surface Methodology (RSM) and Artificial Neural Network (ANN) techniques. *MethodsX*, *6*, 1779–1797. https://doi.org/10.1016/j.mex.2019.07.016

Inkson, B. J. (2016). Scanning electron microscopy (SEM) and transmission electron microscopy (TEM) for materials characterization. In *Materials Characterization Using Nondestructive Evaluation (NDE) Methods* (pp. 17–43). Elsevier. https://doi.org/10.1016/B978-0-08-100040-3.00002-X

Jahan, I., Erci, F., & Isildak, I. (2021). Rapid green synthesis of non-cytotoxic silver nanoparticles using aqueous extracts of "Golden Delicious" apple pulp and cumin seeds with antibacterial and antioxidant activity. *SN Applied Sciences*, *3*(1), Article 1. https://doi.org/10.1007/s42452-020-04046-6

Jamkhande, P. G., Ghule, N. W., Bamer, A. H., & Kalaskar, M. G. (2019). Metal nanoparticles synthesis: An overview on methods of preparation, advantages and disadvantages, and applications. *Journal of Drug Delivery Science and Technology*, *53*, 101174. https://doi.org/10.1016/j.jddst.2019.101174

Jeevanandam, J., Barhoum, A., Chan, Y. S., Dufresne, A., & Danquah, M. K. (2018). Review on nanoparticles and nanostructured materials: History, sources, toxicity and regulations. *Beilstein Journal of Nanotechnology*, *9*, 1050–1074. https://doi.org/10.3762/bjnano.9.98

Jiang, B., Gong, Y., Gao, J., Sun, T., Liu, Y., Oturan, N., & Oturan, M. A. (2019). The reduction of Cr(VI) to Cr(III) mediated by environmentally relevant carboxylic acids: State-of-the-art and perspectives. *Journal of Hazardous Materials*, *365*, 205–226. https://doi.org/10.1016/j.jhazmat.2018.10.070

Kamarudin, N. B., Sharma, S., Gupta, A., Kee, C. G., Chik, S. M. S. B. T., & Gupta, R. (2017). Statistical investigation of extraction parameters of keratin from chicken feather using Design-Expert. *3 Biotech*, *7*(2), Article 2. https://doi.org/10.1007/s13205-017-0767-9

Keat, C. L. (2015). *Biosynthesis of nanoparticles and silver nanoparticles*. *2*, 11. https://doi.org/10.1186/s40643-015-0076-2

Kesić, A., Marković, K., Grujović, M., & Marković, Z. (2023). An Investigation of the Optimal Conditions for the Green Synthesis of Silver Nanoparticles Using an Aqueous Extract from the Agrimonia eupatoria L. Plant. *IOCN 2023*, 1. https://doi.org/10.3390/IOCN2023-14477

Khan, A. (2016). A chemical reduction approach to the synthesis of copper nanoparticles. *Int Nano Lett*, 6.

Khan, I., Saeed, K., & Khan, I. (2019). Nanoparticles: Properties, applications and toxicities. *Arabian Journal of Chemistry*, *12*(7), 908–931. https://doi.org/10.1016/j.arabjc.2017.05.011

Khan, I., Saeed, K., Zekker, I., Zhang, B., Hendi, A. H., Ahmad, A., Ahmad, S., Zada, N., Ahmad, H., Shah, L. A., Shah, T., & Khan, I. (2022). Review on Methylene Blue: Its Properties, Uses, Toxicity and Photodegradation. *Water*, *14*(2), 242. https://doi.org/10.3390/w14020242

Khan, S. A., Khan, S. B., Khan, L. U., Farooq, A., Akhtar, K., & Asiri, A. M. (2018). Fourier Transform Infrared Spectroscopy: Fundamentals and Application in Functional Groups and Nanomaterials Characterization. In S. K. Sharma (Ed.), *Handbook of Materials Characterization* (pp. 317–344). Springer International Publishing. https://doi.org/10.1007/978-3-319-92955-2_9

Kuang, Y., Guo, X., Hu, J., Li, S., Zhang, R., Gao, Q., Yang, X., Chen, Q., & Sun, W. (2020). Occurrence and risks of antibiotics in an urban river in northeastern Tibetan Plateau. *Scientific Reports*, *10*(1), 20054. https://doi.org/10.1038/s41598-020-77152-5

Lele, S. (2017). Sustainable Development Goal 6: Watering down justice concerns. *WIREs Water*, *4*(4), e1224. https://doi.org/10.1002/wat2.1224

Lellis, B., Fávaro-Polonio, C. Z., Pamphile, J. A., & Polonio, J. C. (2019). Effects of textile dyes on health and the environment and bioremediation potential of living organisms. *Biotechnology Research and Innovation*, *3*(2), 275–290. https://doi.org/10.1016/j.biori.2019.09.001

LewisOscar, F., MubarakAli, D., Nithya, C., Priyanka, R., Gopinath, V., Alharbi, N. S., & Thajuddin, N. (2015). One pot synthesis and anti-biofilm potential of copper nanoparticles (CuNPs) against clinical strains of *Pseudomonas aeruginosa*. *Biofouling*, *31*(4), 379–391. https://doi.org/10.1080/08927014.2015.1048686

Li, H., Budarin, V. L., Clark, J. H., North, M., & Wu, X. (2022). Rapid and efficient adsorption of methylene blue dye from aqueous solution by hierarchically porous, activated starbons®: Mechanism and porosity dependence. *Journal of Hazardous Materials*, *436*, 129174. https://doi.org/10.1016/j.jhazmat.2022.129174

Liaqat, N., Jahan, N., Anwar, T., & Qureshi, H. (2022). Green synthesized silver nanoparticles: Optimization, characterization, antimicrobial activity, and cytotoxicity study by hemolysis assay. *Frontiers in Chemistry*, *10*.

Liu, J., Yang, H., Gosling, S. N., Kummu, M., Flörke, M., Pfister, S., Hanasaki, N., Wada, Y., Zhang, X., Zheng, C., Alcamo, J., & Oki, T. (2017). Water scarcity assessments in the past, present, and future: Review on water scarcity assessment. *Earth's Future*, *5*(6), 545–559. https://doi.org/10.1002/2016EF000518

Liu, L., Zhang, X., Yang, L., Ren, L., Wang, D., & Ye, J. (2017). Metal nanoparticles induced photocatalysis. *National Science Review*, *4*(5), 761–780. https://doi.org/10.1093/nsr/nwx019

Lü, X., & Cui, S. (2010). Wool keratin-stabilized silver nanoparticles. *Bioresource Technology*, *101*(12), 4703–4707. https://doi.org/10.1016/j.biortech.2010.01.110

Lukman, A. I., Gong, B., Marjo, C. E., Roessner, U., & Harris, A. T. (2011). Facile synthesis, stabilization, and anti-bacterial performance of discrete Ag nanoparticles using Medicago sativa seed exudates. *Journal of Colloid and Interface Science*, *353*(2), 433–444. https://doi.org/10.1016/j.jcis.2010.09.088

Malik, S., Muhammad, K., & Waheed, Y. (2023). Emerging Applications of Nanotechnology in Healthcare and Medicine. *Molecules*, *28*(18), 6624. https://doi.org/10.3390/molecules28186624

Mancosu, N., Snyder, R., Kyriakakis, G., & Spano, D. (2015). Water Scarcity and Future Challenges for Food Production. *Water*, *7*(12), 975–992. https://doi.org/10.3390/w7030975

Martella, E., Ferroni, C., Guerrini, A., Ballestri, M., Columbaro, M., Santi, S., Sotgiu, G., Serra, M., Donati, D. M., Lucarelli, E., Varchi, G., & Duchi, S. (2018). Functionalized Keratin as Nanotechnology-Based Drug Delivery System for the Pharmacological Treatment of Osteosarcoma. *Int. J. Mol. Sci.*, 16.

Martins, G. R., Monteiro, A. F., Do Amaral, F. R. L., & Da Silva, A. S. (2021). A validated Folin-Ciocalteu method for total phenolics quantification of condensed tannin-rich açaí (Euterpe oleracea Mart.) seeds extract. *Journal of Food Science and Technology*, *58*(12), 4693–4702. https://doi.org/10.1007/s13197-020-04959-5

Matouq, M., Jildeh, N., Qtaishat, M., Hindiyeh, M., & Al Syouf, M. Q. (2015). The adsorption kinetics and modeling for heavy metals removal from wastewater by Moringa pods. *Journal of Environmental Chemical Engineering*, *3*(2), 775–784. https://doi.org/10.1016/j.jece.2015.03.027

Mbewana-Ntshanka, N. G., Moloto, M. J., & Mubiayi, P. K. (2020). Role of the amine and phosphine groups in oleylamine and trioctylphosphine in the synthesis of copper chalcogenide nanoparticles. *Heliyon*, *6*(11), e05130. https://doi.org/10.1016/j.heliyon.2020.e05130

Meili, L., Lins, P. V. S., Costa, M. T., Almeida, R. L., Abud, A. K. S., Soletti, J. I., Dotto, G. L., Tanabe, E. H., Sellaoui, L., Carvalho, S. H. V., & Erto, A. (2019). Adsorption of methylene blue on agroindustrial wastes: Experimental investigation and phenomenological modelling. *Progress in Biophysics and Molecular Biology*, *141*, 60–71. https://doi.org/10.1016/j.pbiomolbio.2018.07.011

Mittal, A. K., Chisti, Y., & Banerjee, U. C. (2013). Synthesis of metallic nanoparticles using plant extracts. *Biotechnology Advances*, *31*(2), 346–356. https://doi.org/10.1016/j.biotechadv.2013.01.003

Mohammad, N., & Atassi, Y. (2020). Adsorption of methylene blue onto electrospun nanofibrous membranes of polylactic acid and polyacrylonitrile coated with chloride doped polyaniline. *Scientific Reports*, *10*(1), 13412. https://doi.org/10.1038/s41598-020-69825-y

Mokrejs, P., Svoboda, P., Hrncirik, J., Janacova, D., & Vasek, V. (2011). Processing poultry feathers into keratin hydrolysate through alkaline-enzymatic hydrolysis. *Waste Management & Research: The Journal for a Sustainable Circular Economy*, *29*(3), 260–267. https://doi.org/10.1177/0734242X10370378

Mourdikoudis, S., Pallares, R. M., & Thanh, N. T. K. (2018). Characterization techniques for nanoparticles: Comparison and complementarity upon studying nanoparticle properties. *Nanoscale*, *10*(27), 12871–12934. https://doi.org/10.1039/C8NR02278J

Mrunal, V. K., Vishnu, A. K., Momin, N., & Manjanna, J. (2019). Cu2O nanoparticles for adsorption and photocatalytic degradation of methylene blue dye from aqueous medium. *Environmental Nanotechnology, Monitoring & Management*, *12*, 100265. https://doi.org/10.1016/j.enmm.2019.100265

Muhammad, W., Ullah, N., Haroon, M., & Abbasi, B. H. (2019). Optical, morphological and biological analysis of zinc oxide nanoparticles (ZnO NPs) using *Papaver somniferum* L. *RSC Advances*, *9*(51), Article 51. https://doi.org/10.1039/C9RA04424H

Mulwa, F., Li, Z., & Fangninou, F. F. (2021). Water Scarcity in Kenya: Current Status, Challenges and Future Solutions. *OALib*, *08*(01), 1–15. https://doi.org/10.4236/oalib.1107096

Musa, M. A., & Idrus, S. (2021). Physical and Biological Treatment Technologies of Slaughterhouse Wastewater: A Review. *Sustainability*, *13*(9), 4656. https://doi.org/10.3390/su13094656

Mustățea, G., Ungureanu, E. L., & Iorga, E. (2019). Protein acidic hydrolysis for amino acid analysis in food—Progress over time: A Short review. *Journal of Hygienic Engineering and Design*.

Nanthavanan, Kandasamy Arungandhi, Sunmathi D, & Niranjana J. (2019). Biological synthesis of keratin nanoparticles from dove feather (columba livia) and it's applications. *Asian Journal of Pharmaceutical and Clinical Research*, 142–146. https://doi.org/10.22159/ajpcr.2019.v12i10.34572

Narayanan, K. B., & Sakthivel, N. (2010). Biological synthesis of metal nanoparticles by microbes. *Advances in Colloid and Interface Science*, *156*(1–2), 1–13. https://doi.org/10.1016/j.cis.2010.02.001

Noimark, S., Bovis, M., MacRobert, A. J., Correia, A., Allan, E., Wilson, M., & Parkin, I. P. (2013). Photobactericidal polymers; the incorporation of crystal violet and nanogold into medical grade silicone. *RSC Advances*, *3*(40), 18383. https://doi.org/10.1039/c3ra42629g

Nuño Martínez, N., Muela Ribera, J., Hausmann-Muela, S., Cevallos, M., Hartinger, S. M., Christen, A., & Mäusezahl, D. (2020). The Meanings of Water: Socio-Cultural Perceptions of Solar Disinfected (SODIS) Drinking Water in Bolivia and Implications for its Uptake. *Water*, *12*(2), 442. https://doi.org/10.3390/w12020442

Oloo, C. M., Onyari, J. M., Wanyonyi, W. C., Wabomba, J. N., & Muinde, V. M. (2020). Adsorptive removal of hazardous crystal violet dye form aqueous solution using Rhizophora mucronata stem-barks: Equilibrium and kinetics studies. *Environmental Chemistry and Ecotoxicology*, *2*, 64–72. https://doi.org/10.1016/j.enceco.2020.05.001

Omari Phanice & Masimba O. Zachary. (2018). Knowledge, Pregnant, Birth, Postpartum, Obstetric danger signs. *Research in Obstetrics and Gynecology*, *6*(1), 16–21. https://doi.org/DOI: 10.5923/j.rog.20180601.03

Osagie, C., Othmani, A., Ghosh, S., Malloum, A., Kashitarash Esfahani, Z., & Ahmadi, S. (2021). Dyes adsorption from aqueous media through the nanotechnology: A review. *Journal of Materials Research and Technology*, *14*, 2195–2218. https://doi.org/10.1016/j.jmrt.2021.07.085

Oztekin, E., & Altin, S. (2016). Wastewater treatment by electrodialysis system and fouling problems. *Journal of Science and Technology*, *6*(1), 91–99.

Pan, F., Lu, Z., Tucker, I., Hosking, S., Petkov, J., & Lu, J. R. (2016). Surface active complexes formed between keratin polypeptides and ionic surfactants. *Journal of Colloid and Interface Science*, *484*(2016), 125–134. https://doi.org/10.1016/j.jcis.2016.08.082

Paşka, O., Ianoş, R., Păcurariu, C., & Brădeanu, A. (2014). Magnetic nanopowder as effective adsorbent for the removal of Congo Red from aqueous solution. *Water Science and Technology*, *69*(6), 1234–1240. https://doi.org/10.2166/wst.2013.827

Patra, J. K., & Baek, K.-H. (2014). Green Nanobiotechnology: Factors Affecting Synthesis and Characterization Techniques. *Journal of Nanomaterials*, *2014*, 1–12. https://doi.org/10.1155/2014/417305

Piri, F., Mollahosseini, A., Khadir, A., & Milani Hosseini, M. (2019). Enhanced adsorption of dyes on microwave-assisted synthesized magnetic zeolite-hydroxyapatite nanocomposite. *Journal of Environmental Chemical Engineering*, *7*(5), 103338. https://doi.org/10.1016/j.jece.2019.103338

Popescu, R. C., Fufă, M. O. M., Grumezescu, A. M., & Holban, A. M. (2017). Nanostructurated membranes for the microbiological purification of drinking water. In *Water Purification* (pp. 421–446). Elsevier. https://doi.org/10.1016/B978-0-12-804300-4.00012-5

Priya, T., Mishra, B. K., & Prasad, M. N. V. (2020). Physico-chemical techniques for the removal of disinfection by-products precursors from water. In *Disinfection By-products in Drinking Water* (pp. 23–58). Elsevier. https://doi.org/10.1016/B978-0-08-102977-0.00002-0

Puneetha, Kottam, N., & A, R. (2021). Investigation of photocatalytic degradation of crystal violet and its correlation with bandgap in ZnO and ZnO/GO nanohybrid. *Inorganic Chemistry Communications*, *125*, 108460. https://doi.org/10.1016/j.inoche.2021.108460

Qomariyah, A., & Hakim, A. K. (2024). *Synthesis of Copper Nanoparticles Using Dragon Fruit (Hylocereus polyrhizus) Extract as a Bio- Reductor and Their Analysis Using a UV-Visible Spectrophotometer*.

Rada-Mendoza, M. D. P., Villamiel-Guerra, M. D. M., Hoyos-Saavedra, O. L., & Alvira, L. F. (2018). Quantification of lead using atomic absorption spectrometry in thermoformed and biodegradable flexible films made from cassava (Manihot esculenta crantz). *DYNA*, *85*(207), 236–242. https://doi.org/10.15446/dyna.v85n207.72347

Rai, P. K., Lee, S. S., Zhang, M., Tsang, Y. F., & Kim, K.-H. (2019). Heavy metals in food crops: Health risks, fate, mechanisms, and management. *Environment International*, *125*, 365–385. https://doi.org/10.1016/j.envint.2019.01.067

Raja, P. M. V., & Barron, A. R. (2020). Physical Methods in Chemistry and Nano Science. *Chem.Libretexts.Org*, 55813.

Ramutshatsha-Makhwedzha, D., Mavhungu, A., Moropeng, M. L., & Mbaya, R. (2022). Activated carbon derived from waste orange and lemon peels for the adsorption of methyl orange and methylene blue dyes from wastewater. *Heliyon*, *8*(8), e09930. https://doi.org/10.1016/j.heliyon.2022.e09930

Rashad, S., Zaki, A. H., & Farghali, A. A. (2019). Morphological effect of titanate nanostructures on the photocatalytic degradation of crystal violet. *Nanomaterials and Nanotechnology*, *9*, 184798041882177. https://doi.org/10.1177/1847980418821778

Rashid, H., Mansoor, M. A., Haider, B., Nasir, R., Abd Hamid, S. B., & Abdulrahman, A. (2020). Synthesis and characterization of magnetite nano particles with high selectivity using in-situ precipitation method. *Separation Science and Technology*, *55*(6), 1207–1215. https://doi.org/10.1080/01496395.2019.1585876

Ray, S. S., Gusain, R., & Kumar, N. (2020). Water purification using various technologies and their advantages and disadvantages. In *Carbon Nanomaterial-Based Adsorbents for Water Purification* (pp. 37–66). Elsevier. https://doi.org/10.1016/B978-0-12-821959-1.00003-9

Restrepo, C. V., & Villa, C. C. (2021). Synthesis of silver nanoparticles, influence of capping agents, and dependence on size and shape: A review. *Environmental Nanotechnology, Monitoring & Management*, *15*, 100428. https://doi.org/10.1016/j.enmm.2021.100428

Sabna, V., Thampi, S. G., & Chandrakaran, S. (2016). Adsorption of crystal violet onto functionalised multi-walled carbon nanotubes: Equilibrium and kinetic studies. *Ecotoxicology and Environmental Safety*, *134*, 390–397. https://doi.org/10.1016/j.ecoenv.2015.09.018

Sadia, B. O., Cherutoi, J. K., & Achisa, C. M. (2021). Optimization, Characterization, and Antibacterial Activity of Copper Nanoparticles Synthesized Using Senna didymobotrya Root Extract. *Journal of Nanotechnology*, *2021*, 1–15. https://doi.org/10.1155/2021/5611434

Sanchez Ramirez, D. O., Vineis, C., Cruz-Maya, I., Tonetti, C., Guarino, V., & Varesano, A. (2022). Wool Keratin Nanofibers for Bioinspired and Sustainable Use in Biomedical Field. *Journal of Functional Biomaterials*, *14*(1), 5. https://doi.org/10.3390/jfb14010005

Santos, C. S. C., Gabriel, B., Blanchy, M., Menes, O., García, D., Blanco, M., Arconada, N., & Neto, V. (2014). Industrial applications of nanoparticles – a prospective overview. *Materials Today*, 12. https://doi.org/10.13140/2.1.5100.6726

Shankar, S., & Rhim, J.-W. (2019). Eco-friendly antimicrobial nanoparticles of keratin-metal ion complex. *Materials Science and Engineering: C*, *105*, 110068. https://doi.org/10.1016/j.msec.2019.110068

Shanker, U., Rani, M., & Jassal, V. (2017). Degradation of hazardous organic dyes in water by nanomaterials. *Environ Chem Lett*, 20.

Sharaf Zeebaree, S. Y., Sharaf Zeebaree, A. Y., Haji Zebari, O. I., & Sharaf Zebari, A. Y. (2021). Sustainable fabrication, optical properties and rapid performance of bio-engineered copper nanoparticles in removal of toxic methylene blue dye in an aqueous medium. *Current Research in Green and Sustainable Chemistry*, *4*, 100103. https://doi.org/10.1016/j.crgsc.2021.100103

Sharma, S., & Bhattacharya, A. (2017). Drinking water contamination and treatment techniques. *Applied Water Science*, *7*(3), 1043–1067. https://doi.org/10.1007/s13201-016-0455-7

Sharma, S., & Gupta, A. (2016). Sustainable Management of Keratin Waste Biomass: Applications and Future Perspectives. *Brazilian Archives of Biology and Technology*, *59*(0). https://doi.org/10.1590/1678-4324-2016150684

Sigei, G., K. Hillary, B., K. Jonah, K., & O. Timothy, O. (2015). Factors Influencing the Choice of Marketing Outlets among Small-Scale Pineapple Farmers in Kericho County, Kenya. *International Journal of Regional Development*, *2*(2), 1. https://doi.org/10.5296/ijrd.v2i2.6237

Sila, M. J., Nyambura, M. I., Abong'o, D. A., Mwaura, F. B., & Iwuoha, E. (2019). Biosynthesis of Silver Nanoparticles from *Eucalyptus corymbia* Leaf Extract at Optimized Conditions. *Nano Hybrids and Composites*, *25*, 32–45. https://doi.org/10.4028/www.scientific.net/NHC.25.32

Sim, S., & Wong, N. (2021). Nanotechnology and its use in imaging and drug delivery (Review). *Biomedical Reports*, *14*(5), 42. https://doi.org/10.3892/br.2021.1418

Singh, A., Gaud, B., & Jaybhaye, S. (2020). Optimization of synthesis parameters of silver nanoparticles and its antimicrobial activity. *Materials Science for Energy Technologies*, *3*, 232–236. https://doi.org/10.1016/j.mset.2019.08.004

Singh, M. R., & Gupta, A. (2016). Water pollution-sources,effects and control. *Pointer Publishers Jaipur.*, 17.

Singh, N., & Goldsmith, B. R. (2020). Role of Electrocatalysis in the Remediation of Water Pollutants. *ACS Catalysis*, *10*(5), 3365–3371. https://doi.org/10.1021/acscatal.9b04167

Sinha, T., & Ahmaruzzaman, M. (2015). Green synthesis of copper nanoparticles for the efficient removal (degradation) of dye from aqueous phase. *Environmental Science and Pollution Research*, *22*(24), 20092–20100. https://doi.org/10.1007/s11356-015-5223-y

Sinkiewicz, I., Śliwińska, A., Staroszczyk, H., & Kołodziejska, I. (2017). Alternative Methods of Preparation of Soluble Keratin from Chicken Feathers. *Waste and Biomass Valorization*, *8*(4), 1043–1048. https://doi.org/10.1007/s12649-016-9678-y

Sıdır, Y. G., Sıdır, İ., Berber, H., & Taşal, E. (2011). UV-spectral changes for some azo compounds in the presence of different solvents. *Journal of Molecular Liquids*, *162*(3), 148–154. https://doi.org/10.1016/j.molliq.2011.07.002

Srivastava, V., & Choubey, A. K. (2021). Investigation of adsorption of organic dyes present in wastewater using chitosan beads immobilized with biofabricated CuO nanoparticles. *Journal of Molecular Structure*, *1242*, 130749. https://doi.org/10.1016/j.molstruc.2021.130749

Stark, W. J., Stoessel, P. R., Wohlleben, W., & Hafner, A. (2015). Industrial applications of nanoparticles. *Chemical Society Reviews*, *44*(16), Article 16. https://doi.org/10.1039/C4CS00362D

Suramwar, N. V., Thakare, S. R., & Khaty, N. T. (2016). One pot synthesis of copper nanoparticles at room temperature and its catalytic activity. *Arabian Journal of Chemistry*, *9*, S1807–S1812. https://doi.org/10.1016/j.arabjc.2012.04.034

Sutanto, N., Saharudin, K. A., Sreekantan, S., Kumaravel, V., & Md Akil, H. (2020). Heterojunction catalysts g-C3N4/-3ZnO-c-Zn2Ti3O8 with highly enhanced visible-light-driven photocatalytic activity. *Journal of Sol-Gel Science and Technology*, *93*(2), 354–370. https://doi.org/10.1007/s10971-019-05101-4

Tasaki, K. (2020). A novel thermal hydrolysis process for extraction of keratin from hog hair for commercial applications. *Waste Management*, *104*(2020), 33–41. https://doi.org/10.1016/j.wasman.2019.12.042

Thakkar, K. N., Mhatre, S. S., & Parikh, R. Y. (2010). Biological synthesis of metallic nanoparticles. *Nanomedicine: Nanotechnology, Biology and Medicine*, *6*(2), 257–262. https://doi.org/10.1016/j.nano.2009.07.002

Thiruvengadam, M., Chung, I.-M., Gomathi, T., Ansari, M. A., Gopiesh Khanna, V., Babu, V., & Rajakumar, G. (2019). Synthesis, characterization and pharmacological potential of green synthesized copper nanoparticles. *Bioprocess and Biosystems Engineering*, *42*(11), Article 11. https://doi.org/10.1007/s00449-019-02173-y

Thomas, S., Harshita, B. S. P., Mishra, P., & Talegaonkar, S. (2015). Ceramic Nanoparticles: Fabrication Methods and Applications in Drug Delivery. *Current Pharmaceutical Design*, *21*(42), Article 42. https://doi.org/10.2174/1381612821666151027153246

Tlili, I., & Alkanhal, T. A. (2019). Nanotechnology for water purification: Electrospun nanofibrous membrane in water and wastewater treatment. *Journal of Water Reuse and Desalination*, *9*(3), 232–248. https://doi.org/10.2166/wrd.2019.057

Vahur, S., Teearu, A., Peets, P., Joosu, L., & Leito, I. (2016). ATR-FT-IR spectral collection of conservation materials in the extended region of 4000-80 cm–1. *Analytical and Bioanalytical Chemistry*, *408*(13), 3373–3379. https://doi.org/10.1007/s00216-016-9411-5

Wang, B., Yang, W., McKittrick, J., & Meyers, M. A. (2016). Keratin: Structure, mechanical properties, occurrence in biological organisms, and efforts at bioinspiration. *Progress in Materials Science*, *76*, 229–318. https://doi.org/10.1016/j.pmatsci.2015.06.001

Wang, D., Yang, X.-H., Tang, R.-C., & Yao, F. (2018). Extraction of Keratin from Rabbit Hair by a Deep Eutectic Solvent and Its Characterization. *Polymers*, *10*(9), 993. https://doi.org/10.3390/polym10090993

Wang, K., Li, R., Ma, J. H., Jian, Y. K., & Che, J. N. (2016). Extracting keratin from wool by using L -cysteine. *Green Chemistry*, *18*(2), 476–481. https://doi.org/10.1039/C5GC01254F

Wanyonyi, W. C., Onyari, J. M., & Shiundu, P. M. (2014). Adsorption of Congo Red Dye from Aqueous Solutions Using Roots of Eichhornia Crassipes: Kinetic and Equilibrium Studies. *Energy Procedia*, *50*, 862–869. https://doi.org/10.1016/j.egypro.2014.06.105

Wasike, P. W., Nawiri, M. P., & Wanyonyi, A. A. (2019). Levels of Heavy Metals (Pb, Mn, Cu and Cd) in Water from River Kuywa and the Adjacent Wells. *Environment and Ecology Research*, *7*(3), 135–138. https://doi.org/10.13189/eer.2019.070303

Wegmann, M., & Scharr, M. (2018). Synthesis of Magnetic Iron Oxide Nanoparticles. In *Precision Medicine* (pp. 145–181). Elsevier. https://doi.org/10.1016/B978-0-12-805364-5.00008-1

William Kajjumba, G., Emik, S., Öngen, A., Kurtulus Özcan, H., & Aydın, S. (2019). Modelling of Adsorption Kinetic Processes—Errors, Theory and Application. In S. Edebali (Ed.), *Advanced Sorption Process Applications*. IntechOpen. https://doi.org/10.5772/intechopen.80495

Wu, Y. (2017). The Removal of Methyl Orange by Periphytic Biofilms. In *Periphyton* (pp. 367–387). Elsevier. https://doi.org/10.1016/B978-0-12-801077-8.00016-8

Xu, H., Shi, Z., Reddy, N., & Yang, Y. (2014). Intrinsically Water-Stable Keratin Nanoparticles and Their in Vivo Biodistribution for Targeted Delivery. *J. Agric. Food Chem.*, 6.

Yardimci, B. (2021). Nanoparticle-based with surface plasmon resonance capability colorimetric sensors developed for the detection of some heavy metal ions using UV-Visible Spectrophotometer. *Turkish Journal of Science and Health*, *2*(1), Article 1.

Yildiz, H. B., Cevik, E., & Bezgin Carbas, B. (2019). Nanotechnology for biological photovoltaics; industrial applications of nanomaterials. In *Industrial Applications of Nanomaterials* (pp. 65–89). Elsevier. https://doi.org/10.1016/B978-0-12-815749-7.00003-7

Ying, S., Guan, Z., Ofoegbu, P. C., Clubb, P., Rico, C., He, F., & Hong, J. (2022). Green synthesis of nanoparticles: Current developments and limitations. *Environmental Technology & Innovation*, *26*, 102336. https://doi.org/10.1016/j.eti.2022.102336

Zhang, L., Sellaoui, L., Franco, D., Dotto, G. L., Bajahzar, A., Belmabrouk, H., Bonilla-Petriciolet, A., Oliveira, M. L. S., & Li, Z. (2020). Adsorption of dyes brilliant blue, sunset yellow and tartrazine from aqueous solution on chitosan: Analytical interpretation via multilayer statistical physics model. *Chemical Engineering Journal*, *382*, 122952. https://doi.org/10.1016/j.cej.2019.122952

Zhang, X., Kuang, Y., & Zhou, S. (2020). Adsorption of Methylene Blue in Water onto Activated Carbon by Surfactant Modification. *Water*, *12*(2), 587. https://doi.org/10.3390/w12020587

Zubrik, A., Jáger, D., Mačingová, E., Matik, M., & Hredzák, S. (2023). Spontaneous degradation of methylene blue adsorbed on magnetic biochars. *Scientific Reports*, *13*(1), 14773. https://doi.org/10.1038/s41598-023-39976-9

Zuo, R., Du, G., Zhang, W., Liu, L., Liu, Y., Mei, L., & Li, Z. (2014). Photocatalytic Degradation of Methylene Blue Using TiO $_2$ Impregnated Diatomite. *Advances in Materials Science and Engineering*, *2014*, 1–7. https://doi.org/10.1155/2014/170148

APPENDICES

Appendix I: Data for Standardization of Folin Ciocalteu Method

conc	Abs
0.0011	2.13
0.00088	1.68
0.00077	1.493
0.00066	1.3
0.00055	1.09
0.00044	0.9
0.00033	0.707
0.00022	0.478
0.00011	0.24

Appendix II: Effect of Time on Hydrolysis of Keratin

Time	Abs I	Abs II	Average	**Conc**
0	0	0	0	0
1	0.228	0.22	0.224	0.000082
2	0.562	0.565	0.5635	0.000252
3	0.566	0.567	0.5665	0.000253
4	0.602	0.624	0.613	0.000277
5	0.623	0.664	0.6435	0.000292
6	0.729	0.719	0.724	0.000332
7	0.744	0.721	0.7325	0.000336
8	0.865	0.823	0.844	0.000392
9	0.786	0.941	0.8635	0.000402
10	0.746	0.977	0.8615	0.000401
11	0.795	0.877	0.836	0.000388
12	0.788	0.905	0.8465	0.000393

Appendix III: Effect of Mass of Hooves on Keratin Hydrolysis

Time (Hours)	1 g	3 g	5 g	7 g	9 g	11 g	14 g
0	0	0	0	0	0	0	0
1	0.4505	0.598	0.8295	0.7535	1.095	1.272	1
2	0.494	0.6725	1.0425	1.0565	1.175	1.358	1.3155
3	0.617	0.7835	1.1465	1.1655	1.303	1.424	1.4045
4	0.6235	0.9185	1.2265	1.278	1.4835	1.4955	1.548
5	0.6455	0.923	1.3085	1.244	1.4035	1.458	1.4715
6	0.648	1.05	1.316	1.4175	1.4785	1.567	1.633
7	0.671	1.134	1.334	1.4205	1.452	1.5695	1.656
8	0.6915	1.1405	1.3225	1.4325	1.562	1.5855	1.702
9	0.726	1.116	1.433	1.466	1.5765	1.68	1.684
10	0.7735	1.0645	1.419	1.448	1.564	1.646	1.575
11	0.772	1.053	1.393	1.466	1.575	1.545	1.596
12	0.683	1.1125	1.617	1.849	1.7255	1.739	1.787

Appendix IV: Effect of pH on Keratin Hydrolysis

Absorbance at various pH

Time (Hrs)	2	3	4	5	6	7	8	9	10	11	12	13
0	0	0	0	0	0	0	0	0	0	0	0	0
1	0.003	0.008	0.007	0.008	0.001	0	0.005	0.006	0.011	0.022	0.12	0.109
2	0.004	0.013	0.007	0.011	0.002	0.001	0.009	0.01	0.012	0.026	0.234	0.235
3	0.011	0.014	0.011	0.013	0.003	0.001	0.012	0.012	0.015	0.1	0.387	0.384
4	0.019	0.017	0.021	0.022	0.011	0.004	0.027	0.015	0.137	0.131	0.483	0.488
5	0.023	0.029	0.037	0.024	0.015	0.006	0.03	0.018	0.139	0.149	0.567	0.593
6	0.024	0.031	0.038	0.035	0.017	0.008	0.032	0.02	0.152	0.171	0.675	0.652
7	0.026	0.032	0.037	0.042	0.019	0.009	0.043	0.04	0.153	0.175	0.819	0.71
8	0.027	0.036	0.039	0.044	0.029	0.01	0.046	0.044	0.157	0.184	0.963	0.782
9	0.028	0.049	0.04	0.046	0.047	0.012	0.053	0.067	0.163	0.207	1.128	0.784
10	0.029	0.056	0.042	0.048	0.041	0.015	0.056	0.068	0.256	0.296	1.059	0.837
11	0.029	0.056	0.061	0.091	0.045	0.021	0.064	0.072	0.29	0.338	1.128	0.961
12	0.028	0.049	0.061	0.091	0.047	0.021	0.076	0.078	0.289	0.366	1.127	0.957
13	0.028	0.055	0.06	0.089	0.046	0.02	0.083	0.078	0.303	0.337	1.128	0.96

Appendix V: Effect of Temperature on Keratin Hydrolysis

	Temperature				
Time(Hours)	30	40	60	70	80
0	0	0	0	0	0
1	0.0755	0.115	0.2565	0.28	0.5815
2	0.148	0.1735	0.71	0.6765	0.81
3	0.275	0.2865	0.9355	1.108	1.052
4	0.288	0.41	1.1685	1.446	1.2305
5	0.3465	0.464	1.225	1.584	1.23
6	0.428	0.497	1.2935	1.601	1.2425
7	0.483	0.589	1.233	1.6555	1.281
8	0.505	0.613	1.2485	1.6625	1.2605
9	0.5815	0.685	1.311	1.6525	1.3055
10	0.718	0.736	1.326	1.628	1.3955
11	0.804	0.805	1.2905	1.6275	1.3095
12	0.8565	0.8095	1.2615	1.6285	1.317

Appendix VI: Effect of Concentration of NaOH on Keratin Hydrolysis

Time(hrs)	0.50%	1%	1.50%	2%	2.50%	3%	3.50%	4%
0	0	0	0	0	0	0	0	0
1	0.143	0.225	0.251	0.167	0.224	0.252	0.1595	0.221
2	0.252	0.5255	0.5555	0.3545	0.5635	0.3015	0.418	0.3925
3	0.363	0.614	0.623	0.6265	0.5665	0.4685	0.4555	0.423
4	0.4795	0.775	0.807	0.68	0.613	0.5845	0.54	0.707
5	0.558	0.8735	0.9475	0.7415	0.6435	0.653	0.5625	0.7685
6	0.6095	0.9105	1.072	0.8295	0.724	0.6825	0.603	0.827
7	0.718	1.0345	1.11	0.827	0.7325	0.8235	0.7425	0.825
8	0.745	1.1535	1.116	0.8235	0.844	0.848	0.8125	0.825
9	0.7515	1.169	1.1215	0.85	0.8635	0.8405	0.8185	0.877
10	0.847	1.197	1.114	0.856	0.8615	0.885	0.842	0.87
11	1.1155	1.249	1.097	0.8305	0.836	0.889	0.834	0.8475
12	1.117	1.241	1.18	0.8065	0.8465	0.8505	0.822	0.856

Appendix VII: Changes in pH of solution with Time during Hydrolysis of Keratin, obtained using 11 g and 14 g of hooves

Time (Hours)	11 g	14 g
0	12.69	12.69
1	11.835	11.79
2	11.625	11.67
3	11.545	11.635
4	11.51	11.545
5	11.485	11.485
6	11.455	11.45
7	11.425	11.435
8	11.38	11.395
9	11.36	11.345
10	11.35	11.34
11	11.345	11.335
12	11.315	11.19

Appendix VIII: Data for standardization of Crystal Violet

Conc(ppm)	Absorbance
5	0.908
4.5	0.82
4	0.724
3.5	0.656
3	0.583
2.5	0.492
2	0.41
1.5	0.321
1	0.26
0.5	0.175

Appendix IX: Data for Standardization of Methylene Blue

Conc(ppm)	Absorbance
5	1.437
4.5	1.281
4	1.164
3.5	1.04
3	0.86
2.5	0.75
2	0.59
1.5	0.48
1	0.332
0.5	0.196

Appendix X: Effect of Time on Adsorption of Crystal Violet using Silver Nanoparticles

Time(min)	Abs 1	Abs 2	Abs av
0	1.319	1.319	1.319
20	0.309	0.305	0.307
40	0.108	0.106	0.107
60	0.05	0.051	0.0505
80	0.055	0.053	0.054
100	0.061	0.058	0.0595
120	0.054	0.054	0.054
140	0.019	0.04	0.0295
160	0.054	0.054	0.054

Appendix XI: Effect of Time on Adsorption of Methylene Blue using Copper Nanoparticles

Time	Abs (Av)
0	1.604
30	0.74
60	0.544
90	0.453
120	0.352
150	0.281
180	0.216
210	0.206
240	0.19
270	0.15
300	0.137
330	0.086
360	0.086
390	0.087

Appendix XII: Effect of Time on Adsorption of Crystal Violet using Fe_3O_4

Time (Min)	qt
0	0
1	9.069839
2	21.86032
3	24.28229
4	24.81459
5	24.81459
6	24.8
7	24.81459
8	24.814
9	24.81459
10	24.81459

Appendix XIII: Effect of Concentration on Adsorption of Crystal Violet using Silver Nanoparticles

	qt (mg/g)					
Time(Min)	20ppm	10 ppm	5 ppm	2.5 ppm	1.25 ppm	0.625 ppm
0	0	0	0	0	0	0
20	13.99071	9.555	5.1725	2.6125	1.039875	0.411125
40	17.16764	10.3575	5.68625	2.675	1.31375	0.489309
60	20.57674	10.3875	5.78375	2.695	1.33625	0.534538
80	21.70088	10.4175	5.91625	2.720142	1.347	0.604438
100	22.6173	10.425	5.9725	2.732794	1.379313	0.686678
120	22.935	10.4325	6.0275	2.745445	1.417	0.686678
140	22.935	10.56	6.0275	2.75125	1.417	0.67023
160	23.326	10.5675	6	2.75125	1.3685	0.682566
180	23.49707	10.5975	5.98625	2.758472	1.3575	0.674343
200	23.49707	10.5825	6.0275	2.75125	1.37375	0.686678

Appendix XIV: Effect of Concentration on Adsorption of Methylene Blue using Copper Nanoparticles

	qt (mg/g)				
time (Min)	0.625	1.25	2.5	5	10
0	0	0	0	0	0
30	0.502261	0.820043	1.469238	2.776718	5.255362
60	0.556786	1.047233	2.246229	3.821792	7.46365
90	0.624943	1.147196	2.368911	4.453381	8.785896
120	0.652206	1.251704	2.564295	4.789622	9.635587
150	0.6931	1.274423	2.782397	4.96683	10.07179
180	0.75217	1.319861	2.755134	5.293984	10.42621
210	0.75217	1.34258	2.77331	5.389404	10.88968
240	0.747626	1.369843	2.777854	5.51663	11.32134
270	0.75217	1.397106	2.895992	5.652944	11.46674
300	0.75217	1.447087	2.90508	5.889222	11.53035
330	0.738538	1.47435	2.950518	6.057343	11.88931
360	0.75217	1.478894	2.936887	6.057343	12.00745
390	0.75217	1.478894	2.950518	6.057343	11.94384

Appendix XV: Effect of Preliminary Concentration on Adsorption of Crystal Violet using Fe_3O_4

Time (min)	0.625 ppm	1.25 ppm	2.5 ppm	10 ppm	20 ppm
0	0	0	0	0	0
1	1.11228	1.072332	2.366976	7.049892	12.98104
2	1.332501	1.22371	2.649161	10.61357	20.45243
3	1.341813	1.370459	2.926219	11.35575	22.04462
4	1.341813	1.370459	3.000422	11.52231	22.7115
5	1.341813	1.370459	3.028475	11.61876	23.23753
6	1.341813	1.370459	3.037524	11.82639	24.08196
7	1.341813	1.370459	3.037524	12.04098	24.42439
8	1.341813	1.370459	3.037524	12.33719	24.8149
9	1.341813	1.370459	3.037524	12.33719	24.8149
10	1.341813	1.370459	3.037524	12.33719	24.8149

Appendix XVI: Effect of Quantity of AgNps on Adsorption of Crystal Violet using Silver Nanoparticles

	qt (mg/g)						
Time(min	0 mg	2 mg	4 mg	6 mg	8 mg	10 mg	12 mg
0	0	0	0	0	0	0	0
20	1.5163	7.619409	8.54814	8.206975	9.5906	10.15	11.5618
40	2.691433	10.66149	11.1259	11.24905	11.486	11.562	11.5713
60	3.857089	11.91243	11.5144	12.13988	12.026	11.571	11.6187
80	4.008719	11.7229	11.7039	12.17779	11.988	11.647	11.6471
100	4.169826	11.91243	11.865	12.16831	11.922	11.685	11.685
120	4.131918	11.90296	12.1304	12.18726	11.988	11.732	11.9314
140	4.956406	11.90296	12.102	12.21569	12.32	11.931	11.9314
160	5.041698	11.71342	12.1304	12.24412	11.988	11.931	11.8935

Appendix XVII: Effect of Quantity of CuNps on Adsorption of Methylene Blue using CuNps

	qt					
Time(Min)	1 mg	2 mg	4 mg	6 mg	8 mg	10 mg
0	0	0	0	0	0	0
30	1.967737	2.291147	2.614557	2.369077	3.366584	3.432824
60	2.31063	2.793797	3.584788	2.840555	4.130299	4.278367
90	2.54442	3.163965	3.87313	3.191241	4.484882	4.652431
120	2.95745	3.596478	4.348504	3.662718	4.878429	4.956359
150	3.331515	3.834165	4.683603	4.067955	5.155081	5.104426
180	3.643236	4.258884	4.956359	4.290056	5.408354	5.404458
210	3.810786	4.488778	4.999221	4.664121	5.466802	5.529146
240	4.067955	4.496571	5.077151	5.069358	5.466802	5.517456
270	4.212126	4.878429	5.170667	5.225218	5.509663	5.5798
300	4.574501	5.084944	5.3577	5.443423	5.716178	5.626559
330	4.858946	5.396665	5.665524	5.770729	5.9149	5.864246
360	4.882325	5.396665	5.646041	5.774626	5.864246	5.829177
390	4.925187	5.42394	5.626559	5.770729	5.899314	5.864246

Appendix XVIII: Effect of Quantity of Fe_3O_4on Adsorption of Crystal Violet

Time (min)	8 mg	6 mg	4 mg	2 mg	1 mg
0	0	0	0	0	0
1	5.390125	10.05125	9.40625	8.7125	3.74625
2	10.21875	11.948	11.782	11.25313	7.4125
3	11.323	12.01875	12.27913	11.84163	9.72
4	11.55188	12.3015	12.33975	12.38861	11.12125
5	11.6665	12.3015	12.34838	12.38861	11.65463
6	11.88725	12.19925	12.34325	12.38861	12.19213
7	12.01313	12.19913	12.34838	12.38861	12.19188
8	12.05056	12.19913	12.3	12.38861	12.19188

Appendix XIX: Effect of Temperature on Adsorption of Crystal Violet using AgNps

Time (min)	25 °C	30 °C	40 °C	50 °C	60 °C
0	0	0	0	0	0
20	9.590599	11.68459	12.09677	11.89068	11.59946
40	11.48597	11.72043	12.13262	12.06093	11.74283
60	12.02142	11.78315	12.02509	12.06093	11.76971
80	12.02142	12.06093	12.02509	12.06093	11.87724
100	12.02142	12.06093	12.02509	12.06093	11.88172
120	12.02142	12.06093	12.02509	12.06093	11.70251

Appendix XX: **Effect of Temperature on Adsorption of Methylene Blue using CuNps**

Time (min)	qt (mg/g) 24 °C	30 °C	40 °C	50 °C	60 °C
0	0	0	0	0	0
30	3.366584	3.015898	4.122506	4.808292	5.275873
60	4.130299	4.851153	5.244701	5.431733	5.903211
90	4.484882	5.396665	5.653834	5.455112	6.020106
120	4.878429	5.59149	5.872039	5.903211	6.016209
150	5.155081	5.716178	5.953865	5.969451	6.020106
180	5.408354	5.735661	6.000623	6.008416	6.008416
210	5.447319	5.762936	6.00452	6.047382	6.012313
240	5.509663	5.770729	6.016209	6.020106	6.020106
270	5.665524	5.872039	6.020106	6.020106	6.047382
300	5.716178	5.918797	6.016209	6.016209	6.024002
330	5.9149	6.00452	6.020106	6.020106	6.020106
360	5.864246	6.00452	6.020106	6.008416	6.047382

Appendix XXI: Effect of Preliminary Colorant pH on Adsorption of Crystal Violet colorant using AgNps

Time(Min)	2	3	4	5	6	7	8	9	10
0	0.513	1.244	1.398	1.358	1.337	1.311	1.392	1.214	0.162
20	0.509	0.0235	0.0425	0.023	0.046	0.03	0.188	0.102	0.053
40	0.458	0.023	0.043	0.0055	0.0045	0.075	0.161	0.064	0.0065
60	0.552	0.016	0.0405	0.006	0.0075	0.034	0.1485	0.044	0.007
80	0.49	0.0155	0.0415	0.026	0.065	0.0345	0.124	0.036	0.0355
100	0.445	0.016	0.039	0.0365	0.0635	0.0355	0.123	0.033	0.039
120	0.419	0.019	0.026	0.036	0.0635	0.036	0.1125	0.033	0.039
140	0.519	0.019	0.027	0.0345	0.0635	0.0525	0.113	0.12	0.04

Appendix XXII: Effect of Preliminary Colorant pH on Adsorption of Methylene Blue colorant using CuNps

Time	2	3	4	5	6	7	8	9	10	11	12	13
0	1.674	1.408	1.369	1.597	1.241	0.725	1.328	1.239	0.784	0.928	0.928	0.927
30	1.553	1.313	1.167	1.27	0.767	0.286	0.986	0.84	0.676	0.827	0.72	0.628
60	1.42	1.18	1.07	1.1	0.65	0.192	0.93	0.722	0.58	0.77	0.71	0.252
90	1.38	0.8	0.98	0.83	0.187	0.096	0.88	0.652	0.512	0.57	0.698	0.184
120	1.373	0.413	0.935	0.785	0.174	0.084	0.815	0.388	0.448	0.45	0.687	0.177
150	1.263	0.239	0.693	0.578	0.112	0.08	0.281	0.286	0.428	0.38	0.31	0.142
180	0.422	0.088	0.141	0.248	0.068	0.077	0.087	0.196	0.422	0.302	0.238	0.137
210	0.127	0.08	0.12	0.153	0.059	0.073	0.073	0.144	0.42	0.232	0.192	0.103
240	0.059	0.079	0.057	0.096	0.06	0.06	0.074	0.111	0.356	0.229	0.102	0.202
270	0.058	0.06	0.051	0.082	0.056	0.06	0.078	0.116	0.315	0.229	0.234	0.164
300	0.062	0.063	0.052	0.056	0.06	0.082	0.08	0.122	0.302	0.202	0.22	0.15
330	0.063	0.06	0.052	0.057	0.059	0.06	0.08	0.118	0.284	0.234	0.244	0.168
360	0.062	0.061	0.053	0.056	0.06	0.058	0.073	0.107	0.234	0.27	0.27	0.183
390	0.06	0.06	0.052	0.06	0.062	0.06	0.073	0.109	0.234	0.27	0.27	0.2

Appendix XIII: Approval Letter by Board of Graduate Studies

UNIVERSITY OF KABIANGA
ISO 9001:2015 CERTIFIED
OFFICE OF THE DIRECTOR, BOARD OF GRADUATE STUDIES

REF: PHD/CHE/002/19 **DATE: 8TH SEPTEMBER, 2023**

Caroline Cheptoo,
MAPS Department,
University of Kabianga,
P.O Box 2030- 20200,
KERICHO.

Dear Ms. Cheptoo,

RE: CLEARANCE TO COMMENCE FIELD WORK/DATA COLLECTION

I am pleased to inform you that the Board of Graduate Studies has considered and approved your PhD research proposal entitled **"Synthesis and Characterization of Nanoparticles using Keratin Extracted from Sheep Hooves for Industrial Applications".**

Subsequently the Board has also approved the following supervisors for appointments.

1. Dr. Wycliffe Chisutia Wanyonyi
2. Dr. Joyce Kiplimo
3. Dr. Edwin S, Madivoli

You may now proceed to commence field work/data collection on condition that you obtain a research permit from NACOSTI and /or an ethical review permit from a relevant ethics review board. .

You are also required to publish two (2) articles in a peer reviewed journal, with all your supervisors, before your oral defense of thesis.

You are required to submit through your supervisors, and HoD, progress reports every three months, to the Director, Board of Graduate Studies.

Please note that it is the policy of the University that you complete your studies within three years from the date of registration. Do not hesitate to consult this office in case of any difficulties encountered in the course of your studies.

I wish you all the best in your research and hope that your study will yield original contribution for the betterment of humanity.

Yours Sincerely,

UNIVERSITY OF KABIANGA
08 SEP 2023
BOARD OF GRADUATE STUDIES

Dr. Ronald K. Rop
DIRECTOR, BOARD OF GRADUATE STUDIES.
RKR/hk

cc 1. Dean, SST
2. HOD, MAPS
3. Supervisors

Appendix XXIV: Research Permit

REPUBLIC OF KENYA

NATIONAL COMMISSION FOR SCIENCE,TECHNOLOGY & INNOVATION

Ref No: **508437**

Date of Issue: **26/September/2023**

RESEARCH LICENSE

This is to Certify that Ms.. Cheptoo Caroline of University of Kabianga, has been licensed to conduct research as per the provision of the Science, Technology and Innovation Act, 2013 (Rev.2014) in Kericho, Nairobi on the topic: Synthesis and characterization of nanoparticles using keratin extracted from sheep hooves for industrial application for the period ending : 26/September/2024.

License No: **NACOSTI/P/23/29833**

508437

Applicant Identification Number

Director General
NATIONAL COMMISSION FOR SCIENCE,TECHNOLOGY & INNOVATION

Verification QR Code

NOTE: This is a computer generated License. To verify the authenticity of this document, Scan the QR Code using QR scanner application.

See overleaf for conditions